UNIVERSITÀ DEGLI STUDI DI TRIESTE

DIPARTIMENTO DI FISICA

DOTTORATO DI RICERCA IN FISICA
XXIX CICLO

Heating Effects and Localization Mechanism in Cold Bose Gases

settore scientifico-disciplinare FIS/02

DOTTORANDO:

Marco Bilardello

RESPONSABILE DOTTORATO DI RICERCA:

Chiar.mo prof. Livio Lanceri (Univ. Trieste)

FIRMA: Livio Lanceri

RELATORE:

Chiar.mo prof. Angelo Bassi (Univ. Trieste)

FIRMA: Angelo Bassi

ANNO ACCADEMICO 2015/2016

UNIVERSITÀ DEGLI STUDI DI TRIESTE

DIPARTIMENTO DI FISICA

DOTTORATO DI RICERCA IN FISICA
XXIX CICLO

Heating Effects and Localization Mechanism in Cold Bose Gases

settore scientifico-disciplinare FIS/02

DOTTORANDO:
Marco Bilardello

RESPONSABILE DOTTORATO DI RICERCA:
Chiar.mo prof. Livio Lanceri (Univ. Trieste)
FIRMA: _____

RELATORE:
Chiar.mo prof. Angelo Bassi (Univ. Trieste)
FIRMA: _____

ANNO ACCADEMICO 2015/2016

Contents

Introduction

Nowadays, quantum mechanics has been tested by experiments in practically all research fields, from sub-nuclear physics [1, 2] to atomic and molecular physics [3, 4] to quantum optics [5]. Nonetheless, several physicists, among whom we mention Leggett [6], Weinberg [7] and Bell [8], believe that quantum mechanics as it is, is not a fundamental theory, but rather a phenomenological one. One of the main problems with quantum mechanics is the notorious measurement problem: usual Schrödinger evolution cannot explain why detectors have well-defined outcomes, and the wavefunction reduction postulate must be used in order to solve this paradox. This poses one simple question: when do we have to use the Schrödinger evolution and when does it stop and the wavefunction reduction postulate applies? To quote Bell [8]: "What exactly qualifies some physical systems to play the role of *measurer*. Was the wave function of the world waiting to jump for thousands of millions of years until a single-celled living creature appeared? Or did it have to wait a little longer for some better qualified system...with a PhD?".
The standard formulation of quantum mechanics does not solve the measurement problem, and several solutions to this problem have been proposed in the last years [9–16]. In this thesis we study one of these solutions, given by dynamical reduction models [17, 18]. In these models the two dynamics of quantum mechanics - the linear and deterministic Schrödinger equation, and the nonlinear and stochastic wavefunction reduction postulate - are substituted by a unique nonlinear and stochastic dynamics. The new dynamics preserves quantum mechanical prediction for microscopic systems, according with experimental results. However, dynamical reduction models are constructed in such a way that macroscopic systems are always localized in space, in contrast with the quantum mechanical superposition principle. This difference between quantum mechanics and dynamical reduction models can be, in principle, tested experimentally. Indeed, research carried out in recent years has set significant bounds on the parameters of dynamical reduction models. The class of experiments ranges from X-rays spontaneous emission [19], to heating effects on cantilevers [20], to matter-wave interferometry [21], to cosmological analysis [22]. In chapter 1 we give a detailed introduction to dynamical reduction models.

In this thesis we analyze the dynamics of the most studied dynamical reduction model, the Continuous Spontaneous Localization (CSL) model, on a new promis-

ing class of systems: cold atomic gases and, more precisely, Bose Einstein condensates [23]. The reasons why Bose Einstein condensates are interesting to test the CSL model are mainly twofold: first of all, these systems have very low temperatures, and they can be used to test some typical effects of the collapse noise, such as heating effects and diffusion processes; secondly, Bose Einstein condensates manifest quantum mechanical properties (as long range coherence) involving a large number N of atoms, $N = 10^3 - 10^{11}$ atoms. The action of the localization mechanism modifies these properties in a way that can, in principle, be tested experimentally.
Other considerations make the study of cold atomic systems in dynamical reduction models very interesting. Indeed, strong theoretical works in describing the quantum mechanical properties of Bose Einstein condensates have been made in the last century. The Bogoliubov theory [24] is at the basis of Bose Einstein condensation of a dilute weekly interacting gas, where the atoms macroscopically occupy the single particle ground state given by the Gross-Pitaevskii equation. Nowadays, common textbooks on cold atomic systems present full theoretical description of several properties, from superfluidity, to vortex creation, to correlation properties of condensates, and many more [25, 26].
On the experimental side, the great effort made in the study of atom-light interaction, together with a very good experimental control on the laser parameters, led to the use of laser for trapping and cooling gases [27]. As a consequence, lower temperature become accessible in the experiments, and in 1995, for the first time a Bose Einstein condensate was created and experimentally observed [28]. Since then, experimentalists performed cold atomic experiments in a huge variety of trapping potentials, from a simple harmonic potential to optical lattices, with a remarkable control on the parameters of the system. Moreover, through the use of Feshbach resonances [29], experimentalists are able to tune the coupling of the atom-atom interaction, thus creating strong or weak interacting gases, and also changing the sign of the coupling. A brief review on cold atomic system is given in chapter 2.

In chapter 3 we study the heating effects of CSL on a Bose Einstein condensate. We first review a recent work [30], were the authors set bounds on the CSL parameters from the experimental observation of the temperature increase of the condensate. Generally, the energy increase of the N-atom system is

$$\frac{1}{N}\frac{dE}{dt} = \frac{1}{N}\frac{dE}{dt}|_{CSL} + \frac{1}{N}\frac{dE}{dt}|_{oth.}, \tag{1}$$

where we separated the CSL contribution from all other contributions due to external sources of heating/cooling of the gas. In [30], the most relevant sources are: evaporative cooling of the gas, leading to a decrease of the temperature of the condensate; three body recombination processes, which increase the temperature of the gas; collisions between the atoms in the condensate and external atoms at room temperature. Usually, these collisions determine atom losses of the condensate, with a resulting energy decrease. Measuring the temperature increase of the gas, and estimating the external sources of heating/cooling, the authors of [30] set the

following bound on the CSL parameters:

$$\frac{\lambda}{r_C^2} < 10^7 \text{ s}^{-1}\text{m}^{-2}\,, \tag{2}$$

where λ is the collapse rate and r_C is the resolution length of the noise. This bound is better than the experimental bound set by interferometric experiments with macromolecules [21], but is weaker than that set by X-rays experiment [19] (see the exclusion plot in fig. 3.6).
In the second part of chapter 3 we study the diffusion process induced by the noise on a free expanding gas. Starting from a recent experimental result [31], where the authors were able to cool a gas down to picokelvin, we computed [32] the modification on the position standard deviation of the gas, due to the noise of CSL, dCSL [33] and cCSL [34, 35] models. For the CSL model, one finds the following expression for the position variance of the gas after a free expansion time t_3:

$$\langle \hat{\mathbf{x}}^2 \rangle_{t_3} = \langle \hat{\mathbf{x}}^2 \rangle_{t_3}^{\text{QM}} + \langle \hat{\mathbf{x}}^2 \rangle_{t_3}^{\text{CSL}}, \tag{3}$$

where we separated the term given by quantum mechanics (QM) from the extra CSL term. Comparing our analytical result with the experimental values, we were able to set the following bound on CSL parameters:

$$\frac{\lambda}{r_C^2} < 5 \times 10^6\, \text{m}^{-2}\text{s}^{-1}. \tag{4}$$

In the exclusion plot in fig. 3.6 we compare this bound with all the other experimental bounds set so far.
We computed the same quantity also for the non-Markovian (cCSL) and dissipative (dCSL) extensions of the CSL model. For the cCSL model, we considered a noise with time correlation function $f(s)$ given by

$$f(s) = \frac{1}{2\tau} e^{-|s|/\tau}\,, \tag{5}$$

where τ is the correlation time of the noise. We observed that, for $r_C \geq 10^{-10}$ m, the predictions with the cCSL are indistinguishable with that of standard CSL model if $\tau^{-1} \geq 10^9$ Hz. Taking into account that, according to cosmological argumentations, the expected value of the correlation time is $\tau^{-1} = 10^{10} - 10^{11}$ Hz, then we can safely say that our bound on the CSL parameters is preserved also in its non-Markovian extension. Nowadays, our work set the strongest bound for the cCSL parameters.
For the dCSL model, we compared the predicted position standard deviation with the measured value. In this model, the new parameter T_{CSL} is introduced, playing the role of the temperature of the noise field. In the limit $T_{\text{CSL}} \to +\infty$ the CSL model is recovered, while if $T_{\text{CSL}} \to 0$ standard quantum mechanics is recovered. Comparing the position standard deviation predicted by dCSL model with the experimental

data, we obtained an exclusion plot in $\lambda - r_C$ for three different values of the noise temperature: $T_{\text{CSL}} = 1, 10^{-6}, 10^{-12}$ K, see the exclusion plot 3.7.

In chapter 4 we study the localization dynamics of the CSL model in Bose Einstein condensates in a double well potential [36]. We specialize the CSL master equation to the double well potential within the two-mode approximation, where the Hamiltonian operator becomes the two-sites Bose Hubbard Hamiltonian. In this case, we are able to solve exactly the master equation if we neglect the hopping term in the Hamiltonian dynamics. We study the localization dynamics for two different classes of initial states: atomic coherent states, and macroscopically entangled states (such as NOON states). We observe that the localization dynamics for the atomic coherent states is negligible with respect to the current experimental times. In fact, atomic coherent states are a coherent factorization of delocalized single particle states, and in the CSL dynamics no amplification mechanism occurs. The situation for a NOON state is different. This many body state is the superposition of the state with N atoms in the left well with the state of N atoms in the right well, thus the amplification mechanism of the CSL dynamics takes place. The collapse rate of the spatial coherences is increased by a N^2 factor, increasing considerably the localization process. This makes NOON states an interesting case for an experimental test of CSL. In fig. 4.2 we represented an hypothetical exclusion plot for the CSL model, where we imaged that the spatial coherence of a NOON state is observed for 1 s. As can be seen, we show that a NOON state with $N \sim 10^3$ with a coherence time of ~ 1 s can constrain the CSL parameters in a region where the other systems presently cannot.
We then extend the localization mechanism to the generic M-sites Bose Hubbard model, describing a Bose Einstein condensate in an optical lattice composed of M sites. We observed no significant modifications of the localization process from the double well case.
In the last part of chapter 4 we determine what requests the experimental values have to satisfy in order to put new bounds for the parameters of the CSL model. We compare the CSL dynamics with two typical decoherence sources, namely, the phase noise and the spontaneous photon emission process. Their density matrix evolution mimics the CSL dynamics, and, usually, they are strong enough to cover CSL effects. We discussed under which conditions CSL effects would become stronger than these decoherence sources. We also compare the results of the CSL dynamics with thermal and three body effects.

Chapter 1

Dynamical Reduction Models

In this chapter we introduce dynamical reduction models. These models solve the measurement problem through a proper non linear and stochastic modification of the Schrödinger equation, such that predictions for microscopic systems result to be indistinguishable from the quantum mechanical predictions. This is a necessary condition in order to avoid contradictions with the experiments. However, quantum mechanics differs from dynamical reduction models if the system is composed by a macroscopic number of particles, where, in the latter case, the dynamics localizes in space the center of mass of the system.

This chapter is organized as follows: we start by introducing the measurement problem, with a focus on the wavefunction reduction postulate. We then describe the first consistent dynamical reduction model, the GRW model. In the last part of this chapter, we describe the CSL model, which is the most studied collapse model, as well as its dissipative (dCSL) and non-white (cCSL) extensions.

1.1 The measurement problem

We start our presentation with a review of the postulates of Quantum Mechanics, and a focus on the measurement problem.

1. Every physical system S is associated to an Hilbert space $\mathbb{H}$. The physical states of the system S are the normalized vectors $|\psi\rangle \in \mathbb{H}$.
2. Every physical observable O of the system S is represented by self-adjoint operator $\hat{O}$ acting on the Hilbert space $\mathbb{H}$. The possible outcomes of a measurement of O are given by its eigenvalues o_n, defined by the relation $\hat{O}|o_n\rangle = o_n|o_n\rangle$, where $|o_n\rangle$ is the related eigenstate. The self-adjointness of the operator $\hat{O}$ guarantees that its eigenvalues are real and its eigenstates form an orthonormal basis of the Hilbert space $\mathbb{H}$. For simplicity, here we assumed that the operator $\hat{O}$ has a discrete and nondegenerate spectrum.

3. Given the initial state $|\psi_0\rangle$ of the system S, its time evolution is described by the Schrödinger equation:

$$i\hbar\frac{d|\psi_t\rangle}{dt} = \hat{H}\,|\psi_t\rangle\,, \tag{1.1}$$

where $\hat{H}$ is the Hamiltonian operator of the system. Once known the initial state $|\psi_0\rangle$ of the system S, the Schrödinger equation (1.1) gives the state $|\psi_t\rangle$ at any time t.

4. The probability $P\,[o_n]$ to have o_n as outcome of a measurement of O on the system S in the state $|\psi\rangle$ is

$$P\,[o_n] = |\langle o_n|\psi\rangle|^2\,. \tag{1.2}$$

5. After the measurement of O with o_n as outcome, the initial state $|\psi\rangle$ of the system S suddenly changes to the eigenstate $|o_n\rangle$:

$$|\psi\rangle \quad \text{before the measurement} \longrightarrow |o_n\rangle \quad \text{after the measurement.} \tag{1.3}$$

This is the so-called wavefunction reduction postulate.

As we can see, Quantum Mechanics is characterized by two very different dynamics.

Firstly, there is the Schrödinger equation (1.1), which gives a *linear* and *deterministic* time evolution for the state of the system. The linearity of the dynamics implies that, if the state of the system at the initial time t_0 is $\alpha\,|\psi_{t_0}\rangle + \beta\,|\phi_{t_0}\rangle$, then at any time t the state is $\alpha\,|\psi_t\rangle + \beta\,|\phi_t\rangle$, *i.e.*, the Schrödinger dynamics preserves the superposition of states. Moreover, as already stated, the Schrödinger equation gives a deterministic time evolution: known the initial state of the system, its future evolution is completely determined.

Secondly, there is the wavefunction reduction postulate (1.3), which is *nonlinear* and *stochastic*. The stochasticity of the measurement process is clearly shown in eq. (1.2). The nonlinearity of eq. (1.3) is due to the fact that, after the measurement process, the state of the system collapses into the eigenstate $|o_n\rangle$ without preserving any initial superposition of states.

For these reasons, the Schrödinger equation (1.1) and the wavefunction reduction postulate (1.3) are two completely different dynamics, and the theory does not explain when we have to apply one or the other. The measurement problem has origin from this ambiguity, as it is well explained by the von Neumann measurement scheme [37] that now we see in detail.

Let us consider the physical system S and one of its observables O. Let M be the device set to measure O on the system S. Let us say that M has a ready state $|A_0\rangle$, which is the initial state of the experimental device when is ready to perform the

measurement, and a set of orthogonal states $|A_n\rangle$ corresponding to different macroscopic states of the device, like, e.g., different positions of a pointer on a scale. Now we assume that the total system $S + M$ is a quantum system evolving under the Schrödinger equation and, to simplify the interaction process between the physical system S and the experimental device M, we assume a perfect correlation between them, *i.e.*,

$$\text{initial state: } |o_n\rangle\,|A_0\rangle \longrightarrow \text{ final state: } |o_n\rangle\,|A_n\rangle\,. \tag{1.4}$$

Eq. (1.4) says nothing more than that to each macroscopically different state of the device (different positions of the pointer on a scale) corresponds a different value of the observable O.
The measurement problem arises when we consider a superposition of eigenstates of $\hat{O}$ as the initial state. According to the linearity of the Schrödinger equation, the final state of the total system $S + M$ is

$$\text{initial state: } \frac{|o_n\rangle + |o_m\rangle}{\sqrt{2}}\,|A_0\rangle \longrightarrow \text{ final state: } \frac{|o_n\rangle\,|A_n\rangle + |o_m\rangle\,|A_m\rangle}{\sqrt{2}}. \tag{1.5}$$

As we can see, in the final state in eq. (1.5) the experimental device does not have a well precise outcome as it should have, leading to the conclusion that the total state of the physical system S and experimental device M does not evolve with the Schrödinger dynamics (or, at least, not for all times). The standard way to solve this problem is to say that, at some time, the Schrödinger evolution stops, and the wavefunction reduction postulate leads the initial state in eq. (1.5) to either $|o_n\rangle\,|A_n\rangle$ or $|o_m\rangle\,|A_m\rangle$ with equal probability. The standard formulation of Quantum Mechanics does not explain precisely when we have to apply the Schrödinger equation or the wavefunction reduction postulate, and unrealistic consequences such as the measurement problem are the consequences of these ambiguities.

We conclude this section on the measurement problem by saying that the above von Neumann measurement scheme has been criticized for its simplicity [13, 14], but it has been proved [17] that also a very general measurement scheme leads to the same problem.

1.2 Possible solutions to the measurement problem

In this section we briefly review some of the solution proposed in the past years to solve the measurement problem. For a more detailed review, see, e.g. [17].

1.2.1 Hidden variables theories and Bohmian Mechanics

One possible way out is saying that the state of the physical system S is not completely defined by a vector $|\psi\rangle$ in an Hilbert space. To complete the theory, new

variables must be introduced besides the vector $|\psi\rangle$.The most famous hidden variable theory is Bohmian Mechanics [9, 10, 38], where the positions $\mathbf{x}_i$ of the particles of the system play the role of the variables in the theory. In this case, particles have always a well-defined position in space, and, in principle, their trajectory in the space can be predicted by knowing the initial positions $\mathbf{x}_i(t_0)$ of the particles of the system and the initial value of the wavefunction $|\psi(t_0)\rangle$ through the following set of dynamical equations:

$$i\hbar\frac{\partial\psi(\mathbf{q}_1,\ldots,\mathbf{q}_N;t)}{\partial t} = \hat{H}\psi(\mathbf{q}_1,\ldots,\mathbf{q}_N;t), \tag{1.6}$$

which is the usual Schrödinger dynamics for the wavefunction represented in the position basis $\mathbf{q}_i$; the trajectory in the real space of the $i-th$ particle with mass m_i is given by the following equation:

$$\frac{d\mathbf{x}_i(t)}{dt} = \frac{\hbar}{m_i}\mathrm{Im}\frac{\psi^*(\mathbf{q}_1,\ldots,\mathbf{q}_N;t)\nabla_i\psi(\mathbf{q}_1,\ldots,\mathbf{q}_N;t)}{|\psi(\mathbf{q}_1,\ldots,\mathbf{q}_N;t)|^2}|_{\mathbf{q}_i=\mathbf{x}_i}\,. \tag{1.7}$$

Taking into account that practically the initial positions $\mathbf{x}_i(t_0)$ of the particles are never known, we can describe the physical system by assign a probability distribution to the positions, namely $\rho(\mathbf{x}_1,\ldots,\mathbf{x}_n;t_0)$. If we impose that $\rho(\mathbf{x}_1,\ldots,\mathbf{x}_n;t_0) = |\psi(\mathbf{x}_1,\ldots,\mathbf{x}_n;t_0)|^2$, with $\psi(\mathbf{x}_1,\ldots,\mathbf{x}_n;t_0)$ the wavefunction of the system evolving with the usual Schrödinger equation, using eqs. (1.6) and (1.7) it can be proven that at any later time t, $\rho(\mathbf{x}_1,\ldots,\mathbf{x}_n;t) = |\psi(\mathbf{x}_1,\ldots,\mathbf{x}_n;t)|^2$. This makes Bohmian Mechanics predictively equivalent to standard Quantum Mechanics.
One peculiar aspect of every hidden variables theory is its contextual nature. In Bohmian Mechanics, for example, given a physical system with a precise wavefunction and well precise positions of the particles, the measurement of e.g. the momentum leads to an outcome which depends on the specific apparatus we chose to perform the measurement. This meas that, in every hidden variable theory, the truly fundamentals entities of the theory are the noncontextual ones (in Bohmian Mechanics, the positions of the particles).

1.2.2 Interaction with an external environment and decoherence

One of the most accepted solution to the measurement problem is decoherence [13, 14, 39], where the superposition of the wavefunction of the system S is suppressed by the action of an external environment E. Let us briefly see how decoherence works through an example. Let us consider a spin-1/2 particle in the following initial state

$$|\psi\rangle = \frac{1}{\sqrt{2}}\left(|\uparrow_z\rangle + |\downarrow_z\rangle\right), \tag{1.8}$$

where $|\uparrow_z\rangle$ ($|\downarrow_z\rangle$) is the state with spin up (down) along the z-direction.
With the statistical operator formalism, the state (1.8) is represented by the follow-

ing projector

$$\begin{aligned} |\psi\rangle\langle\psi| &= \frac{1}{2}\left(|\uparrow_z\rangle\langle\uparrow_z| + |\downarrow_z\rangle\langle\downarrow_z| + |\downarrow_z\rangle\langle\uparrow_z| + |\uparrow_z\rangle\langle\downarrow_z|\right) \\ &= \frac{1}{2}\begin{pmatrix} 1 & 1 \\ 1 & 1 \end{pmatrix} \equiv \hat{\rho}_S, \end{aligned} \tag{1.9}$$

where we expressed the statistical operator in the basis $\{|\uparrow_z\rangle, |\downarrow_z\rangle\}$.
Now let us make the assumption that the spin-1/2 particle interacts with an external environment in an initial state $|\phi\rangle$, or, in the statistical operator formalism, $\hat{\rho}_E = |\phi\rangle\langle\phi|$. Through the interaction, the state of the total system spin-1/2 particle + environment becomes entangled, described by a specific density matrix $\hat{\rho}_{S+E}$. Since we are only interested in the state of the spin-1/2 particle, a statistical average over the degrees of freedom of the external environment is considered. A typical consequences is that the final reduced state of the spin-1/2 particle is given by a diagonal matrix as follows

$$Tr_E\left[\hat{\rho}_{S+E}\right] = \hat{\rho}_S^{'} = \frac{1}{2}\begin{pmatrix} 1 & 0 \\ 0 & 1 \end{pmatrix}, \tag{1.10}$$

which is usually seen as a statistical mixture of spin-1/2 particles with 50% of them in the state $|\uparrow_z\rangle$ and 50% of them in the state $|\downarrow_z\rangle$; in other words, one writes

$$\hat{\rho}_S^{'} = \frac{1}{2}\left(|\uparrow_z\rangle\langle\uparrow_z| + |\downarrow_z\rangle\langle\downarrow_z|\right). \tag{1.11}$$

The main problem here is that the statistical ensemble with density matrix given by eq. (1.10) is not unique. For example, it is easy to see that also the statistical ensemble with 50% of the particles in the state $|\uparrow_x\rangle = \left(|\uparrow_z\rangle + |\downarrow_z\rangle\right)/\sqrt{2}$ and 50% of the particles in the state $|\downarrow_x\rangle = \left(|\uparrow_z\rangle - |\downarrow_z\rangle\right)/\sqrt{2}$ is associated to the statistical operator given by eq. (1.10). From this example it is clear that physically different statistical ensembles have the same statistical operator, and the decoherence dynamics does not tell us if the superposition is suppressed as in eq. (1.11), or is actually still present as in the example above.

1.2.3 Collapse models

Another possible solution is to replace the two dynamics of standard Quantum Mechanics with an unique dynamics leading to the suppression of the superposition during a measurement process. This is the case of Dynamical Reduction Models [17, 18]. The new dynamics must be chosen in such a way that the quantum mechanical predictions for microscopic systems must be preserved, accordingly to experimental results. At the same time, during the interaction between a microscopic system and a macroscopic device, superpositions must be properly suppressed. Since all interactions are ultimately in position, the new dynamics solves

the measurement problem by a proper localization in position of any macroscopic system. It has been proved [40, 41] that the new dynamics must be nonlinear and stochastic, in order to induce the space localization and, at the same time, to avoid faster-than-light signaling.
In the next section we briefly describe the first dynamical reduction model, proposed by Ghirardi, Rimini and Weber (GRW) [42]. After that, we introduce its best known refinement, the Continuous Spontaneous Localization (CSL) model [43], proposed by Ghirardi, Pearle and Rimini. We conclude this chapter on collapse models by describing the dissipative (dCSL) and the non-white (cCSL) extensions of the CSL model.

1.3 GRW model

The GRW model is based on the following postulates:

1. Each particle of any system is subject to random localization processes. The rate of localization follows a Poissonian distribution with mean equal to λ_i, where i is a particle label.

2. The effect of the localization on the i-th particle, around position $\mathbf{a}$, is to suddenly change its state $|\psi\rangle$ as follows:

$$|\psi\rangle \longrightarrow \frac{L^i_{\mathbf{a}}\,|\psi\rangle}{\|L^i_{\mathbf{a}}\,|\psi\rangle\|}, \tag{1.12}$$

   where

$$L^i_{\mathbf{a}} = \left(\pi r_C^2\right)^{-\frac{3}{4}} e^{-\frac{(\hat{\mathbf{x}}_i-\mathbf{a})^2}{2r_C^2}}. \tag{1.13}$$

   In eq. (1.13), $\hat{\mathbf{x}}_i$ is the position operator for the i-th particle, while r_C is a parameter of the model defining the size of the localized function around the point $\mathbf{a}$.

3. The probability that the i-th particle is localized around the point $\mathbf{a}$ is

$$P^i_{\mathbf{a}} = \left\| L^i_{\mathbf{a}}\,|\psi\rangle \right\|^2. \tag{1.14}$$

4. Between two subsequent localizations, the system evolves with the usual Schrödinger equation (1.1).

From the postulates here above, it is clear that the localization process depends on two parameters of the model: the rate of localization λ_i, usually chosen equal for every particle of the same type, and the resolution length r_C. These two parameters must be chosen in such a way that the GRW dynamics preserve the quantum mechanical predictions for microscopic systems (few particles), while localizes in

space the center-of-mass of a macroscopic number of particles.
Let us now consider the master equation for the statistical operator. Let us consider the case of a single particle in the pure state $\hat{\rho}_t = |\psi_t\rangle\langle\psi_t|$, which is suddenly localized around the point $\mathbf{a}$ as described in eq. (1.13) with probability $P_{\mathbf{a}}$ given in eq. (1.14). This means that, due to the GRW localization, the initial pure state $\hat{\rho}_t$ evolves as follows:

$$\begin{aligned}\hat{\rho}_t = |\psi_t\rangle\langle\psi_t| \longrightarrow & \int d\mathbf{a}\, \frac{L_{\mathbf{a}}|\psi_t\rangle\langle\psi_t| L_{\mathbf{a}}}{\|L_{\mathbf{a}}|\psi\rangle\|^2} P_{\mathbf{a}} \\ & = \int d\mathbf{a}\, L_{\mathbf{a}}|\psi_t\rangle\langle\psi_t| L_{\mathbf{a}} \equiv T[\hat{\rho}_t]\,.\end{aligned} \tag{1.15}$$

The GRW localization process has a probability λdt to happen in a time interval dt, while there is a probability $1-\lambda dt$ that, in the same time interval, no localization occurs and the state evolves with the usual Schrödinger dynamics. With these considerations, we can easily find the GRW master equation:

$$\begin{aligned}&\hat{\rho}_{t+dt} = (1-\lambda dt)\left(\hat{\rho}_t - \frac{i}{\hbar}\left[\hat{H},\hat{\rho}_t\right]dt\right) + \lambda dt T[\hat{\rho}_t] \\ &\Rightarrow \frac{d\hat{\rho}_t}{dt} = \frac{-i}{\hbar}\left[\hat{H},\hat{\rho}_t\right] - \lambda\left(\hat{\rho}_t - T[\hat{\rho}_t]\right).\end{aligned} \tag{1.16}$$

It is easy to see that the master equation (1.16) is completely positive and trace preserving, with

$$\frac{d}{dt} Tr\left[\hat{\rho}_t^2\right] < 0, \tag{1.17}$$

which means that pure states evolve in statistical mixtures.

The two main properties of dynamical reduction models we will focus in this thesis are the localization dynamics and the heating effect induced on any physical system. In the next subsection, we describe how eq. (1.16) localizes the state in space for a microscopic system (single particle), and for a macroscopic system (the center-of-mass of N particles). Then, we compute the heating rate induced by GRW dynamics on any physical system.

1.3.1 Localization and amplification mechanism

Let us now see how the master equation (1.16) localizes a state in space. If we focus only on the non-Hamiltonian dynamics, we have that the matrix elements $\langle\mathbf{x}|\hat{\rho}_t|\mathbf{y}\rangle = \rho_t(\mathbf{x},\mathbf{y})$ evolve as follows

$$\frac{d\rho_t(\mathbf{x},\mathbf{y})}{dt} = -\lambda\left(1 - e^{-\frac{(\mathbf{x}-\mathbf{y})^2}{4r_C^2}}\right)\rho_t(\mathbf{x},\mathbf{y}), \tag{1.18}$$

i.e. there is an exponential decrease of the spatial coherences of the particle.

The next property of the GRW model we are interested in is the so-called amplification mechanism, *i.e.*, the rescaling of the collapse rate λ_{CM} of the center-of-mass of a many body system with the number of particles in the system. Let us firstly introduce the many body generalization of the master equation (1.16):

$$\frac{d\hat{\rho}_t}{dt} = \frac{-i}{\hbar}\left[\hat{H}, \hat{\rho}_t\right] - \sum_{i=1}^{N} \lambda_i \left(\hat{\rho}_t - T^i\left[\hat{\rho}_t\right]\right), \tag{1.19}$$

where

$$T^i\left[\hat{\rho}_t\right] = \int d\mathbf{a}\, L^i_{\mathbf{a}} \left|\psi_t\right\rangle \left\langle\psi_t\right| L^i_{\mathbf{a}}, \tag{1.20}$$

and $L^i_{\mathbf{a}}$ is given by eq. (1.13).
Let us now introduce the position operators for the center-of-mass and relative coordinates, respectively, $\hat{\mathbf{X}}$ and $\hat{\mathbf{q}}_i$, $i = 1, \ldots, N-1$, such that

$$\hat{\mathbf{x}}_i = \hat{\mathbf{X}} + \sum_{j=1}^{N-1} c_{i,j}\hat{\mathbf{q}}_j, \tag{1.21}$$

with $c_{i,j}$ real coefficients (their explicit expression is not necessary for proof). We are interested in finding the dynamics of the center-of-mass of the system, *i.e.*, in the reduced statistical operator $\hat{\rho}^{\text{CM}}_t \equiv Tr_{\mathbf{q}}\left[\hat{\rho}_t\right]$. From eq. (1.20) it is possible to see that, $\forall i$,

$$\begin{aligned} Tr_{\mathbf{q}}\left(T^i\left[\hat{\rho}_t\right]\right) &= \int d\mathbf{a}\, L^{\mathbf{X}}_{\mathbf{a}} Tr_{\mathbf{q}}\left(\hat{\rho}_t\right) L^{\mathbf{X}}_{\mathbf{a}} \\ &\equiv T^{\mathbf{X}}\left[Tr_{\mathbf{q}}\left(\hat{\rho}_t\right)\right]. \end{aligned} \tag{1.22}$$

By a Fourier transform of the space integral in eq. (1.20) we have:

$$\begin{aligned} Tr_{\mathbf{q}}\left(T^i\left[\hat{\rho}_t\right]\right) &= Tr_{\mathbf{q}}\left(\int d\mathbf{a}\, \left(\pi r_C^2\right)^{-\frac{3}{2}} e^{-\frac{\left(\hat{\mathbf{x}}_i - \mathbf{a}\right)^2}{2r_C^2}} \hat{\rho}_t e^{-\frac{\left(\hat{\mathbf{x}}_i - \mathbf{a}\right)^2}{2r_C^2}}\right) \\ &= Tr_{\mathbf{q}}\left(\left(\frac{r_C^2}{\pi\hbar^2}\right)^{\frac{3}{2}} \int d\mathbf{p}\, e^{-\frac{\mathbf{p}^2 r_C^2}{2\hbar^2}} e^{\frac{i}{\hbar}\mathbf{p}\left(\hat{\mathbf{X}} + \sum_{j=1}^{N-1} c_{i,j}\hat{\mathbf{q}}_j\right)} \hat{\rho}_t e^{-\frac{i}{\hbar}\mathbf{p}\left(\hat{\mathbf{X}} + \sum_{j=1}^{N-1} c_{i,j}\hat{\mathbf{q}}_j\right)}\right) \\ &= \left(\frac{r_C^2}{\pi\hbar^2}\right)^{\frac{3}{2}} \int d\mathbf{p}\, e^{-\frac{\mathbf{p}^2 r_C^2}{2\hbar^2}} e^{\frac{i}{\hbar}\mathbf{p}\hat{\mathbf{X}}} Tr_{\mathbf{q}}\left(e^{\frac{i}{\hbar}\mathbf{p}\sum_{j=1}^{N-1} c_{i,j}\hat{\mathbf{q}}_j} \hat{\rho}_t e^{-\frac{i}{\hbar}\mathbf{p}\sum_{j=1}^{N-1} c_{i,j}\hat{\mathbf{q}}_j}\right) e^{-\frac{i}{\hbar}\mathbf{p}\hat{\mathbf{X}}} \\ &= \left(\frac{r_C^2}{\pi\hbar^2}\right)^{\frac{3}{2}} \int d\mathbf{p}\, e^{-\frac{\mathbf{p}^2 r_C^2}{2\hbar^2}} e^{\frac{i}{\hbar}\mathbf{p}\hat{\mathbf{X}}} Tr_{\mathbf{q}}\left(\hat{\rho}_t\right) e^{-\frac{i}{\hbar}\mathbf{p}\hat{\mathbf{X}}}. \end{aligned} \tag{1.23}$$

Applying eq. (1.22) in the master equation (1.19) we get

$$\frac{d\hat{\rho}^{\text{CM}}_t}{dt} = \frac{-i}{\hbar}\left[\hat{H}, \hat{\rho}^{\text{CM}}_t\right] - \left(\sum_{i=1}^{N} \lambda_i\right)\left(\hat{\rho}^{\text{CM}}_t - T^{\mathbf{X}}\left[\hat{\rho}^{\text{CM}}_t\right]\right). \tag{1.24}$$

From eq. (1.24) it is immediate to see that the collapse rate for the center-of-mass of an N particles system is $\lambda^{\text{CM}} = \sum_{i=1}^{N} \lambda_i$.

1.3.2 Heating effect

A direct consequence of the master equation (1.16) is a constant energy increase of the system. Indeed, for a generic Hamiltonian operator $\hat{H} = \hat{\mathbf{p}}^2/(2m) + V(\hat{\mathbf{x}})$, by using eqs. (1.16) and (1.13) the rate of energy increase is:

$$\begin{aligned}
&\frac{d}{dt} Tr\left\{\hat{\rho}_t \hat{H}\right\} = -\lambda\left(Tr\left\{\hat{\rho}_t \hat{H}\right\} - Tr\left\{T\left[\hat{\rho}_t\right]\hat{H}\right\}\right) \\
&= \frac{-\lambda}{2}\int d\mathbf{a}\, Tr\left\{\hat{\rho}_t\left[L_{\mathbf{a}}, \left[L_{\mathbf{a}}, \frac{\mathbf{p}^2}{2m}\right]\right]\right\} \\
&= \frac{\lambda\hbar^2}{2mr_C^2}\int d\mathbf{a}\int d\mathbf{x}\,\rho_t(\mathbf{x},\mathbf{x})\frac{(\mathbf{x}-\mathbf{a})^2}{r_C^2} e^{-\frac{(\mathbf{x}-\mathbf{a})^2}{r_C^2}}\left(\pi r_C^2\right)^{-\frac{3}{2}} \\
&= \frac{\lambda\hbar^2}{4mr_C^2}.
\end{aligned} \tag{1.25}$$

In deriving eq. (1.25) we used the unitary trace property of the statistical operator, $\int d\mathbf{x}\,\rho_t(\mathbf{x},\mathbf{x}) = 1$.

As we have seen, the corrections of the GRW model to the quantum mechanical predictions are functions of the two parameters λ and r_C: with too small values, the GRW predictions are indistinguishable from the quantum mechanical ones and the model is not capable of localizing macroscopic objects in space, thus loosing its meaning of a collapse model; too large values are excluded by experiments. In their original paper [42], the authors proposed $\lambda = 10^{-16}$ s^{-1} and $r_C = 10^{-7}$ m. With these values, a single particle localizes every 10^8 years, while a macroscopic object made by 10^{23} particles has a much larger localization rate of $\lambda^{\text{CM}} = 10^7$ s^{-1}, as shown in eq. (1.24). The effect of the choice of these parameters to the energy increase of the system, described in eq. (1.25), is that even for a system composed by 10^{23} particles the energy increase is usually very small. For example, for an ideal mono-atomic gas, the increase in temperature is of order of 10^{-15} K per year. In [44], Adler proposed $r_C = 10^{-7}$ m and $\lambda = 10^{-8\pm2}$ s^{-1}, and $r_C = 10^{-6}$ m and $\lambda = 10^{-6\pm2}$ s^{-1} for the GRW parameters, from the analysis of the process of latent image formation in photography.

The GRW model has all the necessary features that a proper dynamical reduction models must have in order to unify unambiguously the microscopic and macroscopic dynamics. However, the model cannot be applied to systems of identical particles, because the collapse dynamics does not preserve the symmetry of the wavefunction. This problem has been solved by CSL model, which is the subject of the next section.

1.4 Continuous Spontaneous Localization (CSL) model

The CSL model [43] has rapidly become the most popular dynamical reduction models, especially among experimentalists. As for the GRW model, the CSL model preserves the quantum mechanical properties of microscopic systems and, at the same time, it localizes in space the wavefunction of macroscopic systems. But it has two main differences with respect to the GRW model, that we list below:

1. It preserves the symmetry of the wavefunctions for identical particles systems. This is done by a direct expression of the collapse in the second quantization formalism.
2. While in the GRW model the localization of the particle occurs instantaneously through the process described in eq. (1.12), in the CSL model it occurs through a continuous spontaneous localization process due to the action of an external noise field. The noise field is described by a Wiener process that modifies the dynamics of the state of the system in a nonlinear and stochastic way.

The resulting dynamics for the state vector $|\psi_t\rangle$ of the system is described by the following stochastic differential equation, written in the Ito formalism [45]:

$$\begin{aligned} d\,|\psi_t\rangle = \Big[-\frac{i}{\hbar}\hat{H}dt + \frac{\sqrt{\gamma}}{m_0}\int d\mathbf{x}\, \left(\hat{M}(\mathbf{x}) - \langle \hat{M}(\mathbf{x})\rangle\right) dW(\mathbf{x},t) \\ - \frac{\gamma}{2m_0^2}\int d\mathbf{x}\, \left(\hat{M}(\mathbf{x}) - \langle \hat{M}(\mathbf{x})\rangle\right)^2 dt \Big]\, |\psi_t\rangle\,, \end{aligned} \tag{1.26}$$

where $dW(\mathbf{x},t)$ is a Wiener process, with

$$\mathbb{E}[dW(\mathbf{x},t)] = 0 \quad \mathbb{E}[dW(\mathbf{x},t)dW(\mathbf{y},s)] = \gamma dt\delta(\mathbf{x}-\mathbf{y})\delta(t-s) \tag{1.27}$$

and where

$$\hat{M}(\mathbf{x}) = \sum_j m_j \frac{1}{\left(\sqrt{2\pi}r_C\right)^3}\int d\mathbf{y}\, e^{-\frac{(\mathbf{x}-\mathbf{y})^2}{2r_C^2}}\, \hat{a}_j^\dagger(\mathbf{y})\hat{a}_j(\mathbf{y}), \tag{1.28}$$

$$\langle \hat{M}(\mathbf{x})\rangle = \langle\psi_t|\, \hat{M}(\mathbf{x})\, |\psi_t\rangle\,. \tag{1.29}$$

In eq. (1.28) j is a type-of-particle label, with mass m_j and with creation and annihilation operator $\hat{a}_j^\dagger(\mathbf{y}), \hat{a}_j(\mathbf{y})$. The parameter γ is related to the usual collapse rate λ and the resolution length r_C by the relation $\gamma = \lambda\left(4\sqrt{\pi}r_C^2\right)^{3/2}$, while m_0 is a reference mass, which is equal to the nucleon mass. The proof that a dynamics given by eq. (1.26) actually localizes in space is given in [17, 43].

By defining the statistical operator as the following stochastic average:

$$\hat{\rho}_t = \mathbb{E}\left[|\psi_t\rangle\,\langle\psi_t|\right], \tag{1.30}$$

the master equation of the CSL model is found by using the Ito rules for stochastic calculus:

$$\frac{d\hat{\rho}_t}{dt} = -\frac{i}{\hbar}\left[\hat{H},\hat{\rho}_t\right] - \frac{\gamma}{2m_0^2}\int d\mathbf{x}\,\left[\hat{M}(\mathbf{x}),\left[\hat{M}(\mathbf{x}),\hat{\rho}_t\right]\right]. \tag{1.31}$$

From eq. (1.31) it is easy to see that the localization dynamics of a single particle's statistical operator has the same expression as that of equation (1.18), while the localization of macroscopic systems occurs through an amplification mechanism which depends on the spatial coherences $\rho(\mathbf{x},\mathbf{y})$ of the system [17,43]: if the spatial coherences are much larger than r_C, $\rho(\mathbf{x},\mathbf{y}) \gg r_C$,then the collapse rate of the center-of-mass of the system scales linearly with the number of particles, *i.e.*, $\lambda^{\text{CM}} = N\lambda$, as for the GRW model. In the opposite limit $\rho(\mathbf{x},\mathbf{y}) \ll r_C$, the scaling of the collapse rate is quadratic with the number of particles, *i.e.*, $\lambda^{\text{CM}} = N^2\lambda$.
In order to preserve the quantum mechanical predictions for the microscopic systems, and at the same time, to localize macroscopic systems in space, in [43] the values $\lambda = 10^{-17}$ s^{-1} and $r_C = 10^{-7}$ m were proposed. With these values, the center-of-mass of a system composed by 10^{23} particles localizes in 10^{-7} s.

1.4.1 CSL model for many atomic systems

In this thesis we are interested to test the CSL model for many body atomic systems. For this reason, we specialize the CSL master equation (1.31) to the case of interest as done in [30]. Precisely, we want to express the master equation (1.31) in terms of atomic operators instead that in terms of electronic and nucleonic operators. Firstly, we note that we can safely neglect the electronic contribution to the collapse dynamics, due to their lighter mass with respect to the nucleons mass. This means that we can rewrite the master equation (1.31) as follows:

$$\begin{aligned}
&\frac{d\hat{\rho}_t}{dt} = -\frac{i}{\hbar}\left[\hat{H},\hat{\rho}_t\right] - \frac{\gamma}{2}\sum_{j,k}\frac{m_j m_k}{m_0^2}\frac{1}{\left(\sqrt{2\pi}r_C\right)^6}\int d\mathbf{x}\int d\mathbf{y}\int d\mathbf{y}'\, e^{-\frac{(\mathbf{x}-\mathbf{y})^2}{2r_C^2}} e^{-\frac{(\mathbf{x}-\mathbf{y}')^2}{2r_C^2}} \times \\
&\left[\hat{a}_j^\dagger(\mathbf{y})\hat{a}_j(\mathbf{y}),\left[\hat{a}_k^\dagger(\mathbf{y}')\hat{a}_k(\mathbf{y}'),\hat{\rho}_t\right]\right] \\
&= -\frac{i}{\hbar}\left[\hat{H},\hat{\rho}_t\right] - \frac{\lambda}{2}\sum_{j,k}\frac{m_j m_k}{m_0^2}\int d\mathbf{y}\int d\mathbf{y}'\, e^{-\frac{(\mathbf{y}-\mathbf{y}')^2}{4r_C^2}}\left[\hat{a}_j^\dagger(\mathbf{y})\hat{a}_j(\mathbf{y}),\left[\hat{a}_k^\dagger(\mathbf{y}')\hat{a}_k(\mathbf{y}'),\hat{\rho}_t\right]\right] \\
&\approx -\frac{i}{\hbar}\left[\hat{H},\hat{\rho}_t\right] - \frac{\lambda}{2}\int d\mathbf{y}\int d\mathbf{y}'\, e^{-\frac{(\mathbf{y}-\mathbf{y}')^2}{4r_C^2}}\left[\hat{a}_n^\dagger(\mathbf{y})\hat{a}_n(\mathbf{y}),\left[\hat{a}_n^\dagger(\mathbf{y}')\hat{a}_n(\mathbf{y}'),\hat{\rho}_t\right]\right]
\end{aligned} \tag{1.32}$$

where, in the last step, we neglected the contribution of the electrons to the master equation, and we introduced the nucleonic operators $\hat{a}_n(\mathbf{y})$ and $\hat{a}_n^\dagger(\mathbf{y})$ in the position basis.

To move from the nucleonic to the atomic operators, we represent the master equation (1.32) in the position basis $|\mathbf{x}\rangle = |\mathbf{x}_A^N\rangle$, for N atoms with A nucleons each:

$$\begin{aligned}\frac{d\langle\mathbf{x}|\hat{\rho}_t|\mathbf{z}\rangle}{dt} = -\frac{i}{\hbar}\langle\mathbf{x}|\left[\hat{H},\hat{\rho}_t\right]|\mathbf{z}\rangle] - \frac{\lambda}{2}\sum_{\alpha,\beta=1}^{N}\sum_{i,j=1}^{A}\Bigg[e^{-\frac{\left(\mathbf{x}_i^\alpha-\mathbf{x}_j^\beta\right)^2}{4r_C^2}} \\ + e^{-\frac{\left(\mathbf{z}_i^\alpha-\mathbf{z}_j^\beta\right)^2}{4r_C^2}} - 2e^{-\frac{\left(\mathbf{x}_i^\alpha-\mathbf{z}_j^\beta\right)^2}{4r_C^2}}\Bigg]\langle\mathbf{x}|\hat{\rho}_t|\mathbf{z}\rangle\,.\end{aligned} \tag{1.33}$$

Let us represent the equation (1.33) in the center-of-mass $\mathbf{X}^\alpha = \sum_{i=1}^{A}\mathbf{x}_i^\alpha/A$ and relative coordinates $\mathbf{s}_i^\alpha = \mathbf{x}_i^\alpha - \mathbf{X}^\alpha$, for $i = i,\ldots,A-1$:

$$\begin{aligned}\frac{d\langle\mathbf{X},\mathbf{s}|\hat{\rho}_t|\mathbf{Z},\mathbf{s}'\rangle}{dt} = -\frac{i}{\hbar}\langle\mathbf{X},\mathbf{s}|\left[\hat{H},\hat{\rho}_t\right]|\mathbf{Z},\mathbf{s}'\rangle - \frac{\lambda}{2}\sum_{\alpha,\beta=1}^{N}\sum_{i,j=1}^{A}\Bigg[e^{-\frac{\left(\mathbf{s}_i^\alpha-\mathbf{s}_j^\beta+\mathbf{X}^\alpha-\mathbf{X}^\beta\right)^2}{4r_C^2}} \\ +e^{-\frac{\left(\mathbf{s}'^\alpha_i-\mathbf{s}'^\beta_j+\mathbf{Z}^\alpha-\mathbf{Z}^\beta\right)^2}{4r_C^2}} - 2e^{-\frac{\left(\mathbf{s}_i^\alpha-\mathbf{s}'^\beta_j+\mathbf{X}^\alpha-\mathbf{Z}^\beta\right)^2}{4r_C^2}}\Bigg]\langle\mathbf{X},\mathbf{s}|\hat{\rho}_t|\mathbf{Z},\mathbf{s}'\rangle \\ \approx -\frac{i}{\hbar}\langle\mathbf{X},\mathbf{s}|\left[\hat{H},\hat{\rho}_t\right]|\mathbf{Z},\mathbf{s}'\rangle] - \frac{\lambda A^2}{2}\sum_{\alpha,\beta=1}^{N}\Bigg[e^{-\frac{\left(\mathbf{x}^\alpha-\mathbf{x}^\beta\right)^2}{4r_C^2}} + e^{-\frac{\left(\mathbf{z}^\alpha-\mathbf{z}^\beta\right)^2}{4r_C^2}} \\ -2e^{-\frac{\left(\mathbf{x}^\alpha-\mathbf{z}^\beta\right)^2}{4r_C^2}}\Bigg]\langle\mathbf{X},\mathbf{s}|\hat{\rho}_t|\mathbf{Z},\mathbf{s}'\rangle\,.\end{aligned} \tag{1.34}$$

In the last step of eq. (1.34) we used the facts that the nucleus dimension is much smaller than the typical size of wave-function considered in atomic systems, and that it is also much smaller than r_C. Moreover, we assume that the Hamiltonian operator depends only on atomic operators, *i.e.*, it only acts on the center-of-mass coordinates $\mathbf{X}^\alpha$ of each atom. By performing a partial trace over the relative coordinates, and going back to the operatorial form, the following CSL master equation for atomic systems is obtained:

$$\frac{d\hat{\rho}_t}{dt} = -\frac{i}{\hbar}\left[\hat{H},\hat{\rho}_t\right] - \frac{\lambda A^2}{2}\int d\mathbf{y}\int d\mathbf{y}'\,e^{-\frac{(\mathbf{y}-\mathbf{y}')^2}{4r_C^2}}\left[\hat{a}^\dagger(\mathbf{y})\hat{a}(\mathbf{y}),\left[\hat{a}^\dagger(\mathbf{y}')\hat{a}(\mathbf{y}'),\hat{\rho}_t\right]\right], \tag{1.35}$$

where $\hat{a}(\mathbf{x}),\hat{a}^\dagger(\mathbf{x})$ are atomic operators in the position basis.
Similarly to the GRW model (1.25), from eq. (1.35) it is possible to see that the

following energy increase occurs for any Hamiltonian $\hat{H} = \hat{\mathbf{p}}^2/(2m) + V(\hat{\mathbf{x}})$ [30]:

$$\frac{d\,Tr\left[\hat{\rho}_t \hat{H}\right]}{dt} = N\lambda A^2 \frac{3\hbar^2}{4mr_C^2}. \tag{1.36}$$

If, *e.g.*, we consider an hydrogen atom, with $\lambda = 10^{-17}$ s^{-1} and $r_C = 10^{-7}$ m, there is a constant temperature increase of $T \equiv 3\hbar^2/\left(4k_B m r_C^2\right) \approx 50$ μK with a rate of $\lambda = 10^{-17}$ s^{-1}. Here, we used k_B for the Boltzmann constant.

1.5 Dissipative and non-white extensions of CSL model

The problem of an energy divergence in the long-time limit has been widely discussed in the literature [46–50]. If dynamical reduction models are seen as effective models [18], where the noise field plays the role of an external non-quantum environment, then an energy divergence would be in contrast with any reasonable physical principle. Moreover, a white noise description of an external environment makes easier the mathematical treatment of the model, but itis not really physical [18,22,34,35]. In fact, a white noise has an homogeneous energy density, without any high-energy cutoff typical of any realistic environment. These considerations lead directly to the necessity to generalize the CSL model with a more realistic description of the noise field: in [33], the energy divergence problem is solved through a proper dissipative extension of the CSL model; while in [22, 34, 35], an extension of the CSL model with general Gaussian noise is discussed. These two extensions of the CSL model are described here below.

1.5.1 Dissipative CSL model (dCSL)

The dissipative extension of the CSL model is obtained by a proper non-hermitian modification of the mass density function defined in eq. (1.28):

$$\begin{aligned}\hat{M}(\mathbf{x}) \to \hat{\mathbb{L}}(\mathbf{x}) = \sum_j \frac{m_j}{\left(1+k_j\right)^3} \frac{1}{\left(\sqrt{2\pi} r_C\right)^3} \int d\mathbf{y}\, e^{-\frac{(\mathbf{x}-\mathbf{y})^2}{2r_C^2}\left(1+k_j\right)^2} \times \\ \hat{a}_j^\dagger(\mathbf{y}) \hat{a}_j \left(\frac{1-k_j}{1+k_j}\mathbf{y} + \frac{2k_j}{1+k_j}\mathbf{x}\right),\end{aligned} \tag{1.37}$$

where

$$k_j \equiv \frac{\hbar^2}{8m_j r_C^2 k_B T_{\text{CSL}}}. \tag{1.38}$$

As seen in eq. (1.38), in order to have dissipation, a new parameter T_{CSL} is introduced, defining the temperature of the noise field. Thus, this new parameter determines the (finite) value of the long-time limit of the energy of the system. By

comparing eq. (1.37) and eq. (1.28), it is possible to note that the CSL limit is recovered in the infinite noise temperature case, $T_{\text{CSL}} \to +\infty$ ($k_j \to 0$). This is also clear by comparing the CSL stochastic differential equation (1.26) with the modified dynamics for the state vector in the dCSL model:

$$d|\psi_t\rangle = \left[-\frac{i}{\hbar}\hat{H}dt + \frac{\sqrt{\gamma}}{m_0}\int d\mathbf{x}\left(\hat{\mathbb{L}}(\mathbf{x}) - \left\langle\frac{\hat{\mathbb{L}}(\mathbf{x})+\hat{\mathbb{L}}^\dagger(\mathbf{x})}{2}\right\rangle\right)dW(\mathbf{x},t) - \frac{\gamma}{2m_0^2}\times \right.$$
$$\left.\int d\mathbf{x}\left(\hat{\mathbb{L}}^\dagger(\mathbf{x})\hat{\mathbb{L}}(\mathbf{x}) + \left\langle\frac{\hat{\mathbb{L}}(\mathbf{x})+\hat{\mathbb{L}}^\dagger(\mathbf{x})}{2}\right\rangle^2 - 2\left\langle\frac{\hat{\mathbb{L}}(\mathbf{x})+\hat{\mathbb{L}}^\dagger(\mathbf{x})}{2}\right\rangle\hat{\mathbb{L}}(\mathbf{x})\right)dt\right]|\psi_t\rangle\,, \tag{1.39}$$

where $\langle\cdot\rangle = \langle\psi_t|\cdot|\psi_t\rangle$, and where $dW(\mathbf{x},t)$ is the usual Wiener process.

The master equation for the statistical operator is found by using Ito calculus:

$$\frac{d\hat{\rho}_t}{dt} = -\frac{i}{\hbar}\left[\hat{H},\hat{\rho}_t\right] + \frac{\gamma}{m_0^2}\int d\mathbf{x}\left[\hat{\mathbb{L}}(\mathbf{x})\hat{\rho}_t\hat{\mathbb{L}}^\dagger(\mathbf{x}) - \frac{1}{2}\left\{\hat{\mathbb{L}}^\dagger(\mathbf{x})\hat{\mathbb{L}}(\mathbf{x}),\hat{\rho}_t\right\}\right]. \tag{1.40}$$

Eq. (1.40) is a Lindblad master equation [51,52], proving that the dCSL dynamics is Markovian.

In [33], the authors prove that the dCSL model has all the necessary features to be a good dynamical reduction model. In fact, it preserves quantum mechanical properties for microscopic systems, while macroscopic systems are localized in space through a proper amplification mechanism.
Of particular interests for this thesis is the master equation for the single particle reduced density matrix [33]:

$$\frac{d\hat{\rho}_t^{(1)}}{dt} = -\frac{i}{\hbar}\left[\hat{H},\hat{\rho}_t^{(1)}\right] + \frac{\gamma m^2}{(2\pi\hbar)^3 m_0^2}\int d\mathbf{Q}\left[e^{\frac{i}{\hbar}\mathbf{Q}\cdot\hat{\mathbf{x}}}L(\mathbf{Q},\hat{\mathbf{P}})\hat{\rho}_t^{(1)}L(\mathbf{Q},\hat{\mathbf{P}})e^{-\frac{i}{\hbar}\mathbf{Q}\cdot\hat{\mathbf{x}}}\right.$$
$$\left.-\frac{1}{2}\left\{L^2(\mathbf{Q},\hat{\mathbf{P}}),\hat{\rho}_t^{(1)}\right\}\right], \tag{1.41}$$

where

$$L(\mathbf{Q},\hat{\mathbf{P}}) = e^{-\frac{r_C^2}{2\hbar^2}\left|(1+k)\mathbf{Q}+2k\hat{\mathbf{P}}\right|^2}. \tag{1.42}$$

Using eqs. (1.41) and (1.42), in [33] is proved that, for the free-particle case,

$$Tr\left[\hat{\rho}_t^{(1)}\hat{H}\right] \equiv H_t = e^{-\chi t}\left(H_0 - H_{\text{as}}\right) + H_{\text{as}}, \tag{1.43}$$

where the relaxation rate is

$$\chi = \frac{4k\lambda m^2}{(1+k)^5 m_0^2} \tag{1.44}$$

and the asymptotic energy is given by

$$H_{\text{as}} = \frac{3\hbar^2}{16kmr_C^2}. \tag{1.45}$$

1.5.2 Non-white CSL model (cCSL)

The CSL model modifies the usual Schrödinger equation by adding a non-linear and stochastic term, described in terms of a Wiener process. A more realistic extension of CSL model with a general Gaussian noise has been considered in literature [34, 35].
In this case, the second moment of the noise $w(\mathbf{x}, t)$ is

$$\mathbb{E}\left[w(\mathbf{x}, t)w(\mathbf{y}, s)\right] = \gamma\delta\left(\mathbf{x} - \mathbf{y}\right) D(t - s), \tag{1.46}$$

while its average is always zero.
The generalization to a non-white noise implies two main differences on the time evolution of the state vector and on the master equation for the statistical operator [17]:

- The dynamics is no longer described by a Markovian evolution, except in the trivial case where the function $D(t - s) = \delta(t - s)$, *i.e.*, in the white noise case. As a consequence, the time evolution for the statistical operator is no longer described by a master equation of the Lindblad type.
- In general, it is not possible to find an useful form for the time evolution of the state vector $|\psi_t\rangle$, and approximations are necessary. This also means that it is not possible to find an exact closed form for the master equation of the statistical operator.

Since the noise dynamics gives, at least for small times t, a small perturbation to the Hamiltonian dynamics, a perturbative approximation can be used to find a master equation for the statistical operator. Indeed, at the first order in γ, the following master equation can be derived [34, 35]:

$$\frac{d\hat{\rho}_t}{dt} = -\frac{i}{\hbar}\left[\hat{H}, \hat{\rho}_t\right] - \frac{\gamma}{2m_0^2}\int d\mathbf{x}\int_0^t ds\, D(t - s)\left[\hat{M}(\mathbf{x}), \left[\hat{M}(\mathbf{x}, s - t), \hat{\rho}_t\right]\right], \tag{1.47}$$

where

$$\hat{M}(\mathbf{z}, r) = e^{\frac{i}{\hbar}\hat{H}r}\hat{M}(\mathbf{z})e^{-\frac{i}{\hbar}\hat{H}r}. \tag{1.48}$$

Of particular interest for this thesis is the master equation for the single particle reduced density matrix:

$$\frac{d\hat{\rho}_t^{(1)}}{dt} = -\frac{i}{\hbar}\left[\hat{H}, \hat{\rho}_t^{(1)}\right] - \frac{\gamma m^2}{2m_0^2}\int d\mathbf{y}\int_0^t ds\, D(t - s)\left[g(\mathbf{y} - \hat{\mathbf{x}}), \left[g(\mathbf{y} - \hat{\mathbf{x}}(s - t)), \hat{\rho}_t^{(1)}\right]\right], \tag{1.49}$$

where

$$g(\hat{\mathbf{z}}) = \frac{1}{\left(\sqrt{2\pi}r_C\right)^3}e^{-\frac{(\hat{\mathbf{z}})^2}{2r_C^2}}. \tag{1.50}$$

In particular, we will investigate the dynamics described by eq. (1.49) for the following typical noise correlation function:

$$D(r) = \frac{1}{2\tau} e^{-\frac{|r|}{\tau}}, \tag{1.51}$$

where τ defines the characteristic time correlation of the noise. As we can see, in the limit of $\tau \to 0$ the usual CSL model is recovered.

Chapter 2

Cold Bose Gases

Dynamical reduction models solve the measurement problem by localizing in position macroscopic systems, while preserving the quantum mechanical predictions for microscopic systems. Two of the main consequences of the localization process on the state of the systems are: the loss of the spatial coherences, with a rate that increases with the number of particles of the system (amplification mechanism); an energy increase of the system, which, in the long-time limit, can be either divergent (CSL and cCSL models) or convergent to a specific value (dCSL). A promising class of systems to experimentally test dynamical reduction models is represented by cold atomic systems [25, 26, 53–55]. In fact, beside their very low temperature ($T = 10^{-11} - 10^{-7}$ K), cold Bose gases manifest quantum properties (like, *e.g.*, Bose-Einstein condensation and interference properties) involving a large number of particles ($N = 10^3 - 10^{11}$). These are all promising ingredients in order to perform meaningful tests to these models.

In this chapter, we briefly review the main properties of a cold Bose gas. In particular:

1. We describe the phenomenon of Bose-Einstein condensation for an ideal and for a weekly interacting gas;

2. We review the dynamics of a Bose-Einstein condensate (BEC) in a double-well potential. In particular, we focus on its interference properties, and on the possibility to use BECs in a double-well potential to create Schrödinger cat states;

3. We briefly describe the BECs in an optical lattice.

2.1 Bose-Einstein condensation

2.1.1 Ideal gas

The first experimental observation of a BEC [28] was obtained in 1995 by cooling a gas of ^{87}Rb atoms down to ≈ 170 nK. Later experiments achieved Bose-Einstein condensation with gases of ^{1}H, ^{23}Na, ^{174}Yb and many other atomic gases.

The theoretical prediction of BEC dates back to 1925 [23], when Einstein extended an analysis on photon statistics made by Bose [56] to massive particles. Working on an ideal gas, Einstein realized that, below a critical temperature, the atoms occupy the (single particle) ground energy state: this is the so-called Bose-Einstein condensation. Following the line of typical textbooks on this subject [25, 26, 57, 58], in this section we give a brief description of the condensation in an ideal gas, leaving the interacting case to the next section.

Let us consider a gas composed by N non interacting particles in a box of volume V. The Hamiltonian of the system is

$$\hat{H} = \sum_{k=1}^{N} \hat{h}_k = \sum_{k=1}^{N} \frac{\hat{\mathbf{p}}_k^2}{2m}. \tag{2.1}$$

Constraining the gas to stay in a cubic box of side length L, and imposing periodic boundary conditions, it is easy to find the eigenvalues $\epsilon_{\mathbf{n}}$ of the single particle Hamiltonian operator $\hat{h}$:

$$\epsilon_{\mathbf{n}} = \frac{(2\pi\hbar)^2}{2mL^2}\mathbf{n}, \quad \mathbf{n} \in \mathbb{N}^3. \tag{2.2}$$

We are interested in studying the properties of the gas at the thermodynamical limit, *i.e.*,

$$N, V \to +\infty, \quad \frac{N}{V} = \rho \,\text{fixed}\,, \tag{2.3}$$

Even if the physical system we consider is composed by a fixed number N of atoms, we can work in the grand-canonical ensemble -where the system exchanges energy and atoms with an external environment at thermal equilibrium with temperature T, and with μ as chemical potential- since, in the thermodynamical limit, grand-canonical and canonical ensembles are equivalent [59].
The average number of particles in the grand-canonical ensemble is

$$\overline{N} = \sum_{\mathbf{n}} \frac{1}{e^{\beta(\epsilon_{\mathbf{n}}-\mu)} - 1} \equiv N_0 + N_{\text{therm}}\,, \tag{2.4}$$

where N_0 is the occupation number of the ground state ($\mathbf{n} = \mathbf{0}$),

$$\frac{N_0}{V} \equiv \rho_0 = \frac{1}{V}\frac{1}{e^{-\beta\mu} - 1} = \frac{1}{V}\frac{z}{1-z}\,, \tag{2.5}$$

and where $z = \exp[\beta\mu]$ is the so-called fugacity of the gas. N_{therm} is the occupation number of the *thermal* part of the gas, *i.e.*, the occupation number of all the excited states. $\beta = 1/(k_B T)$ is the inverse temperature, and k_B is the Boltzmann constant. Since we have a fixed number N of atoms, $\overline{N} = N$, which means that

$$\frac{N}{V} \equiv \rho = \rho_0 + \rho_{\text{therm}} \tag{2.6}$$

is a fixed quantity. For an ideal Bose gas, the chemical potential is a decreasing monotone function of the temperature, $\mu = \mu(T)$, such that [57,58]

$$-\infty < \beta\mu < 0\,. \tag{2.7}$$

In eq. (2.6) we introduced the thermal density $\rho_{\text{therm}} = N_{\text{therm}}/V$ which, in the thermodynamical limit, can be written as

$$\rho_{\text{therm}} = \left(\frac{2\pi}{\hbar}\right)^3 \int_{\mathbb{R}^3} d\mathbf{p}\, \frac{1}{e^{\beta\left(\frac{\mathbf{p}^2}{2m} - \mu\right)}}\,; \tag{2.8}$$

The thermal density defined in eq. (2.8) is monotonously increasing with μ, and bounded by a critical density defined as follows

$$\rho_{\text{therm}} \leq \rho_{\text{crit}} = g_{3/2}(1) \left(\frac{k_B T m}{2\pi\hbar^2}\right)^{\frac{3}{2}}\,, \tag{2.9}$$

where we introduced the following quantity [26]:

$$g_{3/2}(z) = \sum_{l=1}^{+\infty} \frac{z^l}{l^{3/2}}\,, \tag{2.10}$$

and $g_{3/2}(1) \approx 2.612$.
Having fixed the gas density ρ, at temperature high enough the following inequality holds

$$\rho \leq \rho_{\text{crit}}\,, \tag{2.11}$$

and the fugacity $z = \exp[\beta\mu] \approx 0$. From eq. (2.5), it is clear that the occupation of the ground state is negligible, and all the atoms are in the thermal part. If we decrease the temperature of the gas, preserving the density ρ, the critical density defined in (2.9) decreases, until there is the equality $\rho = \rho_{\text{crit}}$. This identity occurs at the critical temperature

$$T_c = \frac{2\pi\hbar^2}{m k_B} \left(\frac{\rho}{g_{3/2}(1)}\right)^{2/3}\,. \tag{2.12}$$

Below this temperature, the ineq. (2.11) fails, and, from eq. (2.6), a macroscopic occupation of the ground energy state occurs. This phase transition is the Bose-Einstein condensation. From eq. (2.12) it is possible to see the temperature dependence of the condensate fraction in the gas:

$$\frac{N_0}{\overline{N}} = 1 - \left(\frac{T}{T_c}\right)^{3/2} \qquad T \leq T_c\,. \tag{2.13}$$

2.1.2 Weekly interacting gas

The Bose-Einstein condensation theory seen so far holds only for an ideal gas. A first microscopic description of an interacting Bose gas has been achieved in 1947 by Bogolubov [24], where the case of a dilute weekly interacting gas in a box has been considered. Its extension to the nonuniform case has been done in 1961, independently, by Gross [60] and Pitaevskii [61]. Bogolubov's theory provides a successful description of the phenomenology of condensation for an interacting gas, and now we give a brief review of its main steps and results.
Let us start by introducing the Hamiltonian operator for a gas of interacting identical particles in a box:

$$\hat{H} = \sum_{k=1}^{N} \frac{\hat{\mathbf{p}}_k^2}{2m} + \sum_{j<k=1}^{N} V\left(\hat{\mathbf{r}}_j - \hat{\mathbf{r}}_k\right). \tag{2.14}$$

Generally, the gases are dilute enough such that the interacting potential $V\left(\hat{\mathbf{r}}_j - \hat{\mathbf{r}}_k\right)$ can be treated at the mean field level. So, the potential $V\left(\hat{\mathbf{r}}_j - \hat{\mathbf{r}}_k\right)$ can be effectively described by the hard-core potential [62, 63]

$$g \sum_{j<k=1}^{N} \delta\left(\hat{\mathbf{r}}_j - \hat{\mathbf{r}}_k\right), \tag{2.15}$$

where g is the effective coupling constant of the hard-core potential. Imposing the diluted gas condition, the effective interacting range is determined by a unique parameter, *i.e.* the scattering length a_S, which also fixes the strength of the potential:

$$g = \frac{4\pi\hbar^2 a_S}{m}. \tag{2.16}$$

The diluted gas condition can be easily expressed in terms of the scattering length and of the density ρ of the gas [25, 26]:

$$\rho a_S^3 \ll 1. \tag{2.17}$$

If the diluted gas condition (2.17) holds, at zero temperature the Bose Einstein condensation shows itself by the factorization of the many-body state in single particle wave functions,

$$\psi\left(\mathbf{r}_1, \ldots, \mathbf{r}_N\right) = \prod_{i=1}^{N} \phi\left(\mathbf{r}_i\right), \tag{2.18}$$

where $\phi\left(\mathbf{r}\right)$ is the solution of the Gross-Pitaevskii equation, achieved by Gross [60] and Pitaevskii [61] for the general nonuniform case:

$$-\frac{\hbar^2\nabla^2}{2m}\phi\left(\mathbf{r}\right) + U\left(\mathbf{r}\right)\phi\left(\mathbf{r}\right) + g\left|\phi\left(\mathbf{r}\right)\right|^2\phi\left(\mathbf{r}\right) = \mu\phi\left(\mathbf{r}\right), \tag{2.19}$$

where $U(\mathbf{r})$ is the external trapping potential, μ is the chemical potential of the gas, defined as

$$\mu = \frac{\partial E}{\partial N}, \tag{2.20}$$

with E average energy of the gas. For example, in the particular case of an uniform gas, eq. (2.20) takes the simple expression [25,26]

$$\mu = \rho g. \tag{2.21}$$

Rigorous results on the validity of the Gross-Pitaevskii equation (2.19) have been given in recent years [64, 65]. It is also been proved that the condensation of an interacting gas is dynamically preserved in case of a small perturbation of the trapping potential. In this case, the dynamics of the single particle state $\phi(\mathbf{r}, t)$ is given by a time-dependent Gross-Pitaevskii equation [25,26,66]. Extensions of the Gross-Pitaevskii equation have also been made in order to take into account the effects of small thermal clouds interacting with the condensate [67].

2.2 Condensate in a double well potential

One of the most interesting cold-atomic system that can be theoretically studied, and that can actually be implemented in an experimental setup is a BEC in a double well potential [25,26], named also as Bose Josephson junction. In a Bose Josephson junction, when the barrier is high enough (much larger than the chemical potential), the atoms can be only in two states. Each wave function is spatially localized in one of the two wells: the higher the barrier separating the two wells, the lower the overlap between the two wave functions. Experimental quantities such as the height of the barrier and the geometry of each well [26,68], can be tuned with a high degree of control. A Bose Josephson junction can be experimentally implemented *e.g.* by superimposing an optical lattice to a parabolic potential [69,70] or by the use of a laser beam to create the barrier [71].

A phase difference between the two wells emerges as a consequence of the weak link also for a small number of atoms [72] and it can be fixed (giving rise to the so-called phase state). This possibility for example leads to use Bose Josephson junctions as an atom interferometer [73–75]. The quantum mechanical evolution of the phase state is characterized by the typical collapse and revival of the interference fringes, while the CSL dynamics decreases the interference until the fringes disappear and each atom is localized in one of the two wells.

Besides the phase states, Bose Josephson junctions provide as well a promising possibility for creating macroscopic entangled states, including Schrödinger's cat states [76, 77]. The use of squeezed states in atomic interferometers and clocks leading to sub-shot-noise performance has been exploited in experiments [78–81], while the detection of Bell correlations between the spins of ~ 500 atoms in a Bose-Einstein condensate was recently reported in [82].

In this thesis, we focus on two particular types of macroscopic entangled states: the superposition of two phase states, and the NOON state. Even if a Schrödinger's cat state has not been experimentally detected yet, for these two macroscopic entangled states solid theoretical preparation techniques have been studied [83–88]. In the next subsection we briefly describe the theoretical framework usually used to work with BECs in a double well potential, which is within the so-called *two mode approximation* [89]. Then, we use the two mode approximation to describe the physical states and the quantum mechanical dynamics of a BEC in a double well potential.

2.2.1 Two mode approximation

Within the usual two mode approximation [89], valid for large energy barriers between the two wells (and much larger than the chemical potential), one assumes that the atoms can be either in the state $|\psi\rangle_L$ of the left well, or in the state $|\psi\rangle_R$ of the right well. The left and the right states are taken orthogonal $\langle\psi_R|\psi_L\rangle = 0$ (see [89]). Let us firstly rewrite the Hamiltonian (2.14) of a weekly interacting Bose gas in the usual second quantization formalism:

$$\begin{aligned}\hat{H} = \int d\mathbf{x}\, \hat{a}^\dagger(\mathbf{x}) \left(-\frac{\hbar^2\nabla^2}{2m} + V_{\text{ext}}(\mathbf{x}) \right) \hat{a}(\mathbf{x}) + \\ \frac{g}{2} \int d\mathbf{x}\, \hat{a}^\dagger(\mathbf{x})\hat{a}^\dagger(\mathbf{x})\hat{a}(\mathbf{x})\hat{a}(\mathbf{x}),\end{aligned} \tag{2.22}$$

where $V_{\text{ext}}(\mathbf{x})$ is the external trapping potential, that in our case is a double well potential as in fig. 2.1.
To properly describe how the two mode approximation works, let us start by considering the easier case of a noninteracting gas (*i.e.*, $g = 0$), with a separable double well potential:

$$\begin{aligned}V_{\text{ext}}(\mathbf{x}) &= \frac{m\omega^2}{8a^2}(x^2 - a^2)^2 + \frac{1}{2}m\omega^2(y^2 + z^2) \\ &= V_x(x) + V_r(y, z).\end{aligned} \tag{2.23}$$

The two minima of the potential $V_x(x)$ are for $x = \pm a$, and the barrier peak is $V_x(0) = m\omega^2 a^2/8$. Under the hypothesis that $V_x(0) \gg \hbar\omega$, through a WKB approximation [90, 91], it is possible to prove that the double well potential $V_x(x)$ can be effectively described as two distinct harmonic traps, each of them around one minimum $V_x(x = \pm a)$, *i.e.*,

$$V_x(x) = \begin{cases} \frac{1}{2}m\omega^2(x + a)^2, & \text{if } x < 0, \\ \frac{1}{2}m\omega^2(x - a)^2, & \text{if } x > 0, \end{cases} \tag{2.24}$$

The two harmonic wells introduced in (2.24) are weekly connected, with a small

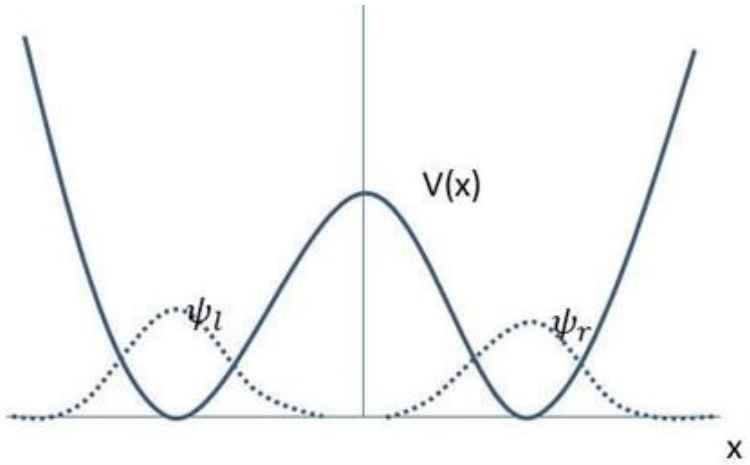

Figure 2.1: Plot of the x-component of the double-well potential represented in eq. (2.23), with the relatives localized wave-functions ψ_l and ψ_r.

tunneling probability. The energy levels of the potential (2.24) are very close to the well known harmonic oscillator energy levels:

$$E_n^{\pm} = \left(n + \frac{1}{2}\right)\hbar\omega \mp \frac{\hbar\omega}{2\pi} e^{-\frac{m\omega a^2}{\hbar}}. \tag{2.25}$$

Under the hypothesis that the system is in a condensate phase, we can safely say that only the low energy states are occupied by the atoms. This means that the atoms are in the ground state for the harmonic potential $V_r(y,z)$, while they occupy only the two low-energy states for the potential $V_x(x)$. Precisely, the only two states that can be occupied by each atom are:

$$\psi^{\pm}(\mathbf{x}) = \psi_0^{\pm}(x)\psi_0(y)\psi_0(z), \tag{2.26}$$

where $\psi_0(s)$ is the ground state of the one dimensional harmonic oscillator, while $\psi_0^{\pm}(x)$ are the eigenstates of the low energy (i.e., $n = 0$) eigenvalues (2.25). Generally, it is possible to write $\psi_0^{\pm}(x)$ as linear combination of the ground state of the harmonic oscillator defined in eq. (2.24):

$$\begin{aligned} \psi_0^{\pm}(x) &= \frac{1}{\sqrt{2}}\left(\psi_0(x-a) \pm \psi_0(x+a)\right) \\ &= \frac{1}{\sqrt{2}}\left(\psi_L(x) \pm \psi_R(x)\right). \end{aligned} \tag{2.27}$$

From eqs. (2.26) and (2.27) we thus define the left and right states characterizing the system:

$$\psi_i(\mathbf{x}) = \psi_i(x)\psi_0(y)\psi_0(z), \quad i = \text{L,R}. \tag{2.28}$$

It is important to note that the hypothesis $V_x(0) \gg \hbar\omega$ is equivalent to saying that the left and right states (2.28) are almost orthogonal:

$$\begin{gathered}\int d\mathbf{x}\, \psi_j^*(\mathbf{x})\psi_k(\mathbf{x}) = \delta_{j,k} + \eta(1-\delta_{j,k}), \\ \text{where } |\eta| = e^{-\frac{a^2 m\omega}{4\hbar}} \ll 1,\ j,k = \text{L,R}.\end{gathered} \tag{2.29}$$

Thus, we can say that, if $V_x(0) \gg \hbar\omega$, each boson of the gas can effectively be described in terms of the left and right states defined in eq. (2.28).

The low-temperature condition we required at the beginning of the section can be now written in a more quantitative way. Precisely, if $k_B T \ll \hbar\omega$, then thermal fluctuation are negligible and the two-mode approximation is preserved.

In general, also the particle-particle interaction introduced in eq. (2.22) must be controlled, in order to preserve the two-mode approximation of the system. A sufficient condition [90] is that the interaction must not modifies the many body ground state of the system. As a consequence, the number of atom in the system is limited:

$$N \ll \frac{l_\omega}{a_S}, \tag{2.30}$$

where $l_\omega = \sqrt{\hbar/(m\omega)}$ is the characteristic length of the harmonic ground energy state, and a_S is the scattering length. If we consider ^{87}Rb atoms, usually used in ultra-cold many-bosons systems, with scattering length $a_S \approx 100 a_0$ [92], where a_0 is the Bohr radius, and frequency trap of $\omega = 10$ Hz, then from eq. (2.30) we have that the number of atoms cannot exceed the limit of $N \approx 10^2$ atoms. However, we must also take into account that the atom-atom interaction can be significantly reduced in the experiment by using the Feshbach resonances [29], increasing the validity of the two mode approximation to larger atomic systems.

In a more general case, the wave functions $\psi_L(\mathbf{x})$, $\psi_R(\mathbf{x})$ are well approximated from the solutions of the time-independent Gross-Pitaevskii equation:

$$-\frac{\hbar^2\nabla^2}{2m}\psi(\mathbf{r}) + V_{\text{ext}}(\mathbf{r})\,\psi(\mathbf{r}) + g\,|\psi(\mathbf{r})|^2\,\psi(\mathbf{r}) = \mu\psi(\mathbf{r}). \tag{2.31}$$

Denoting by ψ_{G} and ψ_{E} the ground and the first-excited states of (2.31), then one has $\psi_L(\mathbf{x}) = (\psi_{\text{G}}(\mathbf{x}) + \psi_{\text{E}}(\mathbf{x}))/\sqrt{2}$ and $\psi_R(\mathbf{x}) = (\psi_{\text{G}}(\mathbf{x}) - \psi_{\text{E}}(\mathbf{x}))/\sqrt{2}$. This way of constructing the wave functions $\psi_L(\mathbf{x})$, $\psi_R(\mathbf{x})$ is typically good if the number of particles per well is not too large and they do not depend on the interactions via the atom numbers N_L and N_R (in that case one has to resort to a nonlinear tight-binding ansatz [93,94]).

The chemical potential in eq. (2.32) is defined in eq. (2.20). In the Thomas-Fermi limit, *i.e.* if the kinetic part in the Gross Pitaevskii equation (2.32) is negligible, the chemical potential has the following expression [26]:

$$\mu = \frac{\hbar\omega}{2}\left(\frac{15 N a_S}{l_\omega}\right)^{2/5}. \tag{2.32}$$

The next step is to rewrite the Hamiltonian (2.22) in terms of the left and right states defined from eq. (2.32). Let us firstly define as $\hat{a}_L^\dagger$ ($\hat{a}_L$) and $\hat{a}_R^\dagger$ ($\hat{a}_R$) the creation (annihilation) operators for, respectively, the left and right states. Condition (2.29) is equivalent to $\left[\hat{a}_i, \hat{a}_j^\dagger\right] = \delta_{i,j}$, where $i, j =$ L,R.
Rewriting the annihilation operators $\hat{a}(\mathbf{x})$ in terms of $\hat{a}_L$ and $\hat{a}_R$ as follows

$$\hat{a}(\mathbf{x}) = \psi_L(\mathbf{x})\hat{a}_L + \psi_R(\mathbf{x})\hat{a}_R, \tag{2.33}$$

(and analogously for its hermitian conjugate), using eq. (2.33) in eq. (2.22) we have that [89, 95]

$$\hat{H} = -J\left(\hat{a}_L^\dagger\hat{a}_R + \hat{a}_R^\dagger\hat{a}_L\right) - U\hat{a}_L^\dagger\hat{a}_L\hat{a}_R^\dagger\hat{a}_R, \tag{2.34}$$

where

$$J = \int d\mathbf{x}\, \psi_L^*(\mathbf{x}) \left(-\frac{\hbar^2\nabla^2}{2m} + V_{\text{ext}}(\mathbf{x})\right) \psi_R(\mathbf{x}) \tag{2.35}$$

$$U = 2g \int d\mathbf{x}\, |\psi_L(\mathbf{x})|^4 . \tag{2.36}$$

For the symmetry of the system, the definition of J and U do not change under the replacement $\psi_L(\mathbf{x}) \leftrightarrow \psi_R(\mathbf{x})$. We fixed the number of atoms in the gas, and we also neglected irrelevant constant terms in eq. (2.34).

We finally observe that in presence of a negative scattering length, the coefficient U can be negative (and yet the two-mode model be valid): a quantum phase transition occurs at a finite value of $|U|$ for which a population imbalance between the two wells has been recently observed [96].

2.2.2 Coherent and entangled states

The preparation of atomic coherent states using Bose Einstein condensates is one of the most important results in many body physics [74, 97–99]. Considering a BEC in a double well potential, the atomic coherent state, or phase state, takes the following expression [26]:

$$|\phi\rangle = \frac{1}{\sqrt{N!2^N}} \left(\hat{a}_L^\dagger + e^{i\phi}\hat{a}_R^\dagger\right)^N |0\rangle \ . \tag{2.37}$$

The phase coherence properties of the state in eq. (2.37) is expressed by the off-diagonal elements of the single particle density matrix defined as follows

$$\rho^{(1)} = \frac{1}{N} \begin{pmatrix} \langle \hat{a}_L^\dagger \hat{a}_L \rangle & \langle \hat{a}_L^\dagger \hat{a}_R \rangle \\ \langle \hat{a}_R^\dagger \hat{a}_L \rangle & \langle \hat{a}_R^\dagger \hat{a}_R \rangle \end{pmatrix}, \tag{2.38}$$

where $\langle\cdot\rangle = \langle\phi|\cdot|\phi\rangle$. Precisely, using eq. (2.37) we have that

$$\langle \hat{a}_L^\dagger \hat{a}_R \rangle = N\frac{e^{i\phi}}{2}. \tag{2.39}$$

Coherence properties of the state (2.37) are detected through the presence of interference fringes in the momentum density of the gas. Indeed, from eq. (2.33) it is easy to see that

$$\hat{a}(\mathbf{p}) = \psi_L(\mathbf{p})\hat{a}_L + \psi_R(\mathbf{p})\hat{a}_R. \tag{2.40}$$

For parity symmetry of the double well potential, we can relate the left and right states as follows:

$$\psi_R(\mathbf{p}) = e^{-i\frac{2ap_x}{\hbar}}\psi_L(\mathbf{p}), \tag{2.41}$$

where we imposed that the right well is displaced $2a$ from the left well along the x-direction.
Using eqs. (2.40) and (2.41), the momentum density operator, averaged on a generic state, becomes:

$$\begin{aligned}\langle \hat{a}^\dagger(\mathbf{p})\hat{a}(\mathbf{p})\rangle &= |\psi_L(\mathbf{p})|^2 \langle \hat{a}_L^\dagger \hat{a}_L\rangle + |\psi_R(\mathbf{p})|^2 \langle \hat{a}_R^\dagger \hat{a}_R\rangle + 2\mathbb{R}\mathrm{e}\left(\psi_L^*(\mathbf{p})\psi_R(\mathbf{p})\langle \hat{a}_L^\dagger \hat{a}_R\rangle\right) \\ &= N|\psi_L(\mathbf{p})|^2\left\{1 + \frac{2}{N}\mathbb{R}\mathrm{e}\left(e^{-i\frac{2ap_x}{\hbar}}\langle \hat{a}_L^\dagger \hat{a}_R\rangle\right)\right\},\end{aligned} \tag{2.42}$$

where we also imposed a fixed number N of atoms. Using eq. (2.39) for the phase state (2.37) in the expression (2.42), we obtain

$$\langle \hat{a}^\dagger(\mathbf{p})\hat{a}(\mathbf{p})\rangle = N|\psi_L(\mathbf{p})|^2\left\{1 + \cos\left(\phi - \frac{2ap_x}{\hbar}\right)\right\}. \tag{2.43}$$

We must also take into account that the phase coherence (2.39) is not, generally, a constant of motion of the Hamiltonian (2.34), due to the presence of the interaction term. In fact, in the case of negligible tunneling, *i.e.* with $J = 0$, the time evolution of the phase coherence (2.39) is (see the appendix A)

$$\langle \hat{a}_L^\dagger \hat{a}_R\rangle_t = \langle \phi| e^{\frac{i}{\hbar}\hat{H}t}\hat{a}_L^\dagger \hat{a}_R e^{-\frac{i}{\hbar}\hat{H}t}|\phi\rangle = N\frac{e^{i\phi}}{2}\left[\cos\left(\frac{tU}{\hbar}\right)\right]^{N-1}. \tag{2.44}$$

For small time $t \ll \hbar/U$, and large number of atoms $N \gg 1$ we have the collapse of the phase coherence (phase diffusion [100, 101]):

$$\langle \hat{a}_L^\dagger \hat{a}_R\rangle_t \approx N\frac{e^{i\phi}}{2}\left[1 - \left(\frac{tU}{\hbar}\right)^2\right]^N \approx N\frac{e^{i\phi}}{2}e^{-N\left(\frac{tU}{\hbar}\right)^2}, \tag{2.45}$$

As can be noted, the phase coherence is periodically reestablished [98, 102], with a revival time T_r given by [103, 104]:

$$T_r = \frac{q\hbar\pi}{U}, \quad q \in \mathbb{Z}. \tag{2.46}$$

Precisely, the interference fringes of an initial phase state, with phase ϕ_0 at time $t = 0$, after a time T_r will be reconstructed around the new phase ϕ_r given by the

following expression [104]:

$$\phi_r = \begin{cases} \phi_0 + \frac{q\pi}{2}, & \text{if } N \text{ is even;} \\ \phi_0, & \text{if } N \text{ is odd;} \end{cases} \tag{2.47}$$

BECs in a double well potential are also one of the most promising systems to create macroscopically entangled states. In this thesis, we mainly focus on two of them: the superposition of phase states and the NOON state.

The superposition of phase states as (2.37) can be dynamically created from a single phase state, with dynamics given by the Hamiltonian (2.34) with $J = 0$ [88]. In particular, after a time $t_2 = \hbar\pi/(2U)$, the initial phase state (2.37) is evolved into

$$|\phi_{t_2}\rangle = \frac{1}{\sqrt{2}}\left(|\phi\rangle + e^{i\beta}\,|\phi+\pi\rangle\right), \tag{2.48}$$

where β is a fixed phase difference between the two phase states. The state (2.48) does not show any single-particle coherence properties as in eq. (2.39), but it shows N-particles coherence. Precisely, it can be proved that (see appendix A)

$$\langle\phi|\,\hat{a}_L^{\dagger k}\hat{a}_R^k\,|\phi+\pi\rangle = \begin{cases} 0, & \text{if } k < N; \\ \frac{N!e^{iN\phi}}{2^N}, & \text{if } k = N. \end{cases} \tag{2.49}$$

Eq. (2.49) means that the only way to distinguish the state (2.48) from the statistical mixture $\hat{\rho} = \left(|\phi\rangle\langle\phi| + |\phi+\pi\rangle\langle\phi+\pi|\right)/2$ is through a measure of N-particles observables, *i.e.*, the reduced density matrix at k-particles does not show any coherences, except if $k = N$.

The second macroscopically entangled state considered here is the so-called NOON state, defined as

$$|\text{NOON}\rangle = \frac{1}{\sqrt{2N!}}\left(\hat{a}_L^{\dagger N} + \hat{a}_R^{\dagger N}\right)|0\rangle\,. \tag{2.50}$$

The NOON state (2.50) is the ground state of the Hamiltonian (2.34) with $J = 0$ and with $U < 0$ [83–88].Even though several proposals have been formulated to create a NOON state in a double well (see e.g. [83–87, 105]), its very short life-time with respect to decoherence makes its experimental realization an open problem. A first step in this direction has been done recently [96], where the experimental realization of double well bosonic systems with negative and controllable scattering length was achieved.

A similar relation to eq. (2.49) is found (see the appendix A)

$$\langle\text{NOON}|\,\hat{a}_L^{\dagger k}\hat{a}_R^k\,|\text{NOON}\rangle = \begin{cases} 0, & \text{if } k < N; \\ \frac{(N!)^2}{2}, & \text{if } k = N. \end{cases} \tag{2.51}$$

The meaning of eq. (2.51) is the same as for eq. (2.49): the only way we have to distinguish the NOON state (2.50) from the statistical mixture $\hat{\rho} = (|N_L, 0_R\rangle\langle N_L, 0_R| +$

$|0_L, N_R\rangle \langle 0_L, N_R|) /2$ is by looking at N-particles observables.

From this point of view, the difference between the atomic coherent state (2.37) and the macroscopic entangled states (2.48) and (2.50) it's quite evident. In fact, in the coherent state all the atoms are in the same superposition of single particle states. Single particle observables are enough to detect the quantumness of coherent state. On the contrary, in the macroscopic entangled states, the superposition is at the level of the whole system and, in order to detect it, the proper N-particles observables are required.

Differently from the coherence properties expressed in eq. (2.39) of the phase state (2.37), the N-particles coherences (2.49) and (2.51) are left unchanged by the Hamiltonian (2.34) with $J = 0$ (see the appendix A).

2.3 Cold atoms in optical lattice

In the last decades, great strides have been made in quantum optics and, in particular, in the study of light-matter interaction. Indeed, nowadays, one of the most powerful way to trap atomic clouds at very low temperature is through the interaction of the atoms with a laser [27, 70, 106, 107]. The atom-light interaction is described in terms of dipole interactions, where the dipole moment $\mathbf{d}$ of the atom is linearly coupled with the far-off resonant electric field $\mathbf{E}(\mathbf{r})$ of the laser. This interaction results in an effective external potential for the atoms given by [108, 109]

$$V_{\text{ext}} \propto \frac{|\mathbf{E}(\mathbf{r})|^2}{\Delta}, \tag{2.52}$$

where $\Delta = \omega_L - \omega_0$, ω_L is the laser frequency and ω_0 is the resonance frequency of the atom. Thus, a spatially oscillating potential can be created by using two counter-propagating laser with same optical properties, with the following optical potential:

$$V_{\text{ext}} \propto \frac{\cos^2(\mathbf{k} \cdot \mathbf{r})}{\Delta}. \tag{2.53}$$

If $\Delta < 0$, the laser is said to be red-detuned, and the atoms are attracted towards the high intensity regions; while, if $\Delta > 0$, the laser is said to be blue-detuned, and the laser pushes the atoms out of the high intensity regions.
The optical lattice created by the potential (2.53) is periodic with lattice length given by $\lambda/2$, with λ the wave length of the trapping laser. All the properties of the optical lattice such as the depth of the potential or the lattice length can be tuned experimentally [70, 107].

The eigenstates $\phi_{n,\mathbf{q}}(\mathbf{r})$ of the periodic single-particle Hamiltonian operator

$$\hat{h} = -\frac{\hbar^2 \nabla^2}{2m} + V_{\text{ext}}(\mathbf{r}) \tag{2.54}$$

are given by applying Bloch's theorem [110]:

$$\phi_{n,\mathbf{q}}(\mathbf{r}) = e^{i\mathbf{q}\cdot\mathbf{r}} u_{n,\mathbf{q}}(\mathbf{r}), \tag{2.55}$$

where $u_{n,\mathbf{q}}$ has the periodicity of the Hamiltonian (2.54). The eigenstates (2.55) are labeled by a band index $n \in \mathbb{N}$, and by the so-called quasi-momentum $\mathbf{q}$, with vector components $q_i \in [-2\pi/\lambda, 2\pi/\lambda)$.

From the Bloch states (2.55) it is possible to define a new basis, composed by states localized in site position, called Wannier functions [110,111]:

$$\psi_{n,\mathbf{R}}(\mathbf{r}) = \left(\frac{\lambda}{4\pi}\right)^3 \int d\mathbf{q}\, e^{-i\mathbf{q}\cdot\mathbf{R}} \phi_{n,\mathbf{q}}(\mathbf{r}), \tag{2.56}$$

where $\mathbf{R}$ indicates the site position in space.
Usually, the temperature of cold atomic systems in optical lattices is low enough to consider only the first band state, *i.e.*, $n = 0$. Thus, the state of the atoms is completely defined by a discrete site index i, indicating the i-th site of the lattice. In the second quantization formalism, it is common to define the operators $\hat{a}_i$, $\left[\hat{a}_i, \hat{a}_j^\dagger\right] = \delta_{i,j}$, ($i, j$ are site indices),such that

$$\langle \mathbf{r}|\, \hat{a}_i^\dagger\, |0\rangle = \psi_{0,\mathbf{R}_i}(\mathbf{r}). \tag{2.57}$$

From now on, we will use the discrete index for the sites position in the optical lattices.

The lattice potential is usually so deep that the tunneling probabilities of the atoms are non negligible only for nearest neighbor sites. From these considerations, it is possible to obtain the famous Bose-Hubbard Hamiltonian for Bose Einstein condensates in optical lattices [70,107]:

$$\hat{H} = -J \sum_{\langle i,j\rangle} \left(\hat{a}_i^\dagger \hat{a}_j + \hat{a}_j^\dagger \hat{a}_i\right) + \frac{U}{2} \sum_i \hat{a}_i^\dagger \hat{a}_i \left(\hat{a}_i^\dagger \hat{a}_i - 1\right), \tag{2.58}$$

where $\langle i, j\rangle$ means nearest neighbor sites, and J and U have a similar definition to eq. (2.35) and eq. (2.36), respectively. Indeed, we can say that the two mode model for a condensate in a double well potential can be seen as a two mode Bose Hubbard model.
Eqs. (2.57) and (2.58) are all we need to describe the states and the dynamics of a BEC in an optical lattice.

Chapter 3

Heating effects on a Bose Einstein condensate

Two of the main effects of dynamical reduction models on a physical system are the heating effect and the localization mechanism. Even if these processes are generally small, these effects can modify a BEC in a way that can be, in principle, experimentally detected. In this chapter we focus on the heating effects on a BEC given by CSL model and by its dissipative and non-Markovian extensions.

In particular, in this chapter:

1. We review the heating effect of CSL model on a BEC in an harmonic trap. We show the experimental bounds founds in [30] by taking into account several other heating sources;

2. We consider a recent experimental result [31], where an atomic ensemble has been cooled down to picokelvins. By comparing the experimental results with the theoretical predictions of the CSL model (and of its dissipative and non-Markovian extensions), we show the resulting experimental bounds [32].

3.1 Temperature increase in a condensate: experimental bounds

As seen in eq. (1.36), CSL model induces an heating effect on any physical system. On a BEC, this effect leads to a decrease of the number of atoms on the condensate, as seen in eq. (2.13) for the case of an ideal gas in a box. If the heating is strong enough, an experimentally detectable decrease of the condensate fraction should be observed. This is the idea that the authors of [30] used to bound the parameters of the CSL model. Of course, in an experiment there are several external sources

that lead to an increase or a decrease of the temperature of the condensate. So, in general, the increasing energy per particle can be written as:

$$\frac{1}{N}\frac{dE}{dt} = \frac{1}{N}\frac{dE}{dt}|_{CSL} + \frac{1}{N}\frac{dE}{dt}|_{oth.}, \tag{3.1}$$

where we split the CSL contribution,

$$\frac{1}{N}\frac{dE}{dt}|_{CSL} = \lambda A^2 \frac{3\hbar^2}{4mr_C^2}, \tag{3.2}$$

from the other heating and cooling sources. The sources that the authors of [30] considered are:

1. the rate of atoms in the gas with energy high enough to leave the trap. This process is at the basis of the so-called evaporative cooling, and it reduces the energy average of the gas [112], $dE_1/\,(dt) < 0$;

2. the rate of inelastic collisions between atoms, leading to the formation of bi-atomic molecules, that usually are energetic enough to leave the trap. This process is called three-body recombination [113–115], and it is usually an heating source for the gas, $dE_2/\,(dt) > 0$;

3. collisions of the atoms in the gas with external atoms at room temperature. These collisions, with high probability, lead the atom in the gas to leave the trap, with an energy loss in the gas that can be estimated from the literature [116], $dE_3/\,(dt) < 0$;

4. laser beam and laser intensity fluctuations that lead to an energy increase of the gas [117], $dE_4/\,(dt) > 0$.

Besides these, there are other possible external heating sources that are unknown or that cannot be estimated, $dE_{\rm un}/\,(dt) > 0$. Thus we can rewrite eq. (3.1) as follows:

$$\frac{1}{N}\frac{dE}{dt} = \frac{1}{N}\frac{dE}{dt}|_{CSL} + \sum_{i=1}^{4}\frac{1}{N}\frac{dE}{dt}|_i + \frac{1}{N}\frac{dE}{dt}|_{\rm un}\,. \tag{3.3}$$

Measuring the left side of eq. (3.3) and making reasonable estimations for the known heating/cooling external sources, it is possible to find an upper bound of the heating rate due to the CSL model. In this way, the authors of [30] put the bounds of

$$\frac{\lambda}{r_C^2} < 10^7\ \mathrm{s}^{-1}\mathrm{m}^{-2}. \tag{3.4}$$

As can be noted in the exclusion plot in fig. 3.6, the bound expressed in eq. (3.4) turns out to be better than that coming from matter-wave interferometry [21], but

is beaten by the X-rays experiments [19], by cantilever experiments (for $r_C \geq 10^{-7}$ m) [20], and, in particular, by diffusion effects on a free expanding gas [32] which is the topic of the next sections.

3.2 Diffusion effects on a free expanding gas

The spontaneous localization mechanism of collapse models induces a Brownian motion in all physical systems. This effect is very weak, but experimental progress in creating ultra-cold atomic systems can be used to detect it. In [32], we considered a recent experiment [31], where an atomic ensemble was cooled down to picokelvins. Any Brownian motion induces an extra increase of the position variance of the gas. We study this effect by solving the dynamical equations for the CSL model, as well as for its non-Markovian and dissipative extensions.

In the experiment [31], a gas of ^{87}Rb atoms is cooled down to very low temperatures ($T = 50^{+50}_{-30}$ pK) by using a "delta-kick" technique. The gas is initially (t=0) trapped by a harmonic potential with standard deviation in position equal to 56 μm. The cooling process comprises the following three steps:

Step 1: The harmonic trap is removed and the gas evolves freely for a relatively long time, $\Delta t_1 = 1.1$ s. This allows atoms with the same average momentum to be approximatively at the same distance from the initial localized state of the gas.

Step 2: Delta-kick. A Gaussian laser beam interacts with the atoms, the laser-atom interaction being modeled by an external harmonic potential. By choosing the proper harmonic frequency and interaction time, the potential reduces the kinetic energy of the atoms. The interaction lasts for a short time, $\delta t_2 \simeq 35$ ms.

Step 3: The gas evolves again freely for a relatively long time, $\Delta t_3 = 1.8$ s. The position variance of the gas is then measured, from which the temperature of the gas is inferred.

The frequency of the delta-kick harmonic potential is $\omega \approx 6.7$ Rad/s [32]. In Fig. 3 of [31], the experimental data are shown. However, the only experimental value, explicitly reported together with error-bars, is the minimum value of the position standard deviation, $120^{+40}_{-40}\,\mu$m, detected at delta-kick time of $\delta t_2 = 35$ ms. This is the experimental value we use to compute the bounds on the collapse parameters.

3.2.1 Expansion of the gas according to the CSL model

We compute the time evolution of the variance in position, as well as the increase of energy of the gas, during the cooling process described in the previous section,

according to the CSL model. The effect of CSL is to increase the temperature of the gas, and consequently its spread in position.

We start from the CSL master equation (1.35), with Hamiltonian operator given by

$$\hat{H} = \sum_{\gamma=1}^{N} \hat{H}_\gamma := \sum_{\gamma=1}^{N} \left(\frac{\hat{\mathbf{p}}_\gamma}{2m} + \frac{1}{2} m\omega^2 \hat{\mathbf{x}}_\gamma^2 \right), \tag{3.5}$$

where γ is a particle index. The quantities we need to compute are: the average position variance

$$\langle \hat{\mathbf{X}}^2 \rangle_t \equiv \frac{1}{N} \sum_{\gamma=1}^{N} \left(\langle \hat{\mathbf{x}}_\gamma^2 \rangle_t - \langle \hat{\mathbf{x}}_\gamma \rangle_t^2 \right), \tag{3.6}$$

the average momentum variance

$$\langle \hat{\mathbf{P}}^2 \rangle_t \equiv \frac{1}{N} \sum_{\gamma=1}^{N} \left(\langle \hat{\mathbf{p}}_\gamma^2 \rangle_t - \langle \hat{\mathbf{p}}_\gamma \rangle_t^2 \right) \tag{3.7}$$

and the average position-momentum correlation

$$\langle \hat{\mathbf{X}}\hat{\mathbf{P}} + \hat{\mathbf{P}}\hat{\mathbf{X}} \rangle_t \equiv \frac{1}{N} \sum_{\gamma=1}^{N} \langle \hat{\mathbf{x}}_\gamma \hat{\mathbf{p}}_\gamma + \hat{\mathbf{p}}_\gamma \hat{\mathbf{x}}_\gamma \rangle_t. \tag{3.8}$$

Since all atoms are identical and are in the same initial state, the average quantities simply correspond to the expectation values for a single atom, which is what we will focus on, in the following. Taking into account that the initial average position and momentum are $\langle \hat{\mathbf{x}} \rangle_{t_0} = \langle \hat{\mathbf{p}} \rangle_{t_0} = 0$, then it's easy to see that (see the appendix B for the details):

$$\langle \hat{\mathbf{x}} \rangle_t = \langle \hat{\mathbf{p}} \rangle_t = 0 \tag{3.9}$$

i.e. CSL does not affect the average motion in position and momentum of the atoms. However, the same is not true for the standard deviations. In fact, from eq. (1.35) and eq. (3.5), one gets B

$$\langle \hat{\mathbf{x}}^2 \rangle_t = \langle \hat{\mathbf{x}}^2 \rangle_{t_0} + \frac{1}{2\omega m} \Big[\mathcal{B}(\omega) \sin\left(2\omega(t-t_0)\right) - \mathcal{A}(\omega) \left(1 - \cos\left(2\omega(t-t_0)\right)\right) \Big], \tag{3.10}$$

$$\langle \hat{\mathbf{p}}^2 \rangle_t = \langle \hat{\mathbf{p}}^2 \rangle_{t_0} + m\omega^2 \mathcal{C}(\omega)(t-t_0) - \frac{m\omega}{2} \Big[\mathcal{B}(\omega) \sin\left(2\omega(t-t_0)\right) - \mathcal{A}(\omega) \left(1 - \cos\left(2\omega(t-t_0)\right)\right) \Big] \tag{3.11}$$

and

$$\langle \hat{\mathbf{x}} \cdot \hat{\mathbf{p}} + \hat{\mathbf{p}} \cdot \hat{\mathbf{x}} \rangle_t = \mathcal{A}(\omega) \sin\left(2\omega(t-t_0)\right) + \mathcal{B}(\omega) \cos\left(2\omega(t-t_0)\right) + \mathcal{C}(\omega), \tag{3.12}$$

where the real parameters $\mathcal{A}(\omega)$, $\mathcal{B}(\omega)$, $\mathcal{C}(\omega)$, are fixed by the initial conditions of the system at the initial time $t = t_0$:

$$\begin{aligned}\mathcal{A}(\omega) &= m\omega\langle\hat{\mathbf{x}}^2\rangle_{t_0} - \frac{\langle\hat{\mathbf{p}}^2\rangle_{t_0}}{m\omega},\\ \mathcal{B}(\omega) &= \langle\hat{\mathbf{x}}\cdot\hat{\mathbf{p}} + \hat{\mathbf{p}}\cdot\hat{\mathbf{x}}\rangle_{t_0} - \mathcal{C}(\omega),\\ \mathcal{C}(\omega) &= \frac{3\lambda A^2\hbar^2}{2mr_C^2\omega^2}.\end{aligned} \tag{3.13}$$

The free evolution (i.e. without the harmonic trap) for $\langle\hat{\mathbf{x}}^2\rangle_t$, $\langle\hat{\mathbf{p}}^2\rangle_t$ and $\langle\hat{\mathbf{x}}\cdot\hat{\mathbf{p}} + \hat{\mathbf{p}}\cdot\hat{\mathbf{x}}\rangle_t$ can be obtained by taking the limit $\omega \to 0$ in eqs. (3.10), (3.11) and (3.12). In such a case we have:

$$\langle\hat{\mathbf{x}}^2\rangle_t = \langle\hat{\mathbf{x}}^2\rangle_{t_0} + \frac{\langle\hat{\mathbf{x}}\cdot\hat{\mathbf{p}} + \hat{\mathbf{p}}\cdot\hat{\mathbf{x}}\rangle_0}{m}(t-t_0) + \frac{\langle\hat{\mathbf{p}}^2\rangle_{t_0}}{m^2}(t-t_0)^2 + \frac{\lambda A^2\hbar^2}{2m^2r_C^2}(t-t_0)^3, \tag{3.14}$$

$$\langle\hat{\mathbf{p}}^2\rangle_t = \langle\hat{\mathbf{p}}^2\rangle_{t_0} + \frac{3\lambda A^2\hbar^2}{2r_C^2}(t-t_0),, \tag{3.15}$$

and for the correlation

$$\langle\hat{\mathbf{x}}\cdot\hat{\mathbf{p}} + \hat{\mathbf{p}}\cdot\hat{\mathbf{x}}\rangle_t = \langle\hat{\mathbf{x}}\cdot\hat{\mathbf{p}} + \hat{\mathbf{p}}\cdot\hat{\mathbf{x}}\rangle_{t_0} + \frac{2\langle\hat{\mathbf{p}}^2\rangle_{t_0}}{m}(t-t_0) + \frac{3\lambda A^2\hbar^2}{2mr_C^2}(t-t_0)^2. \tag{3.16}$$

Given the above equations, we can easily compute the evolution of $\langle\hat{\mathbf{x}}^2\rangle_t$ during the experiment. From $t = 0$ to $t = t_1$ the system evolves freely ($\omega = 0$) accordingly to eqs. (3.14)–(3.16); from $t = t_1$ to time $t = t_2$ it evolves harmonically as described in eqs. (3.10)–(3.12) and then again freely up to time $t = t_3$. Imposing the continuity condition during the whole process, one arrives at the final result:

$$\langle\hat{\mathbf{x}}^2\rangle_{t_3} = \langle\hat{\mathbf{x}}^2\rangle^{\text{QM}}_{t_3} + \langle\hat{\mathbf{x}}^2\rangle^{\text{CSL}}_{t_3}, \tag{3.17}$$

where $\langle\hat{\mathbf{x}}^2\rangle^{\text{QM}}_t$ is the value of the position variance according to the standard Schrödinger evolution, and $\langle\hat{\mathbf{x}}^2\rangle^{\text{CSL}}_t$ is the modification induced by CSL. In particular, the CSL contribution is given by

$$\begin{aligned}\langle\hat{\mathbf{x}}^2\rangle^{\text{CSL}}_{t_3} =& \frac{\lambda A^2\hbar^2}{r_C^2 8m^2\omega^3}\Big[A^{\text{CSL}}(\omega,t_1,t_3,\delta t_2) + B^{\text{CSL}}(\omega,t_1,t_3,\delta t_2)\cos(2\omega\delta t_2) + \\ & C^{\text{CSL}}(\omega,t_1,t_3,\delta t_2)\sin(2\omega\delta t_2)\Big],\end{aligned} \tag{3.18}$$

with

$$A^{\text{CSL}} = 6\omega t_3 + 2\omega^3\left[t_2^3 + 2t_3^3 + t_1^3 - 3t_3^2t_2\right] + 2t_1^3\left(t_3 - t_2\right)^2\omega^5; \tag{3.19a}$$

$$B^{\text{CSL}} = -2\omega\left[3(t_3 - \delta t_2) + \omega^2 t_1(2t_1^2 - 3(t_3 - \delta t_2)^2) + \omega^4 t_1^3(t_3 - t_2)^2\right]; \tag{3.19b}$$

$$C^{\text{CSL}} = 3 + 3\omega^2\left[(t_3 - t_2)^2 - 2(t_3 - \delta t_2)^2\right] + 2\omega^4 t_1^2(t_3 - t_2)(3t_3 - t_1 - 3\delta t_2). \tag{3.19c}$$

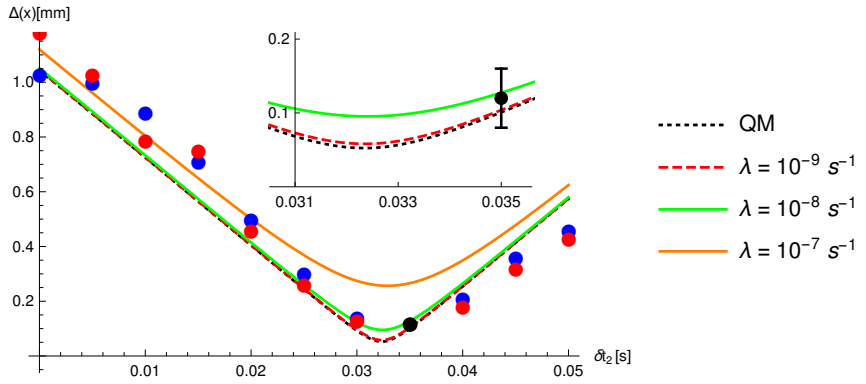

Figure 3.1: Position's standard deviation $\Delta(x) \equiv \langle \hat{\mathbf{x}}^2 \rangle_{t_3}^{1/2}$ at the detector (time $t = t_3$) as a function of the delta-kick time δt_2, for three different values of the collapse rate λ. For each curve, we fixed $r_C = 10^{-7}$ m. The inset shows the curves near the minimum value detected in [31], $\Delta(x)_{\text{EXP}} = 120^{+40}_{-40}\mu$m, indicated by the black bars. The black dotted line shows the quantum-mechanical predictions. The red and blue points represent the experimental data deducted from fig. 3 in [31].

We can see that the CSL contribution $\langle \hat{\mathbf{x}}^2 \rangle_{t_3}^{\text{CSL}}$ to the final variance is independent from the initial state of the gas (contrary to $\langle \hat{\mathbf{x}}^2 \rangle_{t_3}^{\text{QM}}$) and depends, in a rather complicated way, only on the relevant times of the experiment (t_1, $\delta t_2 = t_2 - t_1$, t_3) and the frequency ω of the delta-kick.

In fig. 3.1 we plot the final position variance $\langle \hat{\mathbf{x}}^2 \rangle_{t_3}$ as a function of the delta-kick time δt_2. To highlight the CSL effect, we computed the quantum-mechanical prediction and the CSL predictions for three different values of λ and at fixed $r_C = 10^{-7}$ m. As we can see, for small λ the quantum-mechanical predictions, compatible with the experimental data, are recovered. For larger values of λ the variance $\langle \hat{\mathbf{x}}^2 \rangle_{t_3}$ increases, till it disagrees with the experimental data. This is the expected behavior: the larger λ, the stronger the Brownian fluctuations and the larger the spread of the cloud.

Similarly, in fig. 3.2 we plot the average energy of the gas at the end of the process as a function of δt_2, for different values of λ and again at fixed $r_C = 10^{-7}$ m. We see that the cooling effect is maximum when the delta-kick last for $\delta t_2 \approx 20$ ms, leading to a theoretical kinetic energy of $E \approx 10^{-34}$ J, corresponding to a temperature of order $T \approx 10$ pK. This theoretical value is compatible with the experimental value $T_{min} = 50^{+50}_{-30}$ pK measured in [31]. We also note that the heating effect due to CSL becomes significant for $\lambda \geq 10^{-7}\,\text{s}^{-1}$, leading to an energy increase greater than 5×10^{-33} J, which is about 5 times greater than the value of the energy increase measured during the experiment ($(4 \pm 6) \times 10^{-34}$ J).

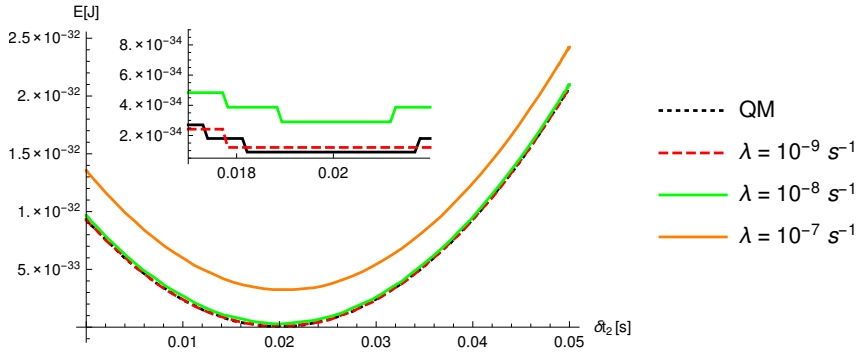

Figure 3.2: Kinetic energy $E \equiv \langle \hat{\mathbf{p}}^2 \rangle_{t_3}/2m$ at the detector (time $t = t_3$) as a function of the delta-kick time δt_2, for three different values of the collapse rate λ. For each curve, we fixed $r_C = 10^{-7}$ m. The inset shows the minimum of the curves, which is $E \sim 10^{-34}$J, corresponding to a temperature $T \simeq 10$ pK, for $\delta t_2 \approx 20$ ms. The black dotted line shows the quantum-mechanical predictions.

3.2.2 Expansion of the gas according to the non-white CSL model

We now consider the predictions of CSL with a non-white noise (cCSL) on the expansion of the gas. The (single particle) cCSL master equation [34, 35], to the first perturbative order in λ, is [1]:

$$\begin{aligned}\frac{d\rho\left(t\right)}{dt} = &-\frac{i}{\hbar}\left[H,\rho\left(t\right)\right] - \lambda 8\pi^{3/2} r_C^3 A^2 \int_0^t ds\, f\left(s\right) \\ &\times \int d\mathbf{Q}\, \tilde{g}(\mathbf{Q})\tilde{g}(-\mathbf{Q}) \left[e^{-\frac{i}{\hbar}\mathbf{Q}\cdot\hat{\mathbf{x}}}, \left[e^{\frac{i}{\hbar}\mathbf{Q}\cdot\hat{\mathbf{x}}(-s)}, \rho\left(t\right)\right]\right],\end{aligned} \tag{3.20}$$

where

$$\tilde{g}(\mathbf{Q}) = \frac{1}{\left(2\pi\hbar\right)^{3/2}} e^{-\frac{\mathbf{Q}^2 r_C^2}{2\hbar^2}}, \tag{3.21}$$

the function $f\left(s\right)$ is the time correlation function of the non-white noise, and $\hat{\mathbf{x}}(-s)$ is the position operator in the interaction picture, evolved backwards to the time $-s$:

$$\hat{\mathbf{x}}(-s) = e^{-\frac{i}{\hbar}Hs}\, \hat{\mathbf{x}}\, e^{\frac{i}{\hbar}Hs}. \tag{3.22}$$

In the white noise limit the correlation function $f(s)$ becomes a Dirac-delta and the standard CSL master equation (1.35) with $N = 1$ is recovered.

From eq. (3.20) it is easy to derive the evolution equation for a generic operator O:

$$\begin{aligned}\frac{d\langle\hat{O}\rangle_t}{dt} = &-\frac{i}{\hbar}\langle[\hat{O},\hat{H}]\rangle_t - \lambda 8\pi^{3/2} r_C^3 A^2 \int_0^t ds f\left(s\right) \\ &\times \int d\mathbf{Q}\, \tilde{g}(\mathbf{Q})\tilde{g}(-\mathbf{Q}) \langle[[\hat{O}, e^{-\frac{i}{\hbar}\mathbf{Q}\cdot\hat{\mathbf{x}}}], e^{\frac{i}{\hbar}\mathbf{Q}\cdot\hat{\mathbf{x}}(-s)}]\rangle_t.\end{aligned} \tag{3.23}$$

[1] Here we report only the single-atom master equation because, similarly to the case of white noise CSL model, we only need to focus on single-atom observables in order to describe the gas.

This non-Markovian master equation cannot be solved exactly for a general non-white noise. We can proceed as follows, noting that any realistic correlation function has a cut-off time τ (to which a frequency cut-off Ω corresponds). When τ is much smaller than the typical timescales of the system, the new dynamics is expected to be indistinguishable from the white-noise case. We will assess for which values of τ the white noise limit is recovered. More precisely we are interested in determining when we can approximate:

$$e^{\frac{i}{\hbar}\mathbf{Q}\cdot\hat{\mathbf{x}}(-s)} \simeq e^{\frac{i}{\hbar}\mathbf{Q}\cdot\hat{\mathbf{x}}}. \tag{3.24}$$

Given the harmonic Hamiltonian in eq. (3.5), the position operator in the interaction picture evolves as follows:

$$\hat{\mathbf{x}}\,(-s) = \cos(\omega s)\,\hat{\mathbf{x}} - \frac{\sin(\omega s)}{m\omega}\hat{\mathbf{p}} \tag{3.25}$$

which implies

$$e^{\frac{i}{\hbar}\mathbf{Q}\cdot\hat{\mathbf{x}}(-s)} = e^{\frac{i}{\hbar}\cos(\omega s)\mathbf{Q}\cdot\hat{\mathbf{x}}}\, e^{-\frac{i}{\hbar}\frac{\sin(\omega s)}{m\omega}\mathbf{Q}\cdot\hat{\mathbf{p}}}\, e^{-\frac{i}{\hbar}\frac{\sin(2\omega s)}{4m\omega}\mathbf{Q}^2}. \tag{3.26}$$

We perform the analysis under the assumption that

$$\tau \ll t \simeq 10^{-2}\ \text{s}, \tag{3.27}$$

which is the order of magnitude of the delta-kick time. This assumption is necessary in order to obtain conditions, which depend only on the noise cut-off τ and not on the time t of evolution. Then, according to eq. (3.26), the approximation in eq. (3.24) is fulfilled when:

$$\omega\tau \ll 1 \quad \Rightarrow \quad \tau \ll \omega^{-1} \simeq 0,94\text{s}, \tag{3.28}$$

and:

$$\frac{|\mathbf{Q}||\mathbf{p}_{max}|\tau}{\hbar m} \ll 1 \quad \Rightarrow \quad \tau \ll 10^3 \left(\frac{r_C}{1\text{m}}\right)\text{s}, \tag{3.29}$$

and also:

$$\frac{\tau}{2m\hbar}\mathbf{Q}^2 \ll 1 \quad \Rightarrow \quad \tau \ll 10^9 \left(\frac{r_C^2}{1\text{m}^2}\right)\text{s}, \tag{3.30}$$

where $m = 1,44 \times 10^{-25}$ Kg is the Rb mass, the maximum momentum is $|\mathbf{p}_{max}| = \langle\hat{\mathbf{p}}\rangle + \langle\hat{\mathbf{p}}^2\rangle^{1/2} \simeq 10^{-29}$ Kg m/s (we took $\langle\hat{\mathbf{p}}\rangle = 0$ and $\langle E\rangle = \langle\hat{\mathbf{p}}^2/2m\rangle \simeq 10^{-32}$ J) and $|\mathbf{Q}| \leq \hbar/r_C$, which is imposed by the Gaussian factors $\tilde{g}(\mathbf{Q})$ defined in eq. (3.21). Given the assumption in eq. (3.27), the condition in eq. (3.28) is always fulfilled, as well as conditions in eqs. (3.29) and (3.30), as long as $r_C \geq 10^{-5}$ m. On the other hand, for $r_C \leq 10^{-5}$ m, the strongest bound comes from the conditions in eqs. (3.29) and (3.30).

Under these conditions, the evolution equation for a generic operator O becomes:

$$\frac{d\langle\hat{O}\rangle_t}{dt} = -\frac{i}{\hbar}\langle[\hat{O},\hat{H}]\rangle_t - \frac{\lambda 8\pi^{3/2} r_C^3 A^2 \tilde{f}(0)}{2}\int d\mathbf{Q}\,\tilde{g}(\mathbf{Q})\tilde{g}(-\mathbf{Q})\langle[[\hat{O},\, e^{-\frac{i}{\hbar}\mathbf{Q}\cdot\hat{\mathbf{x}}}],\, e^{\frac{i}{\hbar}\mathbf{Q}\cdot\hat{\mathbf{x}}}]\rangle_t\,, \tag{3.31}$$

where

$$\tilde{f}(\omega) := \int_{-\infty}^{+\infty} f(s) e^{i\omega s} ds\,, \tag{3.32}$$

and where we assumed $f(s) = f(-s)$ and used the fact that for $t > \tau$

$$\int_0^t ds f(s) \simeq \int_0^\infty ds f(s) = \frac{1}{2}\int_{-\infty}^{\infty} ds f(s) = \frac{\tilde{f}(0)}{2}. \tag{3.33}$$

Therefore, under the assumption (3.27) and when conditions (3.29) and (3.30) are fulfilled, the non-white noise case is well approximated by the white-noise case discussed in the previous section, with the replacement $\lambda \to \lambda \tilde{f}(0)/2$.

A more detailed analysis is possible for a system with spatial extension smaller than r_C. In our case $\langle \hat{\mathbf{x}}^2 \rangle^{1/2} \approx 50\,\mu$m, implying that the approximation holds for $r_C \geq 10^{-4}$ m. Imposing this condition on the Gaussian factors $\tilde{g}(\mathbf{Q})$ defined in eq. (3.21) gives $|\mathbf{Q}| \leq \hbar/r_C$, which guarantees that we can expand the exponentials in the second line of eq. (3.23) as $e^{-\frac{i}{\hbar}\mathbf{Q}\cdot\hat{\mathbf{x}}} \simeq 1 - \frac{i}{\hbar}\mathbf{Q}\cdot\hat{\mathbf{x}}$, leading to

$$\sum_{i,j=1}^{3} \left(\frac{1}{\hbar^2} \int d\mathbf{Q} \tilde{g}(\mathbf{Q}) \tilde{g}(-\mathbf{Q}) Q_i Q_j \right) \langle [[\hat{O},\, \hat{x}_i],\, \hat{x}_j(-s)] \rangle_t. \tag{3.34}$$

The integration over $\mathbf{Q}$ gives the factor

$$\frac{1}{\hbar^2} \int d\mathbf{Q} \tilde{g}(\mathbf{Q}) \tilde{g}(-\mathbf{Q}) Q_i Q_j = \frac{\delta_{ij}}{2^4 \pi^{3/2} r_C^5} \tag{3.35}$$

and therefore eq. (3.23) becomes

$$\frac{d\langle \hat{O} \rangle_t}{dt} = -\frac{i}{\hbar}\langle [\hat{O}, \hat{H}] \rangle_t - \frac{\lambda A^2}{2 r_C^2} \int_0^t ds f(s) \sum_{j=1}^{3} \langle [[\hat{O},\, \hat{x}_j],\, \hat{x}_j(-s)] \rangle_t. \tag{3.36}$$

An explicit calculation is also possible, if we take a specific expression for the noise correlator, e.g.:

$$f(s) = \frac{1}{2\tau} e^{-|s|/\tau}. \tag{3.37}$$

which, in the limit $\tau \to 0$, reduces to a Dirac delta. From eq. (3.36) it is easy to see that the dynamical equations for $\hat{\mathbf{x}}$ and $\hat{\mathbf{p}}$ are not modified by the noise. Similarly, for $\hat{\mathbf{x}}^2$ we have:

$$\frac{d\left\langle \hat{\mathbf{x}}^2 \right\rangle_t}{dt} = \frac{\langle \hat{\mathbf{x}}\hat{\mathbf{p}} + \hat{\mathbf{p}}\hat{\mathbf{x}} \rangle_t}{m}. \tag{3.38}$$

From eq. (3.36), it is also straightforward obtain the following equations:

$$\frac{d\left\langle \hat{\mathbf{x}}\hat{\mathbf{p}} + \hat{\mathbf{p}}\hat{\mathbf{x}} \right\rangle_t}{dt} = \frac{2\left\langle \hat{\mathbf{p}}^2 \right\rangle_t}{m} - 2m\omega^2 \left\langle \hat{\mathbf{x}}^2 \right\rangle_t + \frac{3\lambda A^2 \hbar^2}{m r_C^2} \int_0^t ds\, \frac{e^{-\frac{s}{\tau}} \sin(s\omega)}{2\omega\tau}; \tag{3.39}$$

$$\frac{d\left\langle \hat{\mathbf{p}}^2\right\rangle_t}{dt} = -m\omega^2\left\langle \hat{\mathbf{x}}\hat{\mathbf{p}} + \hat{\mathbf{p}}\hat{\mathbf{x}}\right\rangle_t + \frac{3\lambda A^2\hbar^2}{2r_C^2}\int_0^t ds\,\frac{e^{-\frac{s}{\tau}}\cos(s\omega)}{2\tau}. \tag{3.40}$$

The system of eqs. (3.38), (3.39) and (3.40) can be solved exactly. The solution of eq. (3.39) is:

$$\begin{aligned}\left\langle \hat{\mathbf{x}}\hat{\mathbf{p}} + \hat{\mathbf{p}}\hat{\mathbf{x}}\right\rangle_t = \left\langle \hat{\mathbf{x}}\hat{\mathbf{p}} + \hat{\mathbf{p}}\hat{\mathbf{x}}\right\rangle_0\cos(2\omega t) + \left(\frac{\left\langle \hat{\mathbf{p}}^2\right\rangle_0}{m\omega} - m\omega\left\langle \hat{\mathbf{x}}^2\right\rangle_0\right)\sin(2\omega t)\\ + \frac{3\lambda A^2\hbar^2}{2\omega m r_C^2}\int_0^t ds\, g(s)\sin(2\omega(t-s)),\end{aligned} \tag{3.41}$$

where

$$g(x) = \int_0^x dy\,\frac{e^{-\frac{y}{\tau}}\cos(\omega y)}{2\tau} + \frac{e^{-\frac{x}{\tau}}\sin(\omega x)}{2\omega\tau}. \tag{3.42}$$

Using eq. (3.41) in eqs. (3.38) and (3.40) we get the related solutions:

$$\begin{aligned}\left\langle \hat{\mathbf{x}}^2\right\rangle_t = \left\langle \hat{\mathbf{x}}^2\right\rangle_0 + \frac{1}{2m\omega}\left[\sin(2\omega t)\left\langle \hat{\mathbf{x}}\hat{\mathbf{p}} + \hat{\mathbf{p}}\hat{\mathbf{x}}\right\rangle_0 - \left(\frac{\left\langle \hat{\mathbf{p}}^2\right\rangle_0}{m\omega} - m\omega\left\langle \hat{\mathbf{x}}^2\right\rangle_0\right)(1-\cos(2\omega t))\right]\\ + \frac{3\lambda A^2\hbar^2}{2\omega m^2 r_C^2}\int_0^t ds_2\int_0^{s_2} ds_1\, g(s_1)\sin(2\omega(s_2-s_1));\end{aligned} \tag{3.43}$$

$$\begin{aligned}\left\langle \hat{\mathbf{p}}^2\right\rangle_t = \left\langle \hat{\mathbf{p}}^2\right\rangle_0 - \frac{m\omega}{2}\left[\sin(2\omega t)\left\langle \hat{\mathbf{x}}\hat{\mathbf{p}} + \hat{\mathbf{p}}\hat{\mathbf{x}}\right\rangle_0 - \left(\frac{\left\langle \hat{\mathbf{p}}^2\right\rangle_0}{m\omega} - m\omega\left\langle \hat{\mathbf{x}}^2\right\rangle_0\right)(1-\cos(2\omega t))\right]\\ + \frac{3\lambda A^2\hbar^2}{2r_C^2}\left[\int_0^t ds_2\int_0^{s_2} ds_1\left(\frac{e^{-\frac{s_1}{\tau}}\cos(\omega s_1)}{2\tau} - \omega g(s_1)\sin(2\omega(s_2-s_1))\right)\right].\end{aligned} \tag{3.44}$$

From a direct computation of the function (3.42), it is possible to note that, if $\tau\omega \ll 1$ and $\tau \ll t$, then the solutions eqs. (3.41), (3.43) and (3.44) are practically indistinguishable from eqs. (3.10), (3.11) and (3.12) derived in the white noise case. In the experiment under consideration, we have $\omega = 6.7$ rad/s and $t = \delta t_2 \approx 35$ ms. The white noise limit is therefore a good approximation for any noise with cut-off $\tau \leq 10^{-3}$s.

In the free evolution limit $\omega \to 0$, Eqs. (3.41), (3.43) and (3.44) reduce to:

$$\left\langle \hat{\mathbf{p}}^2\right\rangle_t = \left\langle \hat{\mathbf{p}}^2\right\rangle_0 + \frac{3\lambda A^2\hbar^2}{2r_C^2}\left[t - \tau\left(1 - e^{-\frac{t}{\tau}}\right)\right]; \tag{3.45}$$

$$\left\langle \hat{\mathbf{x}}\hat{\mathbf{p}} + \hat{\mathbf{p}}\hat{\mathbf{x}}\right\rangle_t = \left\langle \hat{\mathbf{x}}\hat{\mathbf{p}} + \hat{\mathbf{p}}\hat{\mathbf{x}}\right\rangle_0 + \frac{2\left\langle \hat{\mathbf{p}}^2\right\rangle_0 t}{m} + \frac{3\lambda A^2\hbar^2}{2mr_C^2}\left[t^2 - \tau t\left(1 - e^{-\frac{t}{\tau}}\right)\right]; \tag{3.46}$$

$$\left\langle \hat{\mathbf{x}}^2 \right\rangle_t = \left\langle \hat{\mathbf{x}}^2 \right\rangle_0 + \frac{\langle \hat{\mathbf{x}}\hat{\mathbf{p}} + \hat{\mathbf{p}}\hat{\mathbf{x}} \rangle_0 \, t}{m} + \frac{\left\langle \hat{\mathbf{p}}^2 \right\rangle_0 t^2}{m^2} + \frac{3\lambda A^2 \hbar^2}{m^2 r_C^2} \left[\frac{t^3}{6} - \frac{t\tau}{2} \left(\frac{1}{2} + e^{-\frac{t}{\tau}} \right) + \frac{\tau^3}{2} \left(1 - e^{-\frac{t}{\tau}} \right) \right]. \tag{3.47}$$

In this case the white noise limit is recovered when $\tau \ll t$. The free time evolution is $t \approx 1$s, which implies $\tau \leq 10^{-2}$s.

To conclude, we can safely say that the bounds we obtain for the CSL model shown in fig. 3.6 hold also for a more general and realistic non-white noise extension of the model if

$$\tau \leq 10^{-3}\,\mathrm{s} \quad \Longrightarrow \quad \Omega \geq 10^{3}\,\mathrm{Hz} \tag{3.48}$$

for $r_C \geq 10^{-5}\,\mathrm{m}$,

$$\tau \ll 10^{3} \left(\frac{r_C}{1\mathrm{m}} \right) \mathrm{s} \quad \Longrightarrow \quad \Omega \gg 10^{-3} \left(\frac{1\mathrm{m}}{r_C} \right) \mathrm{Hz} \tag{3.49}$$

for $10^{-6} \leq r_C \leq 10^{-5}\,\mathrm{m}$,

$$\tau \ll 10^{9} \left(\frac{r_C^2}{1\mathrm{m}^2} \right) \mathrm{s} \quad \Longrightarrow \quad \Omega \gg 10^{-9} \left(\frac{1\mathrm{m}^2}{r_C^2} \right) \mathrm{Hz} \tag{3.50}$$

for $r_C \leq 10^{-6}\,\mathrm{m}$. Taking into account that typical cosmological cut-offs are of order $10^{10} - 10^{11}$ Hz, our analysis shows that for $r_C \geq 10^{-10}$ m and for a typical cosmological collapse noise, the cCSL predictions (therefore also the upper bounds) are indistinguishable from the standard CSL predictions.

3.2.3 Expansion of the gas according to the dCSL model

As in the case of the standard CSL model, it is easy to prove that for a gas of non-interacting atoms, the problem can be reduced to the study of single-atom observables. Thus, from the single particle master equation (1.41), it's possible to find the following differential equations B:

$$\frac{d\langle \hat{\mathbf{x}}^2 \rangle_t}{dt} = \frac{1}{m} \langle \hat{\mathbf{x}} \cdot \hat{\mathbf{p}} + \hat{\mathbf{p}} \cdot \hat{\mathbf{x}} \rangle_t + \frac{6\lambda A^2 r_C^2 k^2}{(1+k)^3}, \tag{3.51a}$$

$$\frac{d \langle \hat{\mathbf{x}} \cdot \hat{\mathbf{p}} + \hat{\mathbf{p}} \cdot \hat{\mathbf{x}} \rangle_t}{dt} = \frac{2}{m} \left\langle \hat{\mathbf{p}}^2 \right\rangle_t - 2m\omega^2 \left\langle \hat{\mathbf{x}}^2 \right\rangle_t - \frac{2\lambda A^2 k}{(1+k)^4} \langle \hat{\mathbf{x}} \cdot \hat{\mathbf{p}} + \hat{\mathbf{p}} \cdot \hat{\mathbf{x}} \rangle_t, \tag{3.51b}$$

$$\frac{d \left\langle \hat{\mathbf{p}}^2 \right\rangle_t}{dt} = -m\omega^2 \langle \hat{\mathbf{x}} \cdot \hat{\mathbf{p}} + \hat{\mathbf{p}} \cdot \hat{\mathbf{x}} \rangle_t - \chi \left\langle \hat{\mathbf{p}}^2 \right\rangle_t + \chi \left\langle \hat{\mathbf{p}}^2 \right\rangle_{as}, \tag{3.51c}$$

where

$$\chi := \frac{4k\lambda A^2}{(1+k)^5}, \qquad \left\langle \hat{\mathbf{p}}^2 \right\rangle_{as} := \frac{3\hbar^2}{8kr_C^2}. \tag{3.52}$$

In the limit of free evolution (*i.e.* $\omega \to 0$), the solutions of the set of eqs. (3.51) are:

$$\left\langle \hat{\mathbf{x}}^2 \right\rangle_t = \left\langle \hat{\mathbf{x}}^2 \right\rangle_{t_0} + \frac{2(\left\langle \hat{\mathbf{p}}^2 \right\rangle_{t_0} - \left\langle \hat{\mathbf{p}}^2 \right\rangle_{as})}{m^2(B-\chi)} \left(\frac{1-e^{-\chi(t-t_0)}}{\chi} - \frac{1-e^{-B(t-t_0)}}{B} \right)$$
$$+ \left(\langle \hat{\mathbf{x}} \cdot \hat{\mathbf{p}} + \hat{\mathbf{p}} \cdot \hat{\mathbf{x}} \rangle_{t_0} - \frac{2\left\langle \hat{\mathbf{p}}^2 \right\rangle_{as}}{mB} \right) \frac{1-e^{-B(t-t_0)}}{mB} + \left(\alpha + \frac{2\left\langle \hat{\mathbf{p}}^2 \right\rangle_{as}}{m^2 B} \right) (t-t_0); \tag{3.53a}$$

$$\langle \hat{\mathbf{x}} \cdot \hat{\mathbf{p}} + \hat{\mathbf{p}} \cdot \hat{\mathbf{x}} \rangle_t = \frac{2(\left\langle \hat{\mathbf{p}}^2 \right\rangle_{t_0} - \left\langle \hat{\mathbf{p}}^2 \right\rangle_{as})}{m(B-\chi)} \left(e^{-\chi(t-t_0)} - e^{-B(t-t_0)} \right) + \frac{2m\left\langle \hat{\mathbf{p}}^2 \right\rangle_{as}}{mB}$$
$$+ e^{-B(t-t_0)} \left(\langle \hat{\mathbf{x}} \cdot \hat{\mathbf{p}} + \hat{\mathbf{p}} \cdot \hat{\mathbf{x}} \rangle_{t_0} - \frac{8m\left\langle \hat{\mathbf{p}}^2 \right\rangle_{as}}{B} \right); \tag{3.53b}$$

$$\left\langle \hat{\mathbf{p}}^2 \right\rangle_t = \left\langle \hat{\mathbf{p}}^2 \right\rangle_{as} + e^{-\chi(t-t_0)} \left(\left\langle \hat{\mathbf{p}}^2 \right\rangle_{t_0} - \left\langle \hat{\mathbf{p}}^2 \right\rangle_{as} \right), \tag{3.53c}$$

where $B := \frac{1+k}{2}\chi$ and $\alpha := \frac{6\lambda A^2 r_C^2 k^2}{(1+k)^3}$.

We should study also the case of an harmonically trapped atom ($\omega \neq 0$). The system of eqs. (3.51) can still be solved exactly. However, the solutions are too complicated and of little practical use. In fact, the duration of the delta-kick is much shorter than the free evolution and, as shown in [32], the dCSL effects during the delta-kick can be neglected and safely be replaced by the standard quantum mechanical evolution.

We can now derive the position variance $\langle \hat{\mathbf{x}}^2 \rangle_{t_3}$ at the final time t_3 as predicted by the dCSL model. During steps 1 and 3 of the experiment (free expansion of the gas) we use the exact solutions given in eqs. (3.53), while during step 2 (the delta-kick) we use the quantum mechanical solution for an harmonic oscillator. In a similar way, one can compute the time evolution of the average kinetic energy. We do not report explicitly the final formula for $\langle \hat{\mathbf{x}}^2 \rangle_{t_3}$ since it is very long and does not help in getting any insight on the physics.

In fig. 3.3 and fig. 3.4 the minimum values of the final position variance and of the average kinetic energy are plotted as a function of the noise temperature T_{CSL} for different values of λ, while keeping $r_C = 10^{-7}$m, and for fixed values of the delta-kick time (we took the values of δt_2 which maximize the delta-kick effects). We can see that in both cases the effect of dissipation is to reduce the increase of the variance and of the energy due to the CSL noise. In particular, for the values of r_C and λ here considered, when $T_{\text{CSL}} < 10^{-7}$ K the effect of the noise is negligible and the predictions are practically equivalent to the standard quantum ones. In the range 10^{-7} K $< T_{\text{CSL}} < 10^{-6}$ K the noise effects are present but are reduced by

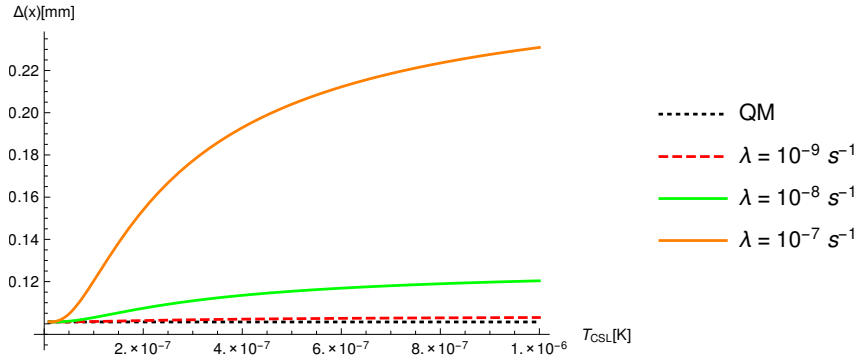

Figure 3.3: Position's standard deviation $\Delta(x) \equiv \langle \hat{\mathbf{x}}^2 \rangle_{t_3}^{1/2}$ at the detector (time $t = t_3$) as a function of the CSL noise temperature T_{CSL}, for three different values of the collapse rate λ. For each curve, we fixed $r_C = 10^{-7}$ m and the delta-kick time $\delta t_2 = 35$ ms, which corresponds to the smallest measured value (black point in fig. 3.1). We plot also the quantum-mechanical value for comparison.

dissipation. When $T_{\text{CSL}} > 10^{-6}$ K the effects of dissipation become negligible and the predictions are indistinguishable from the $T_{\text{CSL}} = +\infty$ case (CSL).

dCSL model with boost

The dCSL model is not Galilei invariant, since the noise selects a preferred reference frame, the one where it is at rest. In the previous section, we implicitly considered the situation where the lab reference frame was at rest with respect to the noise. This is unlikely. If the noise has a cosmological origin, then much likely it is at rest with the cosmic frame, with respect to which the Earth moves. In this section we analyse the case where the collapse noise is moving with some velocity $\mathbf{u}$ with respect to the laboratory system.
The master equation for the boosted dCSL model has the same structure as that in eq. (1.41) with $L(\mathbf{Q}, \hat{\mathbf{p}})$ in Eq. (1.42) replaced by:

$$L(\mathbf{Q}, \hat{\mathbf{p}}, \mathbf{u}) = e^{-\frac{r_C^2}{2\hbar^2}|(1+k)\mathbf{Q}+2k(\hat{\mathbf{p}}-m\mathbf{u})|^2}. \tag{3.54}$$

It is convenient to introduce the boosted momentum operator:

$$\hat{\mathbf{p}}_{\mathbf{u}} := \hat{\mathbf{p}} - m\mathbf{u} \tag{3.55}$$

which allows to rewrite the boosted dCSL master equation as

$$\frac{d\hat{\rho}}{dt} = \left.\frac{d\hat{\rho}^{\text{dCSL}}}{dt}\right|_{\hat{\mathbf{p}}\to\hat{\mathbf{p}}_{\mathbf{u}}} - \frac{i}{\hbar}[\hat{\mathbf{p}}_{\mathbf{u}} \cdot \mathbf{u}, \hat{\rho}] \tag{3.56}$$

where the first term is the master equation of the dCSL as given by eq. (1.41), with $\hat{\mathbf{p}}_{\mathbf{u}}$ in place of $\hat{\mathbf{p}}$. Note that $\hat{\mathbf{p}}_{\mathbf{u}}$ has the same commutation relations as $\mathbf{p}$. The equa-

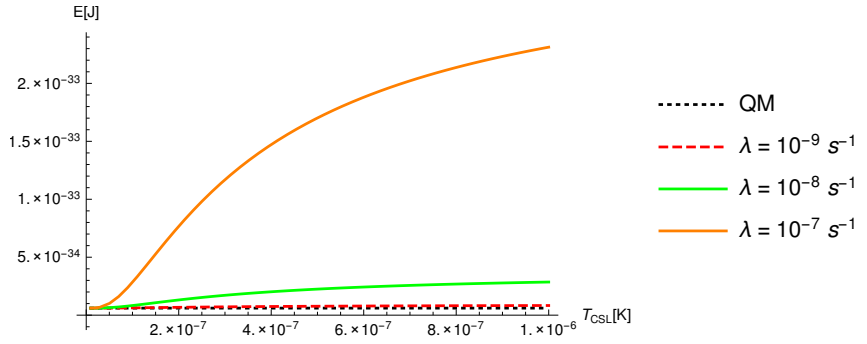

Figure 3.4: Kinetic energy $E \equiv \langle \hat{\mathbf{p}}^2 \rangle_{t_3} / 2m$ at the detector (time $t = t_3$) as a function of the CSL noise temperature T_{CSL}, for three different values of the collapse rate λ. For each curve, we fixed $r_C = 10^{-7}$ m and $\delta t_2 = 20$ ms, associated to the theoretical minimum of the momentum standard deviation (see fig. 3.2). We plot also the quantum-mechanical value for comparison.

tion for the time evolution of a generic operator O is:

$$\frac{d\langle O \rangle_t}{dt} = \frac{d\langle O \rangle_t^{\mathrm{dCSL}}}{dt}\bigg|_{\hat{\mathbf{p}} \to \hat{\mathbf{p}}_{\mathbf{u}}} - \frac{i}{\hbar} \langle [O, \hat{\mathbf{p}}_{\mathbf{u}} \cdot \mathbf{u}] \rangle_t \tag{3.57}$$

where $\langle O \rangle_t^{\mathrm{dCSL}}$ is the expectation value of the operator O given by the dCSL dynamics without boost, again with $\hat{\mathbf{p}}_{\mathbf{u}}$ in place of $\hat{\mathbf{p}}$. Therefore, we can now write the equations for the expectation values $\langle \hat{\mathbf{x}}^2 \rangle_t$, $\langle \hat{\mathbf{p}}_{\mathbf{u}}^2 \rangle_t$ and $\langle \hat{\mathbf{x}} \cdot \hat{\mathbf{p}}_{\mathbf{u}} + \hat{\mathbf{p}}_{\mathbf{u}} \cdot \hat{\mathbf{x}} \rangle_t$ using the results already derived for the dCSL model without boost; we only need to compute the extra commutator of eq. (3.57).
Actually, to get a good estimate of the effect of the boost, it is sufficient to analyze the equations for $\langle \hat{\mathbf{x}} \rangle_t$ and $\langle \hat{\mathbf{p}} \rangle_t$, instead of those for the variances, which are much more complicated. The first equation can be easily derived, while the second one involves lengthier calculations, which however are analogue to those carried out in the previous section, when deriving the equation for $\langle \hat{\mathbf{x}} \cdot \hat{\mathbf{p}} \rangle_t$. The final result is:

$$\frac{d\langle \hat{\mathbf{x}} \rangle_t}{dt} = \frac{\langle \hat{\mathbf{p}}_{\mathbf{u}} \rangle_t}{m} + \mathbf{u}, \qquad \frac{d\langle \hat{\mathbf{p}}_{\mathbf{u}} \rangle_t}{dt} = -B \langle \hat{\mathbf{p}}_{\mathbf{u}} \rangle_t, \tag{3.58}$$

where B is the parameter defined after eq. (3.53). The solution of this system of equations for a free gas ($\omega = 0$) with initial average position $\langle \hat{\mathbf{x}} \rangle_{t_0}$ and initial average momentum $\langle \hat{\mathbf{p}} \rangle_{t_0}$, written in terms of the real momentum $\hat{\mathbf{p}}$, are:

$$\langle \hat{\mathbf{x}} \rangle_t = \langle \hat{\mathbf{x}} \rangle_{t_0} + \mathbf{u}(t - t_0) + \left(\frac{\langle \hat{\mathbf{p}} \rangle_{t_0}}{m} - \mathbf{u} \right) \frac{1 - e^{-B(t-t_0)}}{B}; \tag{3.59}$$

$$\langle \hat{\mathbf{p}} \rangle_t = \langle \hat{\mathbf{p}} \rangle_{t_0} e^{-B(t-t_0)} + m\mathbf{u} \left(1 - e^{-B(t-t_0)} \right); \tag{3.60}$$

We can now argue as follows. The change of the average position of the gas must be smaller than the measured standard deviation, as in [31] no significant variation to the average position of the center-of-mass of the cloud was observed. From

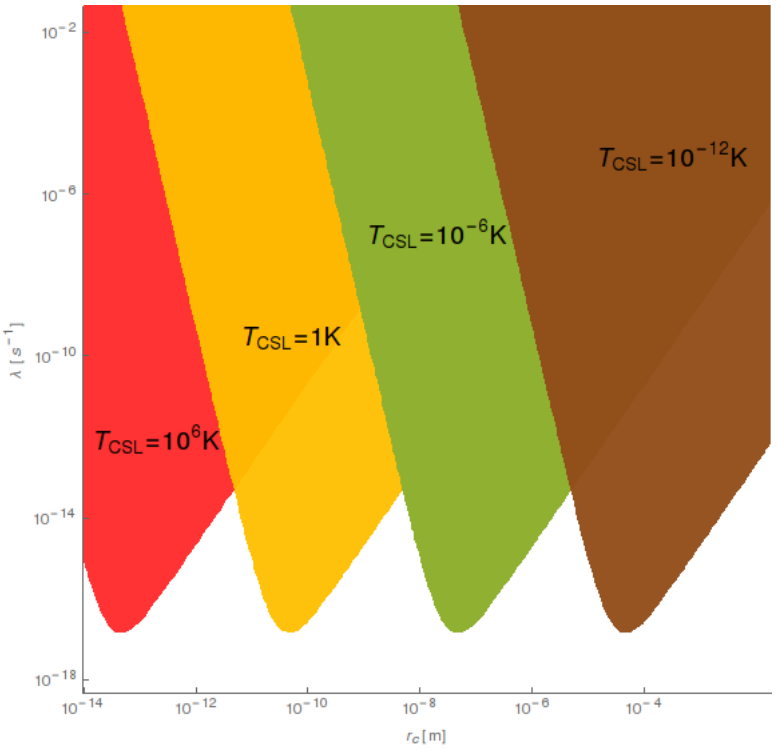

Figure 3.5: Exclusion plot for the boosted dCSL model, considering a boost with $|\mathbf{u}| = 10^7$ ms^{-1} for four different values of the dCSL temperature T_{CSL}.

eq. (3.59), taking into account that for the experiment considered here $\langle \hat{\mathbf{p}} \rangle_{t_0} = 0$ and $t - t_0 \approx 3$ s, and that for any value of the parameters of the dCSL model $B(t - t_0) \ll 1$, we can safely say that

$$\frac{1}{2} |\mathbf{u}| \, B(t - t_0)^2 \leq 1 \, \mu\text{m}. \tag{3.61}$$

where $B = 2\lambda A^2 k/(1 + k)^4$. Considering, for example, the standard values for the dCSL parameters $\lambda = 10^{-17}$ s^{-1}, $r_C = 10^{-7}$ m and $T_{\text{CSL}} = 1$ K, we obtain the bound:

$$|\mathbf{u}| \leq 10^{13} \, \text{m s}^{-1}. \tag{3.62}$$

From cosmological arguments [21] a possible value of the noise boost is $|\mathbf{u}| = 10^7$ ms^{-1}. Using this value in eq. (3.62) an exclusion plot in the parametric space $\lambda - r_C$ is found, as shown in fig. 3.5.

3.2.4 Experimental bounds on the collapse parameters

We now discuss the bounds on the collapse parameters against the experiment here considered. We compare the position's standard deviation, computed for each particular model, with the experimental value $\Delta(x)_{\text{EXP}} = 120^{+40}_{-40} \, \mu$m reported in [31];

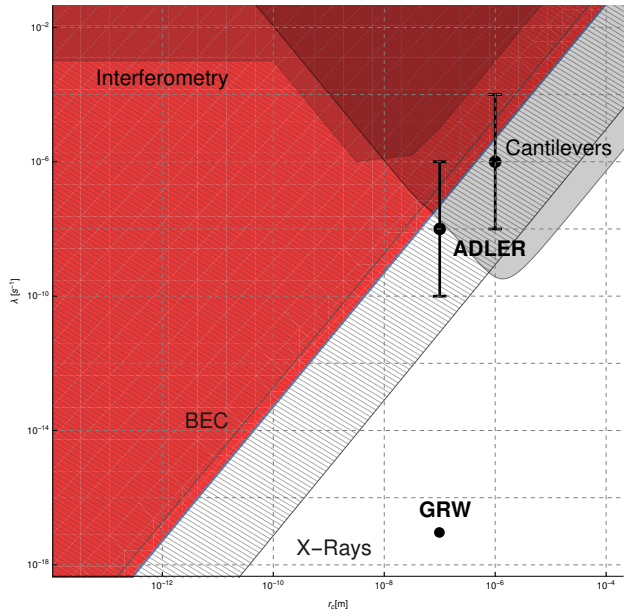

Figure 3.6: Exclusion plot for the CSL model. The red region shows the excluded area, according to the analysis here performed. The picture shows also the bounds coming from matter-wave interferometry [21], cantilevers [20], heating effect on Bose-Einstein Condensates (BECs) [30], and spontaneous X-rays emission [19]. The black points and bars represents the reference values proposed by GRW [42] and Adler [44].

we refer to this value since it is the only one with explicit error bars associated to it. Assuming that this value is distributed according to a normal distribution with mean value $\mu = 120\,\mu$m and $\sigma = 40\,\mu$m, then $\Delta(x) \in [42; 198]\,\mu$m with a confidence level of 95% The exclusion plots in fig. 3.6 and fig. 3.7 show which points in the parameters space predict a CSL-induced position's standard deviation outside the considered range (with a T_{CSL} dependence in the dCSL case).

We start with analysing the CSL model. As shown in eq. (3.18), the increase of the position variance at the final time $t = t_3$ due to the CSL noise is:

$$\langle \hat{\mathbf{x}}^2 \rangle_{t_3}^{\mathrm{CSL}} = \frac{\lambda}{r_C^2} K \tag{3.63}$$

where K is a function of the initial state of the gas, the times $t_1, \delta t_2, t_3$ and the frequency ω of the external harmonic potential, but otherwise contains no dependence on the CSL parameters. By inserting the numerical values, we arrive at the bound:

$$\frac{\lambda}{r_C^2} < 5 \times 10^6\,\mathrm{m}^{-2}\mathrm{s}^{-1}. \tag{3.64}$$

This result is in agreement with the plot in fig. 3.6, where a comparison with bounds coming from other relevant experiments is shown. As one can see, the

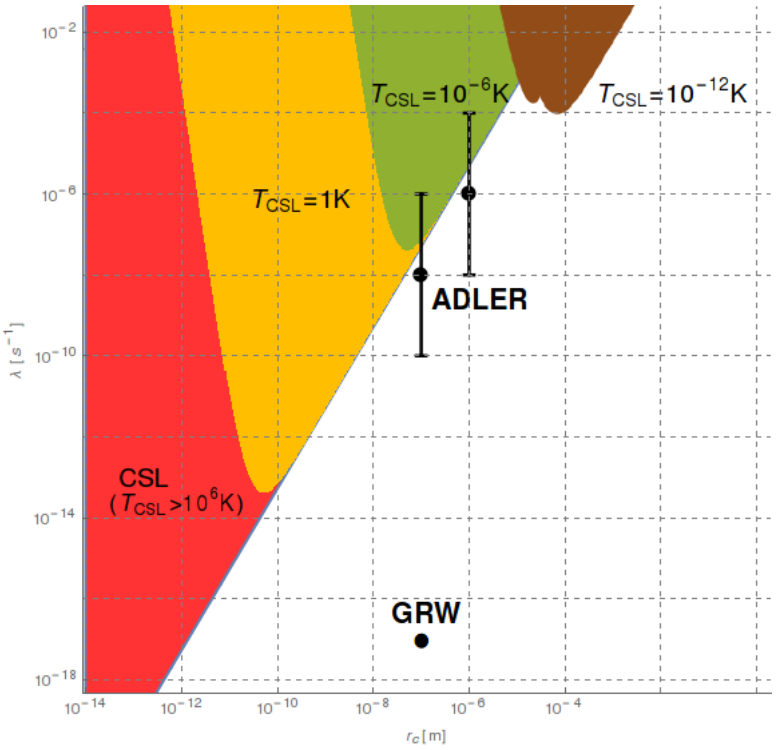

Figure 3.7: Exclusion plot for the dCSL model. The red area represents the excluded region for the CSL model ($T = \infty$) and for any dCSL model with noise temperatures $T_{CSL} > 10^6$ K (due to the finite parametric region considered). Bounds for dCSL for three different noise temperatures are also represented: in yellow the case with $T_{CSL} = 1$ K, in green that for $T_{CSL} = 10^{-6}$ K, and in brown $T_{CSL} = 10^{-12}$ K. The black points and bars represents the parametric values proposed by GRW [42] and Adler [44].

bound is better than that coming from matter-wave interferometry [21] and that related to BECs [30] while, for $r_C \leq 10^{-7}$, it is beaten only by X-rays experiments [19]. Here a comment is at order. As shown in [118–120], CSL predictions for spontaneous photon emission are very sensitive to the type of noise and, when a frequency cut-off is introduced in its spectrum, the CSL effect is significantly decreased. In particular, for X-ray detection, any cutoff smaller than 10^{18} Hz washes the effect away. Since typical cut-offs of cosmological spectra are significantly smaller than 10^{18} Hz [22], and assuming that the CSL noise has the properties of a typical cosmological random background, then one expects bounds related to spontaneous X-ray emission not to play a significant role. On the other hand, our result is robust against changes in the noise. As shown in Sec. 3.2.2, providing $r_C \geq 10^{-7}$ m, for any cutoff larger than 10^6 Hz (which is the case of cosmological noises), the effect is equivalent to that of the standard CSL model.

The situation si different for the dCSL model. The result is reported in fig. 3.7, for three different temperatures of the noise: $T_{CSL} = 1, 10^{-6}, 10^{-12}$ K. As one can see,

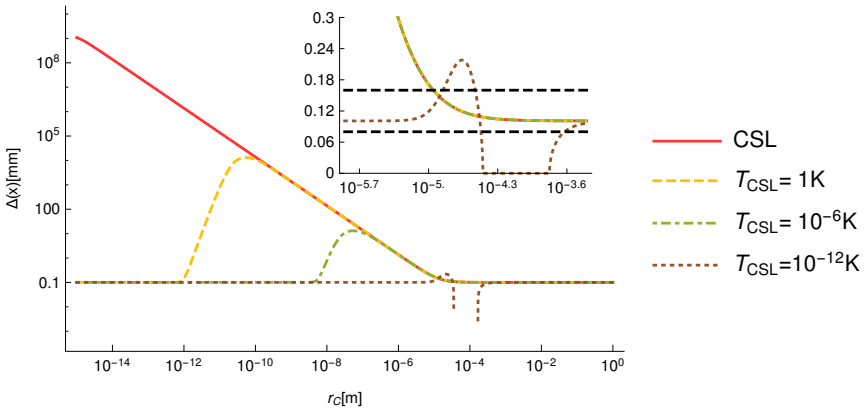

Figure 3.8: Position's standard deviatio of the gas at the detector (time $t = t_3$), as a function of r_C. Four different curves are represented, each corresponding to a different value of the noise temperature T_{CSL}. In each case, $\lambda = 10^{-3.5}$ s^{-1} and $\delta t_2 =$ 35 ms. For $T_{\text{CSL}} = 10^{-12}$ K, an insignificant numerical error appears in the interval $10^{-4.4}$ m $< r_C < 10^{-3.7}$ m, due to very small values of the position's standard deviation. No numerical instabilities appear outside this interval. The experimental value 120^{+40}_{-40} μm is indicated by the dashed black lines in the inset.

the smaller the temperature, the smaller the exclusion region. The reason is that dissipation reduces the Brownian motion fluctuations of the atoms, therefore also the extra spread of the position variance predicted by CSL. The case $T_{\text{CSL}} = 10^{-12}$ is significant. In fact, a noise temperature of the order of 1 picokelvin is lower than the system's temperature, and the dissipative dynamics cools the system, reducing its position and momentum spread. For this reason, the excluded area in the parameter spaces it is fundamentally different from the other, high-temperature situations.
Also the shape of the curve for $T_{\text{CSL}} = 10^{-12}$ K is different from the other cases. This can be better seen in fig. 3.8 where, for fixed T_{CSL} and $\lambda = 10^{-3.5}$ s^{-1}, the final position variance $\langle \hat{\mathbf{x}}^2 \rangle_{t_3}$ is plotted as function of r_C.

To conclude, the bounds on the CSL parameters coming from the experiment in [31] are among the strongest so far analyzed, stronger than direct tests based on matter-wave interferometry. They are robust against changes in the spectrum of the noise, so in this sense they are the strongest for $r_C < 10^{-7}$ m. They become weaker when dissipation is included, still remaining strong down to very small temperatures.

Chapter 4

Localization dynamics in a condensate

In this paper we focus on the use of ultracold atoms to study wave function collapse and we consider atomic gases weakly coupled via a double well potential. Such a setup provides an atomic counterpart of Josephson devices [121, 122] and it is has been experimentally realized and studied for both ultracold bosons [69, 96, 123, 124] and fermions [71]. A Josephson physics and coherent tunneling have been also studied not only in space (as in double well potential) but also between internal levels [78, 79, 125, 126]. Due to the high tunability of experimental parameters, Bose Josephson junction is one of the paradigmatic setups in which to probe and study quantum coherence on mesoscopic/macroscopic scale. For this reason, we use it to study the bounds that can be put on models for the wave function collapse. In particular, we study how CSL affects cold atoms in a double well potential, *i.e.*, a Bose Josephson junction, as qualitatively depicted in fig. 4.1, where we also schematically describe the effect of the collapse of the wave function. In particular, we compute

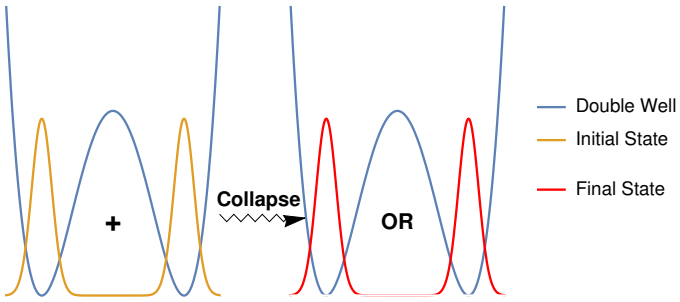

Figure 4.1: Action of the collapse noise on an atom in a double well potential (blue curve). The initial state (yellow curve) is delocalized over the two wells. The interaction of the atom with the collapse noise localizes the atomic state in one of the two wells (red curve).

the effects on the interference fringes of an atomic coherent state, as well as for the collapse of the N-particles coherences of macroscopically entangled states [36]. We study also its natural extension to a BEC in an optical lattice. In the last part, we compare the CSL decoherence with the environmental decoherence, focusing on three main sources: the thermal cloud surroundings the condensate; the three body recombination; and the laser decoherence.

4.1 CSL model for a condensate in a double well potential

In order to apply the CSL model to Bose Josephson junctions, it is convenient to rewrite the master equations (1.35) in terms of the left and right states introduced in eq. (2.32). Using eq. (2.33) in eq. (1.35), we get

$$\frac{d\hat{\rho}(t)}{dt} = -\frac{i}{\hbar}\left[\hat{H}, \hat{\rho}(t)\right] - \frac{\lambda A^2}{2}\sum_{\substack{i,j\\k,l}} \gamma_{k,l}^{i,j}\left[\hat{a}_i^\dagger \hat{a}_j, \left[\hat{a}_k^\dagger \hat{a}_l, \hat{\rho}(t)\right]\right], \tag{4.1}$$

where

$$\gamma_{k,l}^{i,j} = \int d\mathbf{y} \int d\mathbf{y}'\, e^{-\frac{|\mathbf{y}-\mathbf{y}'|^2}{4r_c^2}} \psi_i^*(\mathbf{y})\psi_j(\mathbf{y})\psi_k^*(\mathbf{y}')\psi_l(\mathbf{y}'), \tag{4.2}$$

with $i, j, k, l = L, R$. We can immediately note that couplings with an odd number of the same index, like $\gamma_{L,L}^{L,R}$, are null, due to the orthogonality of the two modes. So, we have to evaluate two types of couplings: $\gamma_{L,L}^{R,R} = \gamma_{R,R}^{L,L} \equiv \gamma_{i,j\neq i}$, where the equality holds for the parity in the CSL Gaussian term; $\gamma_{L,L}^{L,L} = \gamma_{R,R}^{R,R} \equiv \gamma_{i,i}$, where the equality holds for the symmetry of the double well potential.
By taking into account that the total number of particle is fixed, *i.e.*, $\hat{a}_L^\dagger \hat{a}_L + \hat{a}_R^\dagger \hat{a}_R = N\mathbb{I}$, it is possible to find that the dissipative term in the master equation (4.1) has the following expression:

$$\begin{aligned}
&\sum_{i,j=L,R} \gamma_{i,j}\left[\hat{a}_i^\dagger \hat{a}_i, \left[\hat{a}_j^\dagger \hat{a}_j, \hat{\rho}(t)\right]\right] \\
&= \sum_{i=j} \gamma_{i,i}\left[\hat{a}_i^\dagger \hat{a}_i, \left[\hat{a}_i^\dagger \hat{a}_i, \hat{\rho}(t)\right]\right] + \sum_{i\neq j} \gamma_{i,j}\left[\hat{a}_i^\dagger \hat{a}_i, \left[\hat{a}_j^\dagger \hat{a}_j, \hat{\rho}(t)\right]\right] \\
&= \sum_i \left(\gamma_{i,i} - \gamma_{i,j\neq i}\right)\left[\hat{a}_i^\dagger \hat{a}_i, \left[\hat{a}_i^\dagger \hat{a}_i, \hat{\rho}(t)\right]\right] \\
&= \bar{\gamma}\sum_i \left[\hat{a}_i^\dagger \hat{a}_i, \left[\hat{a}_i^\dagger \hat{a}_i, \hat{\rho}(t)\right]\right],
\end{aligned} \tag{4.3}$$

where we have defined

$$\begin{aligned}\bar{\gamma} &= \int d\mathbf{y} \int d\mathbf{y}' \, e^{-\frac{|\mathbf{y}-\mathbf{y}'|^2}{4r_C^2}} \left|\psi_L(\mathbf{y})\right|^2 \left(\left|\psi_L(\mathbf{y}')\right|^2 - \left|\psi_R(\mathbf{y}')\right|^2\right) \\ &\approx 1 - e^{-\frac{a^2}{r_C^2}},\end{aligned} \tag{4.4}$$

the last equality is expected to be satisfied in the two-mode approximation.

The master equation (4.1) so becomes as follows

$$\frac{d\hat{\rho}(t)}{dt} = -\frac{i}{\hbar}\left[\hat{H}, \hat{\rho}(t)\right] - \frac{\lambda A^2 \bar{\gamma}}{2} \sum_{i=L,R} \left[\hat{a}_i^\dagger \hat{a}_i, \left[\hat{a}_i^\dagger \hat{a}_i, \hat{\rho}(t)\right]\right]. \tag{4.5}$$

To have an explicit solution, we neglect the hopping term in the Hamiltonian operator of eq. (2.34). As shown in appendix C, the solution of eq. (4.5) is

$$\begin{aligned}\hat{\rho}(t) &= e^{\frac{4iUt}{\hbar}\hat{a}_L^\dagger \hat{a}_L \hat{a}_R^\dagger \hat{a}_R} e^{-\lambda A^2 \bar{\gamma} t \left(\overleftarrow{\hat{a}_R^\dagger \hat{a}_R} - \overrightarrow{\hat{a}_R^\dagger \hat{a}_R}\right)^2} \hat{\rho}(0) e^{-\frac{4iUt}{\hbar}\hat{a}_L^\dagger \hat{a}_L \hat{a}_R^\dagger \hat{a}_R} \\ &= e^{-\lambda A^2 \bar{\gamma} t \left(\overleftarrow{\hat{a}_R^\dagger \hat{a}_R} - \overrightarrow{\hat{a}_R^\dagger \hat{a}_R}\right)^2} \hat{\rho}_{\mathrm{Sch}}(t),\end{aligned} \tag{4.6}$$

where $\overleftarrow{\hat{a}_R^\dagger \hat{a}_R}\left(\overrightarrow{\hat{a}_R^\dagger \hat{a}_R}\right)$ acts on the left (right) of the density matrix, and

$$\hat{\rho}_{\mathrm{Sch}}(t) = e^{\frac{iUt}{\hbar}\hat{a}_L^\dagger \hat{a}_L \hat{a}_R^\dagger \hat{a}_R} \hat{\rho}(0) e^{-\frac{iUt}{\hbar}\hat{a}_L^\dagger \hat{a}_L \hat{a}_R^\dagger \hat{a}_R} \tag{4.7}$$

is the density matrix evolved under the only Schrödinger dynamics.

4.1.1 Decoherence effects due to CSL model

Let us see how an initial phase state (2.37) evolves under the CSL dynamics, by looking in particular to the coherence properties given by eq. (2.39). From eq. (4.6), it is possible to see that (see Appendix C):

$$\langle \hat{a}_L^\dagger \hat{a}_R \rangle_t^{\mathrm{CSL}} = \mathrm{Tr}\left[\hat{a}_L^\dagger \hat{a}_R \hat{\rho}(t)\right] = e^{-\lambda A^2 \bar{\gamma} t} \langle \hat{a}_L^{\dagger N} \hat{a}_R^N \rangle_t^{\mathrm{Sch}}. \tag{4.8}$$

Taking into account the Schrödinger evolution of the phase state coherence (2.44), we obtain

$$\begin{aligned}\langle \hat{a}_L^\dagger \hat{a}_R \rangle_t^{\mathrm{CSL}} &= N e^{-\lambda A^2 \bar{\gamma} t} \frac{e^{i\phi}}{2} \left[\cos\left(\frac{tU}{\hbar}\right)\right]^{N-1} \\ &\approx N \frac{e^{i\phi}}{2} e^{-\lambda A^2 \bar{\gamma} t} e^{-N\left(\frac{tU}{\hbar}\right)^2},\end{aligned} \tag{4.9}$$

where the last line is true only for $t \ll \hbar/|U|$.
From eq. (4.9), it is cleat that the action of the CSL dynamics is to break the spatial superposition (2.39) of the phase state. Since, in this case, the many-body state is a coherent factorization of delocalized single particle states, then an amplification mechanism is missing, and the CSL collapse rate does not depend on the total number of particles N. Thus, the use of phase states such as (2.37) to set experimental bounds on the CSL parameters is not convenient in general.

As for example, let us consider the experiment [99], where the long coherence time of 200 ms with a gas of ^{23}Na atoms was observed. Using eq. (4.4), we have that the exponential decrease of the coherence in eq. (4.9) induced by CSL dynamics becomes experimentally visible only if $\lambda \geq 1/(tA^2)$. Then from eq. (4.9) it is possible to put a bound of $\lambda \leq 10^{-2}$ s^{-1}. This is a weak bound for two main reasons: firstly, the expected values of the collapse rate λ theoretically predicts by Ghirardi, Rimini and Weber ($\lambda = 10^{-16}$ s^{-1}) and by Adler ($\lambda = 10^{-8\pm2}$ s^{-1} and $\lambda = 10^{-6\pm2}$ s^{-1}) are much smaller than 10^{-2} s^{-1}; secondly, much stronger bounds have been set by other experiments, as can be seen in the exclusion plot 4.2. Let us now consider the CSL evolution of the macroscopically entangled states (2.48) and (2.50). In this case, the N-particles coherence properties (2.49) and (2.51) are preserved by Schrödinger evolution. Using eq. (4.6), as discussed in appendix C it is possible to see that

$$\langle \hat{a}_L^{\dagger N} \hat{a}_R^N \rangle_t^{\mathrm{CSL}} = e^{-\lambda N^2 A^2 \tilde{\gamma} t} \langle \hat{a}_L^{\dagger N} \hat{a}_R^N \rangle_t^{\mathrm{Sch}}. \tag{4.10}$$

Differently from the phase decoherence case (4.9), the exponential decoherence of the macroscopically entangled states (4.10) is faster due to a factor N^2. This is due to the macroscopicity of the states (2.48) and (2.50),*i.e.*, these are superposition of localized N-particles states, which is expressed by the N-particles quantum coherences (2.49) and (2.51). As a consequence, an amplification mechanism occurs in the CSL dynamics, increasing the collapse rate by a factor N^2.

In fig. 4.2 we picture the exclusion plot for an hypothetical experiment involving the macroscopically entangled states (2.48) or (2.50).To proceed further, we have to fix a time t for which the N-particles coherences (2.49) and (2.51) The longer the time t, the smaller the number of atoms needed to use (the dependence on the time is linear, the one on the number is quadratic). An inspection of results show that in order to have both reasonable values for the particle number N and at the same time explore the white region in fig. 4.2, the one not yet excluded by experiments, one has to use $t \sim 1$ s. This is presently a very challenging request, and the goal of the present computation is to clarify and predict what value of t is needed to explore the uncovered region of the CSL parameter space for N going from 10^2 to 10^6.We then choose $t = 1$ s and we considered a Rb gas, with width of each well given by σ, and with the two wells distant d. With $d = 10\mu$ m the ratio U/J is negligleable, and the results for $J = 0$ apply and are plotted in fig. 4.2 for three different values of N (with $\sigma \approx 1\mu$ m). Also reducing d in order to have a finite J does not quantitatively change the region that can be explored in the $\lambda - r_C$ space (actually, we expect it shrinks) - similarly increasing σ, which results in decreasing U, does not change

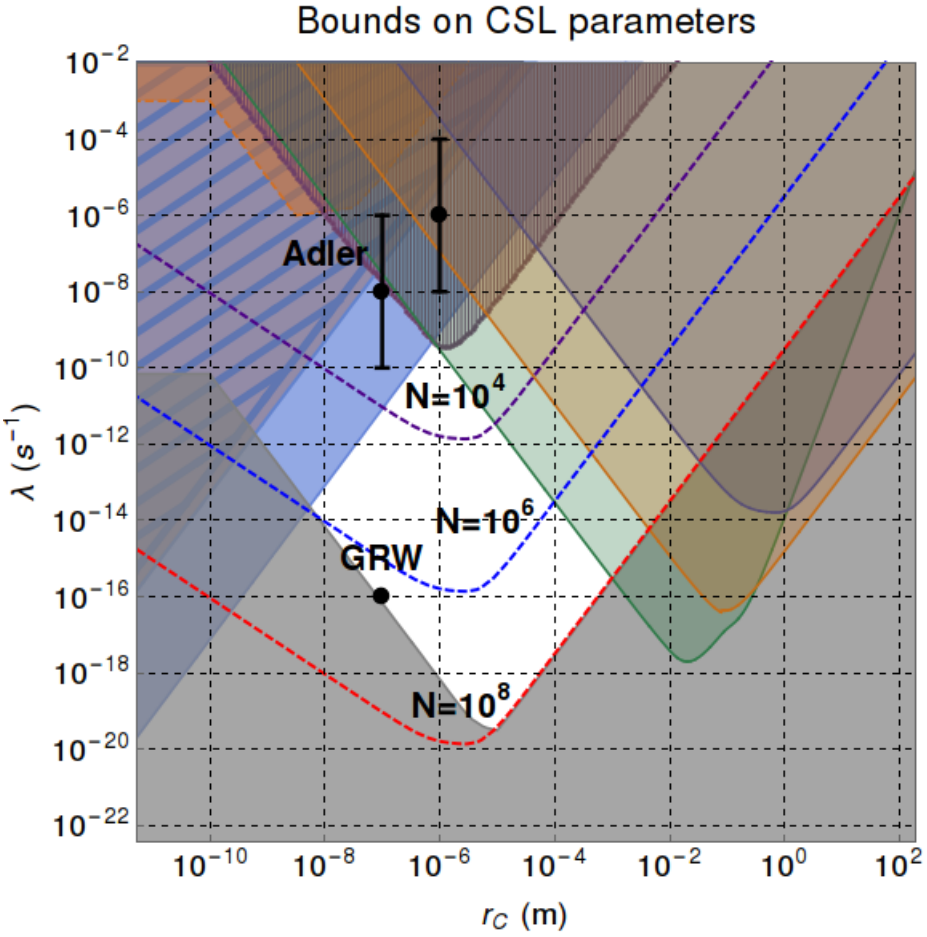

Figure 4.2: Most recent exclusion plot of the CSL model [127](non-white regions), where we added the bounds for an hypothetical experiment involving the macroscopically entangled states (2.48),(2.50). Here, we made the hypothesis that their N-particles coherences are preserved for a time $t = 1$ s, with three different number of particles: $N = 10^4$ (purple dashed line), 10^6 (blue dashed line) and 10^8 (red dashed line). The excluded regions are the upper part of the related dashed line.

the boundaries of the region, as soon as the two-mode approximation holds. We conclude that with $t = 1$ s one needs $N \sim 10^3 - 10^4$ to enter the white region not yet explored and that with the (presently prohibitive) number $N = 10^8$ the whole white region can be probed.

From fig. (4.3), where the time evolution (4.10) is represented, the strong dependence on N is clear.

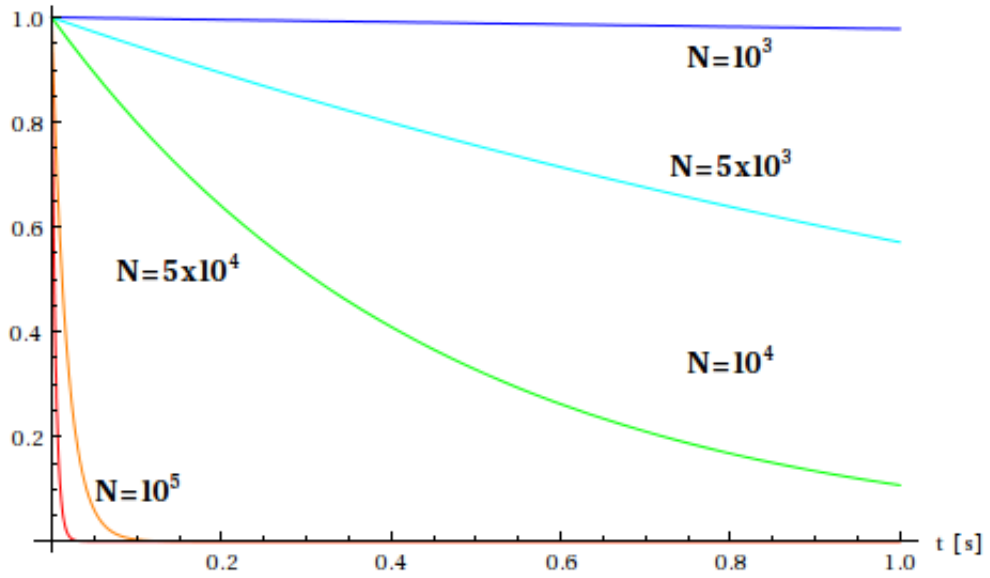

Figure 4.3: Time evolution (4.10) of the normalized N-particles coherences, for different number of atoms. Here we fixed the CSL parameters $\lambda = 10^{-11}\,\mathrm{s}^{-1}$ and $r_C = 10^{-7}$ m, which are among the weakest parameters of the white region in fig. 4.2.

4.2 CSL model for a condensate in an optical lattice

A direct extension of the double well potential to a multi well potential is given by a BEC in an optical lattice described in sec. 2.3. Let us rewrite the CSL master equation (1.35) in the basis of the Wannier functions (2.57) (neglecting the higher bands):

$$\frac{d\hat{\rho}(t)}{dt} = -\frac{i}{\hbar}\left[\hat{H},\hat{\rho}(t)\right] - \frac{\lambda A^2}{2}\sum_{\substack{i,j\\k,l}}\gamma_{k,l}^{i,j}\left[\hat{a}_i^\dagger\hat{a}_j,\left[\hat{a}_k^\dagger\hat{a}_l,\hat{\rho}(t)\right]\right], \tag{4.11}$$

where $\gamma_{k,l}^{i,j}$ has the expression given in eq. (4.2) but, in this case, the single particle wave functions are the Wannier functions (2.57). The Hamiltonian operator is the Bose Hubbard Hamiltonian given in eq. (2.58).
As for a double well potential, here we neglect the hopping term in the Hamiltonian operator (i.e., we set $J = 0$). Then, the solution of the master equation (4.11) is

$$\hat{\rho}(t) = e^{-\lambda A^2 t\sum_{i,j}\gamma_{i,j}\left(\hat{a}_i^\dagger\overleftarrow{\hat{a}_i}-\hat{a}_i^\dagger\overrightarrow{\hat{a}_i}\right)\left(\hat{a}_j^\dagger\overleftarrow{\hat{a}_j}-\hat{a}_j^\dagger\overrightarrow{\hat{a}_j}\right)}\hat{\rho}_{\mathrm{Sch}}(t), \tag{4.12}$$

where $\gamma_{i,j} = \gamma_{j,j}^{i,i}$. This master equation is the extension of the two mode master equation (4.6) to the multi mode case.

Let us consider the coherent state in an optical lattice [25]:

$$|\psi\rangle = \frac{1}{\sqrt{N!}} \left(\frac{1}{\sqrt{M}} \sum_{i=1}^{M} \hat{a}_i^\dagger \right)^N |0\rangle \,, \tag{4.13}$$

where M is the number of sites in the optical lattice, and N is the number of atoms. This state has long range coherence properties, which are expressed by the off-diagonal elements of the single particle density matrix:

$$\langle 0| \, \hat{a}_j \hat{\rho}^{(1)} \hat{a}_i^\dagger \, |0\rangle = \frac{1}{N} \langle \psi| \, \hat{a}_i^\dagger \hat{a}_j \, |\psi\rangle \equiv \frac{1}{N} \langle \hat{a}_i^\dagger \hat{a}_j \rangle. \tag{4.14}$$

Indeed, for the state (4.13) we get

$$\langle \hat{a}_i^\dagger \hat{a}_j \rangle = \frac{N}{M}. \tag{4.15}$$

The effect of the CSL model on the state (4.13) is to destroy the off-diagonal elements (4.15) with an exponential time decay. This is computed using eq. (4.12):

$$\langle \hat{a}_i^\dagger \hat{a}_j \rangle_t^{\mathrm{CSL}} = \mathrm{Tr} \left[\hat{a}_i^\dagger \hat{a}_j \hat{\rho}(t) \right] = e^{-\lambda A^2 \gamma_{i,j} t} \langle \hat{a}_i^\dagger \hat{a}_j \rangle_t^{\mathrm{Sch}}. \tag{4.16}$$

It is easy to note that the dynamics of the two mode coherent state, given in eq. (4.8), and the dynamics of the multi mode coherent state given in eq. (4.16) are the same. As for the two mode case, the decoherence effect induced by CSL to the coherent state (4.13) is not enhanced by the number of atoms in the lattice. The physical reason is the same: in the coherent state all the atoms are in the same delocalized single particle state. The CSL dynamics acts by destroying these single particle delocalizations, and no amplification mechanism occurs.

On the contrary, the amplification mechanism enhances the decoherence effects of the CSL model on the lattice NOON state, defined by

$$|\mathrm{NOON}\rangle = \frac{1}{\sqrt{M(N!)}} \sum_i \left(\hat{a}_i^\dagger \right)^N |0\rangle \,. \tag{4.17}$$

This is a macroscopic entangled state, as seen by the following identities

$$\langle \mathrm{NOON}| \, \hat{a}_i^{\dagger k} \hat{a}_j^k \, |\mathrm{NOON}\rangle = \begin{cases} 0, & \text{if } k < N; \\ \frac{(N!)^2}{M}, & \text{if } k = N. \end{cases} \tag{4.18}$$

The relations expressed in eq. (4.18) are totally equivalent to the two mode case, expressed in eq. (2.51). The CSL effects in this case are increased by the number of atoms in the lattice:

$$\langle \hat{a}_i^{\dagger N} \hat{a}_j^N \rangle_t^{\mathrm{CSL}} = e^{-\lambda N^2 A^2 \gamma_{i,j} t} \langle \hat{a}_i^{\dagger N} \hat{a}_j^N \rangle_t^{\mathrm{Sch}}. \tag{4.19}$$

Comparing eq. (4.19) with the related two mode case, expressed in eq. (4.10), it is evident that the CSL dynamics is the same. Indeed, the CSL model acts by destroying N-particles coherences, thus the amplification mechanism lead to a faster localization process.

From the comparison between the two mode case to the multi mode case, we can thus conclude that the bounds on the CSL paramenters that are expected from the experiments are not modified by an increase of the number of sites in the system. So, at least from a theoretical point of view, searching for experimental bounds on a BEC in a double well potential or on an optical lattice is the same.

4.3 Environmental decoherence on a condensate: comparison with CSL effects

Problems in testing CSL dynamics in experiments usually arise from environmental decoherence sources, leading to similar loss of coherences. This is the topic of this section, in which we compare the decoherence of the CSL noise with the decoherence induced by the external environment. In particular, we focus on four main sources, i.e., the thermal cloud surrounding the condensate, the three body recombination processes, phase noise and the trapping laser. We then study the conditions that experiments have to fulfill in order to reduce the environment decoherence, which is a necessary condition to detect CSL effects.

4.3.1 Interaction with a thermal cloud

Even if the temperature is very low, a small amount of thermally excited atoms is always present. Atoms in excited states interact with the condensate, leading to two main effects: a loss of atoms from the condensate to the thermal cloud; and a decoherence on the condensate in the position basis. As reviewed in appendix C, the master equation describing the dynamics of a condensate interacting with its thermal cloud is:

$$\frac{d\hat{\rho}(t)}{dt} = -\frac{i}{\hbar}\left[\hat{H}, \hat{\rho}(t)\right] + \sum_{i=1,2} \mathcal{L}_t^{(i)}\left[\hat{\rho}(t)\right] , \tag{4.20}$$

where $\mathcal{L}_t^{(1)}\left[\hat{\rho}(t)\right]$ describes the atom losses dynamics, which can be written in the following way for the particular case of a condensate in a double well potential [104]:

$$\mathcal{L}_t^{(1)}\left[\hat{\rho}(t)\right] = \Lambda_{\text{loss}} \sum_{j=L,R} \hat{a}_j \hat{\rho}(t) \hat{a}_j^\dagger - \frac{1}{2}\left\{\hat{a}_j^\dagger \hat{a}_j, \hat{\rho}(t)\right\} , \tag{4.21}$$

where Λ_{loss} is the rate of atom losses from the condensate to the thermal cloud, which, according the discussion in Appendix C is given by the following local correlation function of the thermal cloud

$$\Lambda_{\text{loss}} = \frac{g^2}{\hbar^2} \int d\mathbf{x} \; |\psi_L(\mathbf{x})|^2 \, \text{Tr} \left[\hat{a}^\dagger(\mathbf{x}) \hat{a}^\dagger(\mathbf{x}) \hat{a}^\dagger(\mathbf{x}) \hat{a}(\mathbf{x}) \hat{a}(\mathbf{x}) \hat{a}(\mathbf{x}) \hat{\rho}_{\text{therm}} \right] . \tag{4.22}$$

The term $\mathcal{L}_t^{(2)} [\hat{\rho}(t)]$ introduced in eq. (4.20) describes interactions between the condensate (C) and non condensate (NC) atoms of the type $C + NC \to C + NC$. This interaction is in position, and leads to a decoherence dynamics that preserves the populations of the gas. In particular, for a double well potential, the following identity holds

$$\mathcal{L}_t^{(2)} [\hat{\rho}(t)] = -\frac{\Lambda_{\text{dec}}}{2} \sum_{j=L,R} \left[\hat{a}_j^\dagger \hat{a}_j, \left[\hat{a}_j^\dagger \hat{a}_j, \hat{\rho}(t) \right] \right] , \tag{4.23}$$

where

$$\Lambda_{\text{dec}} = \frac{g^2}{\hbar^2} \int d\mathbf{x} \, \text{Tr} \left[\hat{a}^\dagger(\mathbf{x}) \hat{a}(\mathbf{x}) \hat{a}^\dagger(\mathbf{x}) \hat{a}(\mathbf{x}) \hat{\rho}_{\text{therm}} \right] |\psi_L(\mathbf{x})|^4 . \tag{4.24}$$

Let us consider first the term in eq. (4.22). Neglecting the Hamiltonian dynamics, it is easy to see that the N-particles correlation has the following time dependence:

$$\langle \hat{a}_L^{\dagger N} \hat{a}_R^N \rangle_t^{\text{loss}} = e^{-\Lambda_{\text{loss}} N t} \langle \hat{a}_L^{\dagger N} \hat{a}_R^N \rangle_0 . \tag{4.25}$$

Differently from the CSL case (4.10), the decoherence rate induced by atom losses increases linearly with the number of atoms. If we consider, for example, the experimental setup described in [113], the authors measured $\Lambda_{\text{loss}} \approx 4 \times 10^{-3}$ s^{-1} for a non-homogeneous gas at fractional temperature $T/T_C \approx 1/3$, where T_C is the critical temperature of the gas. Comparing the decay rates of the CSL model in eq. (4.10) with the decay given by the atomic losses as in eq. (4.25) with the parameters given in [113], the CSL damping turns out to be faster only if the NOON state is composed by $N > \Lambda_{\text{loss}} / \left(\lambda A^2 \right) \approx 10^{10}$ atoms, considering the value $\lambda = 10^{-17}$ s^{-1} as proposed in [43], and $A \approx 100$. From eq. (4.22), the decoherence rate induced by the atomic losses can be reduced either by a proper decreasing of the temperature of the gas (so reducing the thermal density) or by decreasing the coupling interaction, which can be achieved by use of Feshbach resonances. We have that

$$\Lambda_{\text{loss}} \approx \frac{g^2 n_{\text{therm}}^3}{\hbar^2} . \tag{4.26}$$

In order to detect CSL effects on a NOON state with, for example $N = 10^8$ atoms (the number of atoms we need in order to probe the whole unexplored region of the parameter space, as shown in fig. 4.2), eq. (4.26) shows that the experimental setup described in [113] must be modified either by reducing the thermal density or by decreasing the coupling constant of one order of magnitude.

Let us now focus on the term in eq. (4.23). We immediately note the similarities between the eq. (4.23) and the CSL master equation (4.5), with $\lambda A^2 \to \Lambda_{\text{dec}}$. Through

eqs. (4.24) and (4.26), it is possible to relate the decoherence rate due to the atomic losses to the decoherence rate described in eq. (4.23) as follows (see Appendix C):

$$\Lambda_{\text{dec}} \approx \frac{\Lambda_{\text{loss}}}{N_{\text{therm}}}, \tag{4.27}$$

where N_{therm} is the number of atoms in the thermal cloud. If we consider again the experiment described in [113], we have roughly that $N_{\text{therm}} \approx N\left(T/T_C\right)^3 \approx 10^4$, where we used the relation between the total number of atoms with the number in the thermal cloud of an ideal gas in an harmonic trap [26]. Using then eq. (4.27) we have $\Lambda_{\text{dec}} \approx 4 \times 10^{-10}\ \text{s}^{-1}$. Taking into account that we need $\Lambda_{\text{dec}} < \lambda A^2 \approx 10^{-13}\ \text{s}^{-1}$, the experimental setup described in [113] must be modified either by reducing the thermal density or by decreasing the coupling constant by two orders of magnitude.

We conclude this part on thermal decoherence by stating that the atomic losses can be further reduced by using a special model for the Bose Einstein condensate [128]. In this case, the condensate is trapped in a deep but narrow spherical potential, chosen in such a way that there is only one single-particle bound state (condensate mode) and a continuum of excited modes (non condensate modes). If the binding energy of the condensate is much higher then the thermal energy of the non condensate atoms, then the fugacity satisfies $z \ll 1$. The presence of condensation, in this model, is due to the depth of the potential. As discussed in [128], this regime allows to neglect the atom losses, and to consider only the term in eq. (4.23).

4.3.2 Three body recombination processes

We consider here the effect of three body recombination processes, according to which atoms leave the trap, with negligible probability that they interact again with other atoms in the trap. We write the effective master equation describing the dynamics of a Bose Einstein condensate with three body recombination processes [104, 129–131] in the form

$$\frac{d\hat{\rho}(t)}{dt} = -\frac{i}{\hbar}\left[\hat{H}, \hat{\rho}(t)\right] + \Lambda_3 \sum_{j=L,R} \hat{a}_j^3 \hat{\rho}(t) \hat{a}_j^{\dagger 3} - \frac{1}{2}\left\{\hat{a}_j^{\dagger 3}\hat{a}_j^3, \hat{\rho}(t)\right\}, \tag{4.28}$$

where

$$\Lambda_3 \approx \frac{\hbar a_S^4}{m} \int d\mathbf{x} \left|\psi_L\left(\mathbf{x}\right)\right|^6 . \tag{4.29}$$

Using eqs. (4.28) and (4.31), one finds the following relation:

$$\langle \hat{a}_L^{\dagger N} \hat{a}_R^N \rangle_3 (t) = e^{-\frac{\hbar a_S^4 n_{\text{BEC}}^2}{m} N t} \langle \hat{a}_L^{\dagger N} \hat{a}_R^N \rangle_0 , \tag{4.30}$$

where n_{BEC} is the condensate density. Comparing the three body decoherence rate in eq. (4.30) with the CSL decoherence rate $\lambda A^2 N^2$, we have a lower bound on the

number of atoms of the NOON state,

$$N \geq \frac{\hbar a_S^4 n_{\text{bec}}^2}{m\lambda A^2}\,. \tag{4.31}$$

Consider, for example, the experimental measure described in [113], where $\hbar a_S^4/m \approx 5\times 10^{-30}$ cm^6/s and the peak density of the condensate is 5×10^{14} cm^{-3}. In this case, the CSL decoherence is faster if $N \geq 10^{13}$ atoms, for the particular case of $\lambda = 10^{-17}$ s^{-1}. The three body decoherence rate can be decreased either by reducing the condensate density or by reducing the scattering length through the use of Feshbach resonance. For example, if we consider an experiment with a condensate density of $\approx 10^{13}$ cm^{-3} and a scattering length $a_S \leq 10^{-9}$ m, the CSL localization dynamics is dominant with $N \geq 10^7$ atoms.

4.3.3 Laser decoherence: phase noise and spontaneous photon emission

A very common technique to trap atoms is by using an external laser source. Thanks to the large experimental control on the laser electric field, several external potentials can be realized, with a large control on the parameters of the trap [27]. However, every optical trap is also a decoherence source for the trapped atomic system, leading to decoherence of the atomic density matrix in the position basis. Two of the main decoherence sources due to the laser are a phase noise, induced by fluctuations of the laser beam pointing [132], and spontaneous photon emission processes from the atoms [108, 109, 133].

Phase noise

The phase noise in a Bose Josephson junction can be studied and treated as a stochastic noise modifying the energy levels of the system [132]. The effective density matrix evolution is given by:

$$\hat{\rho}(t) = \int_{-\infty}^{+\infty} d\phi\, f(\phi,t) e^{-i\phi\hat{a}_R^\dagger\hat{a}_R}\hat{\rho}_{\text{Sch}}(t)e^{i\phi\hat{a}_R^\dagger\hat{a}_R}. \tag{4.32}$$

If the phase noise is a Gaussian noise with null average, then we have that

$$f(\phi,t) = \frac{1}{\sqrt{2\pi}\Delta(t)} e^{-\frac{\phi^2}{2\Delta^2(t)}}. \tag{4.33}$$

where the variance $\Delta^2(t)$ completely characterizes the noise. Using eq. (4.33) in eq. (4.32), the density matrix evolution of a Bose Josephson junction under a Gaussian phase noise is:

$$\hat{\rho}(t) = e^{-\frac{\Delta^2(t)}{2}\left(\hat{a}_R^\dagger\overleftarrow{\hat{a}_R} - \hat{a}_R^\dagger\overrightarrow{\hat{a}_R}\right)^2}\hat{\rho}_{\text{Sch}}(t). \tag{4.34}$$

By comparing eq. (4.34) with the density matrix evolution under the CSL dynamics eq. (1.35), it is clear that the latter one can be tested only if the phase noise is reduced enough in the experiment. In [30], the authors studied the effect of the fluctuations of the laser beam pointing on a single well potential for a gas of ^{133}Cs atoms. In this work, the heating effect induced by the phase noise results to be negligible, compared to the heating of the CSL model, if $\lambda > 10^5 (r_C/(1\,\mathrm{m}))^2\ \mathrm{s}^{-1}$. If we choose the value of $r_C = 10^{-7}$ m (as proposed in [42, 43]), then, for the experimental setup described in [30], the phase noise becomes negligible if $\lambda > 10^{-9}\ \mathrm{s}^{-1}$. This means that the interesting part of the parametric space shown in fig. 4.2 cannot be explored by such experimental setup due to a too strong phase noise. For example, in order to test CSL effects with the parameters $\lambda = 10^{-16}\ \mathrm{s}^{-1}$ $r_C = 10^{-7}$ m, then the phase noise should be reduced by a power 10^{-7}, showing the very high control on the phase noise needed to explore the $\lambda - r_c$ parameter space.

Spontaneous photon emission processes

Another decoherence source related to optical traps is due to the spontaneous photon emission. In [133], the authors derived the master equation for two levels atoms in a far-detuned optical trap, which is given by:

$$\begin{aligned}\frac{d\hat{\rho}(t)}{dt} = &-\frac{i}{\hbar}\left[\hat{H}, \hat{\rho}(t)\right] - \frac{\Gamma}{8\delta^2}\int d\mathbf{y}\int d\mathbf{y}'\,\Omega(\mathbf{y})\Omega(\mathbf{y}')\times \\ &\mathrm{F}\left(k\left(\mathbf{y}-\mathbf{y}'\right)\right)\left[\hat{a}^\dagger(\mathbf{y})\hat{a}(\mathbf{y}), \left[\hat{a}^\dagger(\mathbf{y}')\hat{a}(\mathbf{y}'), \hat{\rho}(t)\right]\right],\end{aligned} \tag{4.35}$$

where Γ is the spontaneous emission rate; $\delta = \omega_l - \omega_0$, ω_l is the frequency of the laser, ω_0 is the frequency resonance of the two levels atoms; $k = \omega_0/c$ with c speed of light in vacuum; $\Omega(\mathbf{x}) = \mathbf{d}\cdot\mathbf{E}(\mathbf{x})/\hbar$ Rabi frequency, related to the effective optical trap by

$$V(\mathbf{x}) = \hbar\frac{|\Omega(\mathbf{x})|^2}{4\delta}. \tag{4.36}$$

The function $\mathrm{F}(\mathbf{z})$ in eq. (4.35) is defined by the following integration:

$$\mathrm{F}(\mathbf{z}) = \int_{\|\mathbf{u}\|=1} d\mathbf{u}\, \mathrm{e}^{-i\mathbf{u}\cdot\mathbf{z}}. \tag{4.37}$$

We note that the spontaneous emission master equation (4.35) has the same form of the CSL master equation (1.35), with the replacement:

$$\lambda A^2 e^{-\frac{(\mathbf{y}-\mathbf{y}')^2}{4r_c^2}} \to \frac{\Gamma}{4\delta^2}\Omega(\mathbf{y})\Omega(\mathbf{y}')\mathrm{F}\left(k\left(\mathbf{y}-\mathbf{y}'\right)\right). \tag{4.38}$$

Using eq. (2.33) in eq. (4.35), with a similar procedure used to find eqs. (4.5) and (4.6), it is possible to write down the density matrix for a gas of atoms trapped in an optical trap with spontaneous emission process:

$$\hat{\rho}(t) = e^{-\frac{\Gamma\bar{\Omega}t}{4\delta^2}\left(\hat{a}_R^\dagger\overleftarrow{\hat{a}_R} - \hat{a}_R^\dagger\overrightarrow{\hat{a}_R}\right)^2}\hat{\rho}_{\mathrm{Sch}}(t), \tag{4.39}$$

where

$$\bar{\Omega} = \int d\mathbf{y} \int d\mathbf{y}' \, \Omega(\mathbf{y})\Omega(\mathbf{y}')\mathrm{F}\left(k\left(\mathbf{y}-\mathbf{y}'\right)\right) \times \\ |\psi_L(\mathbf{y})|^2 \left(\left|\psi_L(\mathbf{y}')\right|^2 - \left|\psi_R(\mathbf{y}')\right|^2\right). \tag{4.40}$$

Compared to the CSL dynamics given in eq. (4.6), the spontaneous emission processes are negligible only if $\lambda A^2 \bar{\gamma} \gg \Gamma\bar{\Omega}/\left(4\delta^2\right)$. For example, let us consider the experimental setup described in [96], where a laser with wavelength of 1064 nm is used to trap a gas of ^{39}K atoms. The resonance frequency of ^{39}K is $\omega_0 \approx 390$ THz. Setting $r_C = 10^{-7}$ m, we have that hypothetical CSL effects would be visible only if $\lambda > 10^{-12}$ s^{-1}. This means that the decoherence induced by spontaneous photon emission is strong enough to cover a large part of the parametric space shown in fig. 4.2. In order to probe the interesting part of the CSL parametric space, the spontaneous photon emission should be reduced by a power 10^4. We conclude that the laser decoherence effects discussed in this and the previous sections are alleviated by using magnetic traps [68].

Conclusions

In this thesis we have studied the effects of dynamical reduction models on Bose Einstein condensates. In particular, in chapter 3 we studied the heating effects induced by the noise, which are mainly two: a temperature increase of the gas, and a diffusion process of the atoms.
For the CSL model, the results are expressed in the exclusion plot in fig. 3.6. The bounds found with cold atomic systems, and in particular the one given by the diffusion processes in a free expanding gas, turn out to be better than the bound set by matter-wave interferometer and, partly, by cantilever experiment. They are beaten by X-rays experiment and, for $r_C \geq 10^{-7}$ m, by cantilever experiment.
We studied the diffusion processes in a free expanding gas also given by cCSL and dCSL model. For the non-Markovian model, we found that our CSL bound result to be robust against changes in the noise frequency cut-off. Precisely, providing $r_C \geq 10^{-7}$ m, for any cutoff larger than 10^6 Hz (which is the case of cosmological noises), the effect in the cCSL model is equivalent to that of the standard CSL model. This is a very important result, because CSL predictions for spontaneous photon emission are very sensitive to the type of noise and, when a frequency cut-off is introduced in its spectrum, the CSL effect is significantly decreased. In particular, for X-ray detection, any cutoff smaller than 10^{18} Hz (typical cut-offs of cosmological spectra are significantly smaller than this value) washes the effect away.
For the dCSL model, the bounds we found are reported in fig. 3.7, for three different temperatures of the noise: $T_{\text{CSL}} = 1, 10^{-6}, 10^{-12}$ K. In this case, the diffusion effect of the noise become weaker, still remaining non-negligible down to very small temperatures.

In chapter 4 we studied the localization dynamics of the CSL model for a condensate in a double well potential. We have seen that coherence properties of atomic coherent states are practically left unchanged by the CSL dynamics. Vice versa, coherence properties of macroscopic entangled states such as the NOON states are exponentially damped by CSL dynamics in a way that can be experimentally tested. We observed that, through an hypothetical experiment observing the N-particles coherence of a NOON state for 1 s, it is possible to probe the unexplored part of the parameters space of the CSL model with reasonable numbers of atoms. The results are summarized in fig. 4.2. In the $\lambda - r_C$ parameter space there is presently a region not yet explored, and we pointed out that having entangled states, as the NOON

state, with $N \gtrsim 10^3$ and coherence time $t \gtrsim 1$ s would make possible to probe such a region. A similar outcome may be obtained when considering entangled states in an array of weakly coupled ultracold bosonic gases described by the Bose-Hubbard model or by varying the distance between (and the width of) the wells.
We have also compared the CSL decoherence with the environmental decoherence due to three main sources: a thermal cloud, the three body recombination processes, and the laser trapping field. Using standard experimental values for the parameters of each source, we noted that the environmental decoherence, generally, covers the effects of the CSL dynamics. We then determined what requests the experimental values have to satisfy in order to put new bounds for the parameters of the CSL model in the white region of fig. 4.2. Although very demanding for current-day experiments, our results together with the recent very promising results on the implementation of squeezed states and the detection multi-particle correlations [82] show that in perspective further advancements in the manipulation of highly-entangled states may open the possibility to study collapse models and to test quantum mechanics with ultracold atoms in double well potentials.

Acknowledgements

I wish to thank my supervisor Prof. Angelo Bassi for all the time he spend for me by reading and correcting the thesis. I want to thank Angelo also for all the time he spend for me during these three years of Ph.D., during which we had several useful physics discussions and good free time.

I wish to thank Dr. Andrea Trombettoni for all the useful discussions we had in the last months. In particular, I want to thank Andrea for all the help he is giving to me during my search for a postdoc position.

I wish to thank all the colleagues that I had the luck to met during these three years. I wish to thank Dr. Andrea Vinante and Dr. Mauro Schiulaz for the useful discussions we had, and, in particular I want to thank Mauro also for all the good free time we had together. I wish to thank all the past and current members of Angelo's group that I had the luck to met, as G. Gasbarri, M. Toros, Dr. S. Donadi, Dr. L. Ferialdi, M. Carlesso, L. Curcuraci, S. Bacchi, S. Marcantoni, M. Caiaffa, Dr. A. Smirne, Dr. A. Großardt, Dr. M. Bahrami for all the physics discussions we had in these three years and for the good free time we had together.

Ringrazio la mia famiglia che mi ha sostenuto e supportato durante questo dottorato. Ringrazio in particolare i miei genitori che mi sono sempre stati vicini in questi anni.

And, last but not least, I wish to thank all my friends for all the good times we had, always ready to go out for a beer and spend some time together!

Appendix A

Bose Einstein condensate in a double well potential: some useful results.

In this appendix we proof some important relations that we introduced in chapter 2 on the double well potential. This results are used in chapter 4 for the study of the localization dynamics of a Bose Einstein condensate due to the CSL model.

A.0.1 Proof of eq. (2.44).

From the definition of atomic coherent state in eq. (2.37), using the Hamiltonian defined in eq. (2.34) with $J = 0$, we have that

$$\begin{aligned}
&\langle \hat{a}_L^\dagger \hat{a}_R \rangle_t = \langle \phi | \, e^{\frac{i}{\hbar}\hat{H}t} \hat{a}_L^\dagger \hat{a}_R e^{-\frac{i}{\hbar}\hat{H}t} \, | \phi \rangle \\
&= \frac{1}{N! 2^N} \sum_{j,k=0}^{N} \binom{N}{k} \binom{N}{j} e^{i\phi(j-k)} \, \langle 0 | \, \hat{a}_L^{N-k} \hat{a}_R^k \\
&e^{-\frac{i}{\hbar}tU\hat{a}_L^\dagger \hat{a}_L \hat{a}_R^\dagger \hat{a}_R} \hat{a}_L^\dagger \hat{a}_R e^{\frac{i}{\hbar}tU\hat{a}_L^\dagger \hat{a}_L \hat{a}_R^\dagger \hat{a}_R} \left(\hat{a}_L^\dagger\right)^{N-j} \left(\hat{a}_R^\dagger\right)^j | 0 \rangle \\
&= \frac{1}{N! 2^N} \sum_{j,k=0}^{N} \binom{N}{k} \binom{N}{j} e^{i\phi(j-k)} e^{-\frac{i}{\hbar}tUk(N-k)} e^{\frac{i}{\hbar}tUj(N-j)} \, \langle 0 | \, \hat{a}_L^{N-k} \hat{a}_R^{k+1} \left(\hat{a}_L^\dagger\right)^{N-j+1} \left(\hat{a}_R^\dagger\right)^j | 0 \rangle \\
&= \frac{e^{i\phi}}{N! 2^N} \sum_{k=0}^{N-1} \binom{N}{k} \binom{N}{k+1} e^{\frac{i}{\hbar}tU[(k+1)(N-k-1)-k(N-k)]} (N-k)!(k+1)! \\
&= N \frac{e^{i\left[\phi + (N-1)\frac{tU}{\hbar}\right]}}{2^N} \sum_{k=0}^{N-1} \binom{N-1}{k} e^{-\frac{2i}{\hbar}tUk} \\
&= N \frac{e^{i\left[\phi + (N-1)\frac{tU}{\hbar}\right]}}{2^N} \left(1 + e^{-\frac{2i}{\hbar}tU}\right)^{N-1} \\
&= N \frac{e^{i\phi}}{2} \left[\cos\left(\frac{tU}{\hbar}\right)\right]^{N-1}.
\end{aligned} \tag{A.1}$$

A.0.2 Proof of eqs. (2.49), (2.51)and their time evolution.

From the definition of atomic coherent state in eq. (2.37), the following result is obtained:

$$\begin{aligned}
&\langle \phi | \, \hat{a}_L^{\dagger k} \hat{a}_R^k \, | \phi + \pi \rangle \\
&= \frac{1}{N! 2^N} \sum_{l,m=0}^{N} \binom{N}{l} \binom{N}{m} e^{i\phi(l-m)} (-1)^m \, \langle 0 | \, \hat{a}_L^{N-l} \hat{a}_R^l \hat{a}_L^{\dagger k} \hat{a}_R^k \left(\hat{a}_L^\dagger\right)^{N-m} \left(\hat{a}_R^\dagger\right)^m | 0 \rangle \\
&= \frac{1}{N! 2^N} \sum_{l,m=0}^{N} \binom{N}{l} \binom{N}{m} e^{i\phi(l-m)} (-1)^m \delta_{l,k+m} l! \, (N-l+k)! \\
&= \frac{N!}{2^N} \sum_{l=0}^{N-k} \binom{N-k}{l} (-1)^{l-k},
\end{aligned} \tag{A.2}$$

from which eq. (2.49) follows. With a similar computation, the time evolution of eq. (A.2) becomes

$$\begin{aligned}
&\langle\phi|\, e^{-\frac{i}{\hbar}tU\hat{a}_L^\dagger\hat{a}_L\hat{a}_R^\dagger\hat{a}_R}\,\hat{a}_L^{\dagger k}\hat{a}_R^k\, e^{\frac{i}{\hbar}tU\hat{a}_L^\dagger\hat{a}_L\hat{a}_R^\dagger\hat{a}_R}\,|\phi+\pi\rangle \\
&= \sum_{l,m=0}^{N}\binom{N}{l}\binom{N}{m}e^{i\phi(l-m)}(-1)^m\delta_{l,k+m}l!\,(N-l+k)!e^{\frac{iUt}{\hbar}[(N-l)l-(N-m)m]} \\
&= \frac{N!}{2^k}\,(-1)^k\,e^{i\phi k}i^{N-k}e^{-\frac{i}{\hbar}Utk^2}\left[\sin\left(\frac{Ukt}{\hbar}\right)\right]^{N-k}
\end{aligned} \tag{A.3}$$

As can be seen from the last identity in eq. (A.3), the unitary time evolution leads to a dephasing process except if $k = N$. The result expressed in eq. (2.51) and its time evolution are proved similarly.

Appendix B

CSL and dCSL dynamics for a free expanding gas

B.1 CSL dynamics: proof of eqs. (3.10), (3.11) and (3.12)

Let us specialize the CSL master equation in eq. (1.35) to the single atom case [32]:

$$\frac{d\hat{\rho}(t)}{dt} = -\frac{i}{\hbar}\left[\hat{H}, \hat{\rho}(t)\right] + \int d\mathbf{y}\left[\mathbb{L}(\mathbf{y})\hat{\rho}(t)\mathbb{L}^{\dagger}(\mathbf{y}) - \frac{1}{2}\left\{\mathbb{L}^{\dagger}(\mathbf{y})\mathbb{L}(\mathbf{y}), \hat{\rho}(t)\right\}\right]. \tag{B.1}$$

where the Hamiltonian is:

$$\hat{H} = \frac{\hat{\mathbf{p}}}{2m} + \frac{1}{2}m\omega^2\hat{\mathbf{x}}^2\,, \tag{B.2}$$

and the Lindblad operators $\mathbb{L}(\mathbf{y})$ are

$$\mathbb{L}(\mathbf{y}) = \sqrt{\frac{\lambda A^2}{\pi^{3/2} r_C^3}} e^{-\frac{|\hat{\mathbf{x}}-\mathbf{y}|^2}{2r_C^2}}\,. \tag{B.3}$$

Given $\langle\hat{\mathbf{x}}\rangle_{t_0} = \langle\hat{\mathbf{p}}\rangle_{t_0} = 0$ at some initial time t_0, from eq. (B.1) it is easy to see that at any time t the following identity holds:

$$\langle\hat{\mathbf{x}}\rangle_t = \langle\hat{\mathbf{p}}\rangle_t = 0 \tag{B.4}$$

i.e. CSL does not affect the average motion in position and momentum of the atoms. However, the same is not true for the standard deviations. In fact, considering the time evolution of $\hat{\mathbf{x}}^2, \hat{\mathbf{p}}^2$ in eq. (B.1), one finds that:

$$\frac{d\langle\hat{\mathbf{x}}^2\rangle_t}{dt} = \frac{1}{m}\langle\hat{\mathbf{x}}\cdot\hat{\mathbf{p}} + \hat{\mathbf{p}}\cdot\hat{\mathbf{x}}\rangle_t, \tag{B.5}$$

$$\frac{d\langle\hat{\mathbf{p}}^2\rangle_t}{dt} = \frac{3\lambda A^2\hbar^2}{2r_c^2} - m\omega^2\langle\hat{\mathbf{x}}\cdot\hat{\mathbf{p}} + \hat{\mathbf{p}}\cdot\hat{\mathbf{x}}\rangle_t. \tag{B.6}$$

In a similar way, one can show that the position-momentum correlation satisfies the equation:

$$\frac{d\langle \hat{\mathbf{x}}\cdot\hat{\mathbf{p}}+\hat{\mathbf{p}}\cdot\hat{\mathbf{x}}\rangle_t}{dt}=\frac{2}{m}\langle\hat{\mathbf{p}}^2\rangle_t-2m\omega^2\langle\hat{\mathbf{x}}^2\rangle_t. \tag{B.7}$$

The solution to the set of differential equations (B.5)–(B.7) are expressed in eqs. (3.10), (3.11) and (3.12).

B.2 dCSL dynamics: proof of the set of eqs. (3.51)

In this case, we start from the single particle master equation of the dCSL model in eq. (1.41). For the computation we have to perform, it is useful to express the master equation (1.41) through its Fourier transform [33]:

$$\begin{aligned}\frac{d\hat{\rho}}{dt}&=-\frac{i}{\hbar}\left[\frac{\hat{\mathbf{p}}^2}{2m}+\frac{1}{2}m\omega^2\hat{\mathbf{x}}^2,\hat{\rho}\right]+\frac{\lambda A^2 r_C^3}{(\sqrt{\pi}\hbar)^3}\\&\int d^3Q\left(e^{\frac{i}{\hbar}\mathbf{Q}\cdot\hat{\mathbf{x}}}L(\mathbf{Q},\hat{\mathbf{p}})\hat{\rho}(t)L(\mathbf{Q},\hat{\mathbf{p}})e^{-\frac{i}{\hbar}\mathbf{Q}\cdot\hat{\mathbf{x}}}\right.\\&\left.-\frac{1}{2}\left\{L^2(\mathbf{Q},\hat{\mathbf{p}}),\hat{\rho}\right\}\right),\end{aligned} \tag{B.8}$$

where

$$L(\mathbf{Q},\hat{\mathbf{p}})=e^{-\frac{r_C^2}{2\hbar^2}|(1+k)\mathbf{Q}+2k\hat{\mathbf{p}}|^2}. \tag{B.9}$$

With the help of the above equation, we can easily derive the equation for the variance in position:

$$\begin{aligned}\frac{d\langle\hat{\mathbf{x}}^2\rangle_t}{dt}&=\frac{1}{m}\langle\hat{\mathbf{x}}\cdot\hat{\mathbf{p}}+\hat{\mathbf{p}}\cdot\hat{\mathbf{x}}\rangle_t-\frac{\lambda A^2 r_C^3}{2(\sqrt{\pi}\hbar)^3}\\&\times\int d^3Q\,\mathrm{Tr}\left\{\hat{\rho}[[\hat{\mathbf{x}}^2,L(\mathbf{Q},\hat{\mathbf{p}})],L(\mathbf{Q},\hat{\mathbf{p}})]\right\}.\end{aligned} \tag{B.10}$$

After a long but straightforward calculation, one finds that

$$\begin{aligned}&[[\hat{\mathbf{x}}^2,L(\mathbf{Q},\hat{\mathbf{p}})],L(\mathbf{Q},\hat{\mathbf{p}})]=\\&-\frac{8k^2r_C^4}{\hbar^2}\left[(1+k)\mathbf{Q}_j+2k\hat{\mathbf{p}}_j\right]^2L^2(\mathbf{Q},\hat{\mathbf{p}}).\end{aligned} \tag{B.11}$$

Using Eq. (B.11) in Eq. (B.10), and performing the trace over the momentum eigenvectors, the following integration appears:

$$\begin{aligned}&\int d^3Q\int d^3p\,\left[(1+k)\mathbf{Q}+2k\mathbf{p}\right]^2e^{-\frac{r_C^2}{\hbar^2}\left[(1+k)\mathbf{Q}+2k\mathbf{p}\right]^2}\times\\&\times\hat{\rho}(p,p,t)=\frac{3}{2}\left(\frac{\sqrt{\pi}}{1+k}\right)^3\left(\frac{\hbar}{r_C}\right)^5\end{aligned} \tag{B.12}$$

Collecting all results, we get:

$$\frac{d\langle\hat{\mathbf{x}}^2\rangle_t}{dt} = \frac{1}{m}\langle\hat{\mathbf{x}}\cdot\hat{\mathbf{p}}+\hat{\mathbf{p}}\cdot\hat{\mathbf{x}}\rangle_t + \frac{6\lambda A^2 r_C^2 k^2}{(1+k)^3}. \tag{B.13}$$

Note that for $k \to 0$ Eq. (B.5) is recovered. In order to solve Eq. (B.13) we need to find $\langle\hat{\mathbf{x}}\cdot\hat{\mathbf{p}}+\hat{\mathbf{p}}\cdot\hat{\mathbf{x}}\rangle_t$. The equation for $\langle\hat{\mathbf{x}}\cdot\hat{\mathbf{p}}\rangle_t$ is:

$$\begin{aligned}\frac{d\langle\hat{\mathbf{x}}\cdot\hat{\mathbf{p}}\rangle_t}{dt} &= \frac{1}{m}\langle\hat{\mathbf{p}}^2\rangle_t - m\omega^2\left\langle\hat{\mathbf{x}}^2\right\rangle_t + \frac{\lambda A^2 r_C^3}{(\sqrt{\pi}\hbar)^3}\\ &\int d^3Q\left(\mathrm{Tr}\left\{e^{\frac{i}{\hbar}\mathbf{Q}\cdot\hat{\mathbf{x}}}L(\mathbf{Q},\hat{\mathbf{p}})\hat{\rho}(t)L(\mathbf{Q},\hat{\mathbf{p}})e^{-\frac{i}{\hbar}\mathbf{Q}\cdot\hat{\mathbf{x}}}\hat{\mathbf{x}}\cdot\hat{\mathbf{p}}\right\}\right.\\ &\left.-\frac{1}{2}\mathrm{Tr}\left\{\left\{L^2(\mathbf{Q},\hat{\mathbf{p}}),\hat{\rho}\right\}\hat{\mathbf{x}}\cdot\hat{\mathbf{p}}\right\}\right)\end{aligned} \tag{B.14}$$

Using the ciclycity of the trace together with

$$e^{-\frac{i}{\hbar}\mathbf{Q}\cdot\hat{\mathbf{x}}}\,\hat{\mathbf{x}}\cdot\hat{\mathbf{p}}\,e^{\frac{i}{\hbar}\mathbf{Q}\cdot\hat{\mathbf{x}}} = \hat{\mathbf{x}}\cdot(\hat{\mathbf{p}}+\mathbf{Q}) \tag{B.15}$$

we can rewrite the trace as

$$\begin{aligned}&\mathrm{Tr}\left\{e^{\frac{i}{\hbar}\mathbf{Q}\cdot\hat{\mathbf{x}}}L(\mathbf{Q},\hat{\mathbf{p}})\hat{\rho}(t)L(\mathbf{Q},\hat{\mathbf{p}})e^{-\frac{i}{\hbar}\mathbf{Q}\cdot\hat{\mathbf{x}}}\hat{\mathbf{x}}\cdot\hat{\mathbf{p}}\right\} -\\ &-\frac{1}{2}\mathrm{Tr}\left\{\left\{L^2(\mathbf{Q},\hat{\mathbf{p}}),\hat{\rho}\right\}\hat{\mathbf{x}}\cdot\hat{\mathbf{p}}\right\} =\\ &=\mathrm{Tr}\left\{\hat{\rho}(t)L(\mathbf{Q},\hat{\mathbf{p}})\hat{\mathbf{x}}\cdot\mathbf{Q}L(\mathbf{Q},\hat{\mathbf{p}})\right\} -\\ &-\frac{1}{2}\mathrm{Tr}\left\{\hat{\rho}(t)\left[\left[\hat{\mathbf{x}}\cdot\hat{\mathbf{p}},L(\mathbf{Q},\hat{\mathbf{p}})\right],L(\mathbf{Q},\hat{\mathbf{p}})\right]\right\}\end{aligned} \tag{B.16}$$

The term in the last line gives no contribution since the double commutator is zero. The integration over $\mathbf{Q}$ of the other term can be rewritten as follows:

$$\begin{aligned}&\int d^3Q\,\mathrm{Tr}\left\{\hat{\rho}(t)L(\mathbf{Q},\hat{\mathbf{p}})\hat{\mathbf{x}}\cdot\mathbf{Q}L(\mathbf{Q},\hat{\mathbf{p}})\right\} =\\ &=\frac{1}{2}\int d^3Q\,\mathrm{Tr}\left\{L^2(\mathbf{Q},\hat{\mathbf{p}})\hat{\rho}\hat{\mathbf{x}}\cdot\mathbf{Q}\right\}\\ &+\frac{1}{2}\int d^3Q\,\mathrm{Tr}\left\{L^2(\mathbf{Q},\hat{\mathbf{p}})\hat{\mathbf{x}}\cdot\mathbf{Q}\hat{\rho}\right\},\end{aligned} \tag{B.17}$$

and expanding the trace over the momentum eigenstates we get

$$\begin{aligned}&=\frac{1}{2}\sum_{j=1}^{3}\int d^3p\left(\int d^3Q L^2(\mathbf{Q},\mathbf{p})Q_j\right)\langle\mathbf{p}|\left(\hat{\rho}\hat{x}_j\right)|\mathbf{p}\rangle\\ &+\frac{1}{2}\sum_{j=1}^{3}\int d^3p\left(\int d^3Q L^2(\mathbf{Q},\mathbf{p})Q_j\right)\langle\mathbf{p}|\left(\hat{x}_j\hat{\rho}\right)|\mathbf{p}\rangle.\end{aligned}$$

Considering that

$$\int d^3Q L^2(\mathbf{Q},\mathbf{p})Q_j = -\frac{2kp_j}{(1+k)}\left(\frac{\hbar\sqrt{\pi}}{(1+k)\,r_C}\right)^3, \tag{B.18}$$

the dCSL contribution to eq. (B.14) is

$$\begin{aligned}&\frac{\lambda A^2 r_C^3}{2(\sqrt{\pi}\hbar)^3}\int d^3Q\,\mathrm{Tr}\Big(\hat{\rho}(t)L(\mathbf{Q},\hat{\mathbf{p}})\hat{\mathbf{x}}\cdot\mathbf{Q}L(\mathbf{Q},\hat{\mathbf{p}})\Big) = \\ &= -\frac{\lambda A^2 k}{(1+k)^4}\left\langle\hat{\mathbf{x}}\cdot\hat{\mathbf{p}}+\hat{\mathbf{p}}\cdot\hat{\mathbf{x}}\right\rangle_t.\end{aligned} \tag{B.19}$$

So, the equation for $\langle\hat{\mathbf{x}}\cdot\hat{\mathbf{p}}\rangle_t$ is:

$$\frac{d\left\langle\hat{\mathbf{x}}\cdot\hat{\mathbf{p}}\right\rangle_t}{dt} = \frac{1}{m}\left\langle\hat{\mathbf{p}}^2\right\rangle_t - m\omega^2\left\langle\hat{\mathbf{x}}^2\right\rangle_t - \frac{\lambda A^2 k}{(1+k)^4}\left\langle\hat{\mathbf{x}}\cdot\hat{\mathbf{p}}+\hat{\mathbf{p}}\cdot\hat{\mathbf{x}}\right\rangle_t \tag{B.20}$$

which implies that:

$$\begin{aligned}&\frac{d\left\langle\hat{\mathbf{x}}\cdot\hat{\mathbf{p}}+\hat{\mathbf{p}}\cdot\hat{\mathbf{x}}\right\rangle_t}{dt} = \frac{2}{m}\left\langle\hat{\mathbf{p}}^2\right\rangle_t - 2m\omega^2\left\langle\hat{\mathbf{x}}^2\right\rangle_t \\ &-\frac{2\lambda A^2 k}{(1+k)^4}\left\langle\hat{\mathbf{x}}\cdot\hat{\mathbf{p}}+\hat{\mathbf{p}}\cdot\hat{\mathbf{x}}\right\rangle_t.\end{aligned} \tag{B.21}$$

The last equation we need is that for the momentum variance $\left\langle\hat{\mathbf{p}}^2\right\rangle_t$. This has been already derived in [33]:

$$\frac{d\left\langle\hat{\mathbf{p}}^2\right\rangle_t}{dt} = -m\omega^2\left\langle\hat{\mathbf{x}}\cdot\hat{\mathbf{p}}+\hat{\mathbf{p}}\cdot\hat{\mathbf{x}}\right\rangle_t - \chi\left\langle\hat{\mathbf{p}}^2\right\rangle_t + \chi\left\langle\hat{\mathbf{p}}^2\right\rangle_{as}, \tag{B.22}$$

where

$$\chi := \frac{4k\lambda A^2}{(1+k)^5}, \qquad \left\langle\hat{\mathbf{p}}^2\right\rangle_{as} := \frac{3\hbar^2}{8kr_C^2}. \tag{B.23}$$

Appendix C

Dynamics in a double well potential

This appendix is divided in two sections. In the first section we obtain the solution of the CSL master equation for a condensate in a double well potential, expressed eq. (4.6). We derive also the CSL decoherence in eqs. (4.8) and (4.10). In the second section we derive the master equation for a condensate interacting with a thermal cloud.

C.1 Proof of eqs. (4.6), (4.8) and (4.10).

The general density matrix in the two-mode approximation can be written as follows:

$$\hat{\rho} = \sum_{k,j=0}^{N} c_{k,j} \left(\hat{a}_L^\dagger\right)^{N-j} \left(\hat{a}_R^\dagger\right)^{j} |0\rangle \langle 0| \left(\hat{a}_L\right)^{N-k} \left(\hat{a}_R\right)^{k}, \tag{C.1}$$

where $c_{k,j}$ are complex coefficients satisfying the self-adjointness and normalization conditions of the density matrix. We use the expansion eq. (C.1) in order to solve eq. (4.5), as follows

$$\begin{aligned}
&\frac{d}{dt} \langle 0| \left(\hat{a}_L\right)^{N-m} \left(\hat{a}_R\right)^{m} \hat{\rho}(t) \left(\hat{a}_L^\dagger\right)^{N-l} \left(\hat{a}_R^\dagger\right)^{l} |0\rangle \equiv \dot{\rho}(m,l,t) \\
&= \frac{iU}{\hbar} \langle 0| \left(\hat{a}_L\right)^{N-m} \left(\hat{a}_R\right)^{m} \left[\hat{a}_L^\dagger \hat{a}_L \hat{a}_R^\dagger \hat{a}_R, \hat{\rho}(t)\right] \left(\hat{a}_L^\dagger\right)^{N-l} \left(\hat{a}_R^\dagger\right)^{l} |0\rangle \\
&- \frac{\lambda A^2 \bar{\gamma}}{2} \sum_{i=L,R} \langle 0| \left(\hat{a}_L\right)^{N-m} \left(\hat{a}_R\right)^{m} \left[\hat{a}_i^\dagger \hat{a}_i, \left[\hat{a}_i^\dagger \hat{a}_i, \hat{\rho}(t)\right]\right] \left(\hat{a}_L^\dagger\right)^{N-l} \left(\hat{a}_R^\dagger\right)^{l} |0\rangle \\
&= \frac{iU}{\hbar} \left[(N-m)\, m - (N-l)\, l\right] \rho(m,l,t) - \lambda A^2 \bar{\gamma} \left(m-l\right)^2 \rho(m,l,t) \\
&\Rightarrow \rho(m,l,t) = e^{\frac{iUt}{\hbar}(l+m-N)(l-m)} e^{-\lambda A^2 \bar{\gamma} t (m-l)^2} \rho(m,l,0).
\end{aligned} \tag{C.2}$$

From eq. (C.2), the density matrix eq. (4.6) is easily obtained.

Regarding eq. (4.8), we have that

$$\begin{aligned}
&\langle \hat{a}_L^\dagger \hat{a}_R \rangle_t^{\mathrm{CSL}} = \mathrm{Tr}\left[\hat{a}_L^\dagger \hat{a}_R \hat{\rho}(t)\right] \\
&= \sum_{k=0}^{N} \frac{1}{(N-k)!k!} \langle 0| \left(\hat{a}_L\right)^{N-k} \left(\hat{a}_R\right)^k \hat{a}_L^\dagger \hat{a}_R e^{-\lambda A^2 \bar{\gamma} t \left(\hat{a}_R^\dagger \overleftarrow{\hat{a}_R} - \hat{a}_R^\dagger \overrightarrow{\hat{a}_R}\right)^2} \hat{\rho}_{\mathrm{Sch}}(t) \left(\hat{a}_L^\dagger\right)^{N-k} \left(\hat{a}_R^\dagger\right)^k |0\rangle \\
&= e^{-\lambda A^2 \bar{\gamma} t} \sum_{k=0}^{N} \frac{1}{(N-k)!k!} \langle 0| \left(\hat{a}_L\right)^{N-k} \left(\hat{a}_R\right)^k \hat{a}_L^\dagger \hat{a}_R \hat{\rho}_{\mathrm{Sch}}(t) \left(\hat{a}_L^\dagger\right)^{N-k} \left(\hat{a}_R^\dagger\right)^k |0\rangle \\
&= e^{-\lambda A^2 \bar{\gamma} t} \langle \hat{a}_L^\dagger \hat{a}_R \rangle_t^{\mathrm{Sch}}.
\end{aligned} \tag{C.3}$$

Eq. (4.10) can be similarly proved.

C.2 Interaction between condensate and thermal cloud: master equation and decoherence rates

In this section we derive the master equation describing the dynamics of a Bose Einstein condensate interacting with its thermal cloud. We start by writing the Hamiltonian of the total system:

$$\hat{H} = \int d\mathbf{x}\, \hat{a}^\dagger(\mathbf{x}) \left(-\frac{\hbar^2 \nabla^2}{2m} + V_{\mathrm{ext}}(\mathbf{x})\right) \hat{a}(\mathbf{x}) + \frac{g}{2} \int d\mathbf{x}\, \hat{a}^\dagger(\mathbf{x}) \hat{a}^\dagger(\mathbf{x}) \hat{a}(\mathbf{x}) \hat{a}(\mathbf{x}), \tag{C.4}$$

We rewrite the Hamiltonian operator in terms of the energy eigenstates $\hat{a}_i^\dagger |0\rangle = |\psi\rangle_i$ of the single particle Hamiltonian $-\frac{\hbar^2\nabla^2}{2m} + V_{\mathrm{ext}}(\mathbf{x})$:

$$\hat{H} = \sum_i \epsilon_i \hat{a}_i^\dagger \hat{a}_i + \frac{1}{2} \sum_{\substack{i,j \\ k,l}} \gamma_{k,l}^{i,j} \hat{a}_i^\dagger \hat{a}_j^\dagger \hat{a}_k \hat{a}_l\,, \tag{C.5}$$

where

$$\gamma_{k,l}^{i,j} = \int d\mathbf{x}\, \psi_i^*(\mathbf{x})\, \psi_i^*(\mathbf{x})\, \psi_k(\mathbf{x})\, \psi_l(\mathbf{x})\,. \tag{C.6}$$

By splitting between the condensate modes $i \in [0, \ldots, J] \equiv \mathcal{C}$ from the thermal modes $i \in [J+1, \ldots, +\infty[\equiv \mathcal{NC}$, the Hamiltonian operator in eq. (C.5) becomes:

$$\hat{H} = \hat{H}_C + \hat{H}_{NC} + \hat{V}_{int}\,, \tag{C.7}$$

where

$$\hat{H}_C = \sum_{i\in\mathcal{C}} \epsilon_i \hat{a}_i^\dagger \hat{a}_i + \frac{1}{2}\sum_{\mathcal{C}} \gamma_{k,l}^{i,j} \hat{a}_i^\dagger \hat{a}_j^\dagger \hat{a}_k \hat{a}_l \,; \tag{C.8}$$

$$\hat{H}_{NC} = \sum_{i\in\mathcal{NC}} \epsilon_i \hat{a}_i^\dagger \hat{a}_i + \frac{1}{2}\sum_{\mathcal{NC}} \gamma_{k,l}^{i,j} \hat{a}_i^\dagger \hat{a}_j^\dagger \hat{a}_k \hat{a}_l \,; \tag{C.9}$$

$$\hat{V}_{int} = \frac{1}{2}\sum_{\mathcal{C}+\mathcal{NC}} \gamma_{k,l}^{i,j} \hat{a}_i^\dagger \hat{a}_j^\dagger \hat{a}_k \hat{a}_l \,. \tag{C.10}$$

In the interaction picture (labeled by I), an initial density matrix $\hat{\rho}_0$ evolves in time as follows:

$$\hat{\rho}^I(t) = \mathrm{T}\left\{ e^{-\frac{i}{\hbar}\int d\tau\, \hat{V}_{int}^I(\tau)} \right\} \hat{\rho}_0 \mathrm{T}\left\{ e^{\frac{i}{\hbar}\int d\tau\, \hat{V}_{int}^I(\tau)} \right\} , \tag{C.11}$$

where $\mathrm{T}\{\cdot\}$ refers to the time ordering operations. In the weak coupling limit [134], we expand the two time ordered exponentials in eq. (C.11) up to the second order in the coupling g, obtaining the following expression

$$\begin{aligned}\hat{\rho}^I(t) =& \hat{\rho}_0 - \frac{i}{\hbar}\int d\tau \left[\hat{V}_{int}^I(\tau), \hat{\rho}_0\right] + \left(\frac{i}{\hbar}\right)^2 \int_0^t d\tau_1 \int_0^{\tau_1} d\tau_2 \left(\hat{V}_{int}^I(\tau_1)\hat{V}_{int}^I(\tau_2)\hat{\rho}_0 \right. \\ &\left. + \hat{\rho}_0 \hat{V}_{int}^I(\tau_2)\hat{V}_{int}^I(\tau_1)\right) - \left(\frac{i}{\hbar}\right)^2 \int_0^t d\tau_1 \int_0^t d\tau_2\, \hat{V}_{int}^I(\tau_1)\hat{\rho}_0 \hat{V}_{int}^I(\tau_2) \,.\end{aligned} \tag{C.12}$$

We work in the Born-Markov approximation [134], with initial state given by

$$\hat{\rho}_0 = \hat{\rho}_{\mathcal{C}} \frac{e^{-\beta \hat{H}_{NC}}}{\mathrm{Tr}\left[e^{-\beta \hat{H}_{NC}}\right]} \,. \tag{C.13}$$

We are interested only on the condensate modes $\mathcal{C}$, thus in eq. (C.12) we perform a partial trace over the non-condensate modes $\mathcal{NC}$. In computing the master equation for the condensate, we neglect the processes that do not conserve the energy of the system, such as $C + C \to NC + NC$ and $C + C \to NC + C$, where C refers to a condensate atom, and NC refers to a non-condensate atom. We thus obtain the following master equation in the Schrödinger picture:

$$\frac{d\hat{\rho}_{\mathcal{C}}(t)}{dt} = -\frac{i}{\hbar}\left[\hat{H}_C, \hat{\rho}_{\mathcal{C}}(t)\right] + \sum_{i=1,2} \widetilde{\mathcal{L}}_t^{(i)}\left[\hat{\rho}_{\mathcal{C}}(t)\right] , \tag{C.14}$$

where

$$\widetilde{\mathcal{L}}_t^{(1)}\left[\hat{\rho}_{\mathcal{C}}(t)\right] = \int d\mathbf{x} \int d\mathbf{y}\, \Lambda_{\mathrm{loss}}(\mathbf{x},\mathbf{y}) \left\{ \hat{a}^\dagger(\mathbf{x})\hat{a}(\mathbf{y})\hat{\rho}_{\mathcal{C}}(t) + \hat{\rho}_{\mathcal{C}}(t)\hat{a}^\dagger(\mathbf{x})\hat{a}(\mathbf{y}) - 2\hat{a}(\mathbf{y})\hat{\rho}_{\mathcal{C}}(t)\hat{a}^\dagger(\mathbf{x}) \right\} ; \tag{C.15}$$

$$\widetilde{\mathcal{L}}_t^{(2)}\left[\hat{\rho}_{\mathcal{C}}(t)\right] = \int d\mathbf{x} \int d\mathbf{y}\, \Lambda_{\mathrm{dec}}(\mathbf{x},\mathbf{y}) \left[\hat{a}^\dagger(\mathbf{x})\hat{a}(\mathbf{x}), \left[\hat{a}^\dagger(\mathbf{y})\hat{a}(\mathbf{y}), \hat{\rho}_{\mathcal{C}}(t)\right]\right] , \tag{C.16}$$

with damping rates given by the following quantities

$$\Lambda_{\text{loss}}(\mathbf{x},\mathbf{y}) = \frac{g^2}{2\hbar^2}\text{Tr}\left[\hat{a}^\dagger(\mathbf{x})\hat{a}(\mathbf{x})\hat{a}(\mathbf{x})\hat{a}^\dagger(\mathbf{y})\hat{a}^\dagger(\mathbf{y})\hat{a}(\mathbf{y})\frac{e^{-\beta\hat{H}_{NC}}}{\text{Tr}\left[e^{-\beta\hat{H}_{NC}}\right]}\right] ; \tag{C.17}$$

$$\Lambda_{\text{dec}}(\mathbf{x},\mathbf{y}) = \frac{g^2}{2\hbar^2}\text{Tr}\left[\hat{a}^\dagger(\mathbf{x})\hat{a}(\mathbf{x})\hat{a}^\dagger(\mathbf{y})\hat{a}^\dagger(\mathbf{y})\frac{e^{-\beta\hat{H}_{NC}}}{\text{Tr}\left[e^{-\beta\hat{H}_{NC}}\right]}\right] . \tag{C.18}$$

Note that the damping rates introduced in eqs. (C.19) and (C.20) are proportional, respectively, to the three-particles correlation and the two-particles correlation of the thermal cloud. For an homogeneous thermal cloud both quantities are strongly peeked around $\mathbf{x} = \mathbf{y}$, so we can further simplify the expressions as follows:

$$\Lambda_{\text{loss}}(\mathbf{x},\mathbf{y}) \approx \frac{g^2}{2\hbar^2}\text{Tr}\left[\hat{a}^\dagger(\mathbf{0})\hat{a}(\mathbf{0})\hat{a}(\mathbf{0})\hat{a}^\dagger(\mathbf{0})\hat{a}^\dagger(\mathbf{0})\hat{a}(\mathbf{0})\frac{e^{-\beta\hat{H}_{NC}}}{\text{Tr}\left[e^{-\beta\hat{H}_{NC}}\right]}\right]\delta(\mathbf{x}-\mathbf{y}) ; \tag{C.19}$$

$$\Lambda_{\text{dec}}(\mathbf{x},\mathbf{y}) = \frac{g^2}{2\hbar^2}\text{Tr}\left[\hat{a}^\dagger(\mathbf{0})\hat{a}(\mathbf{0})\hat{a}^\dagger(\mathbf{0})\hat{a}^\dagger(\mathbf{0})\frac{e^{-\beta\hat{H}_{NC}}}{\text{Tr}\left[e^{-\beta\hat{H}_{NC}}\right]}\right]\delta(\mathbf{x}-\mathbf{y}) , \tag{C.20}$$

where $\delta(\mathbf{x}-\mathbf{y})$ is the Dirac delta. The expressions in eqs. (4.26) and (4.27) are easily found in standard textbooks on cold atomic systems [25]. Imposing the two-mode approximation on the master equation (C.14), the eqs. (4.21) and (4.23) are easily obtained.

Bibliography

[1] C. Davisson and L. Germer, *The scattering of electrons by a single crystal of nickel*. 1927.

[2] J. H. Halban and P. Preiswerk, "Preuve experimentale de la diffraction des neutrons," *Comptes Rendus Acad. Sci. Paris*, vol. 203.

[3] M. Arndt, O. Nairz, J. Vos-Andreae, C. Keller, G. Van der Zouw, and A. Zeilinger, "Wave–particle duality of c60 molecules," *nature*, vol. 401, no. 6754, pp. 680–682, 1999.

[4] S. Gerlich, S. Eibenberger, M. Tomandl, S. Nimmrichter, K. Hornberger, P. J. Fagan, J. Tüxen, M. Mayor, and M. Arndt, "Quantum interference of large organic molecules," *Nature communications*, vol. 2, p. 263, 2011.

[5] M. Planck, *The theory of heat radiation*. Courier Corporation, 2013.

[6] A. J. Leggett, "*I'm inclined to put my money on the idea that if you push quantum mechanics hard enough it will break down and something else will take over - something we can't envisage at the moment*," *New Scientist*, vol. 2766.

[7] S. Weinberg, "Collapse of the state vector," *Physical Review A*, vol. 85, no. 6, p. 062116, 2012.

[8] J. Bell, "Against 'measurement'," *Physics world*, vol. 3, no. 8, p. 33, 1990.

[9] D. Bohm, "A suggested interpretation of the quantum theory in terms of "hidden" variables. i," *Phys. Rev.*, vol. 85, pp. 166–179, Jan 1952.

[10] D. Bohm, "A suggested interpretation of the quantum theory in terms of "hidden" variables. ii," *Phys. Rev.*, vol. 85, pp. 180–193, Jan 1952.

[11] H. Everett III, "The theory of the universal wave function," in *The many-worlds interpretation of quantum mechanics*, Citeseer, 1973.

[12] A. Danieri, A. Loinger, and G. Prosperi, "Quantum theory of measurement and ergodic condition," *Nucl. Phys*, vol. 33, pp. 297–319, 1962.

[13] W. H. Zurek, "Pointer basis of quantum apparatus: Into what mixture does the wave packet collapse?," *Phys. Rev. D*, vol. 24, pp. 1516–1525, Sep 1981.

[14] W. H. Zurek, "Environment-induced superselection rules," *Phys. Rev. D*, vol. 26, pp. 1862–1880, Oct 1982.

[15] D. Dieks, "The formalism of quantum theory: an objective description of reality?," *Annalen der Physik*, vol. 500, no. 3, pp. 174–190, 1988.

[16] J. Javanainen and J. Ruostekoski, "Emergent classicality in continuous quantum measurements," *New Journal of Physics*, vol. 15, no. 1, p. 013005, 2013.

[17] A. Bassi and G. Ghirardi, "Dynamical reduction models," *Physics Reports*, vol. 379, no. 5, pp. 257–426, 2003.

[18] A. Bassi, K. Lochan, S. Satin, T. P. Singh, and H. Ulbricht, "Models of wavefunction collapse, underlying theories, and experimental tests," *Reviews of Modern Physics*, vol. 85, no. 2, p. 471, 2013.

[19] C. Curceanu, S. Bartalucci, A. Bassi, M. Bazzi, S. Bertolucci, C. Berucci, A. Bragadireanu, M. Cargnelli, A. Clozza, L. De Paolis, *et al.*, "Spontaneously emitted x-rays: An experimental signature of the dynamical reduction models," *Foundations of Physics*, pp. 1–6, 2015.

[20] A. Vinante, M. Bahrami, A. Bassi, O. Usenko, G. Wijts, and T. Oosterkamp, "Upper bounds on spontaneous wave-function collapse models using millikelvin-cooled nanocantilevers," *Physical review letters*, vol. 116, no. 9, p. 090402, 2016.

[21] M. Toroš and A. Bassi, "Bounds on collapse models from matter-wave interferometry," *arXiv preprint arXiv:1601.03672*, 2016.

[22] A. Bassi, D.-A. Deckert, and L. Ferialdi, "Breaking quantum linearity: Constraints from human perception and cosmological implications," *EPL (Europhysics Letters)*, vol. 92, no. 5, p. 50006, 2010.

[23] A. Einstein, "Quantentheorie des einatomigen idealen gases," *Sitzungsberichte der Preussischen Akademie der Wissenschaften, Physikalisch-mathematische Klasse*, pp. 3–14, 1925.

[24] N. Bogolubov, "On the theory of superfluidity," *J. Phys*, vol. 11, pp. 23–29, 1966.

[25] C. J. Pethick and H. Smith, *Bose-Einstein condensation in dilute gases*. Cambridge university press, 2002.

[26] L. Pitaevskii and S. Stringari, *Bose-Einstein Condensation*. International Series of Monographs on Physics, Clarendon Press, 2003.

[27] H. J. Metcalf and P. Straten, *Laser cooling and trapping of neutral atoms*. Wiley Online Library, 2007.

[28] M. H. Anderson, J. R. Ensher, M. R. Matthews, C. E. Wieman, and E. A. Cornell, "Observation of bose-einstein condensation in a dilute atomic vapor," *science*, vol. 269, no. 5221, pp. 198–201, 1995.

[29] C. Chin, R. Grimm, P. Julienne, and E. Tiesinga, "Feshbach resonances in ultracold gases," *Reviews of Modern Physics*, vol. 82, no. 2, p. 1225, 2010.

[30] F. Laloë, W. J. Mullin, and P. Pearle, "Heating of trapped ultracold atoms by collapse dynamics," *Physical Review A*, vol. 90, no. 5, p. 052119, 2014.

[31] T. Kovachy, J. M. Hogan, A. Sugarbaker, S. M. Dickerson, C. A. Donnelly, C. Overstreet, and M. A. Kasevich, "Matter wave lensing to picokelvin temperatures," *Physical review letters*, vol. 114, no. 14, p. 143004, 2015.

[32] M. Bilardello, S. Donadi, A. Vinante, and A. Bassi, "Bounds on collapse models from cold-atom experiments," *Physica A: Statistical Mechanics and its Applications*, vol. 462, pp. 764 – 782, 2016.

[33] A. Smirne and A. Bassi, "Dissipative continuous spontaneous localization (csl) model," *Scientific reports*, vol. 5, 2015.

[34] S. L. Adler and A. Bassi, "Collapse models with non-white noises," *Journal of Physics A: Mathematical and Theoretical*, vol. 40, no. 50, p. 15083, 2007.

[35] S. L. Adler and A. Bassi, "Collapse models with non-white noises: Ii. particle-density coupled noises," *Journal of Physics A: Mathematical and Theoretical*, vol. 41, no. 39, p. 395308, 2008.

[36] M. Bilardello, A. Trombettoni, and A. Bassi, "Collapse in ultracold bose josephson junctions," *arXiv preprint arXiv:1612.07691*, 2016.

[37] J. Von Neumann, *Mathematical foundations of quantum mechanics*. No. 2, Princeton university press, 1955.

[38] J. T. Cushing, A. Fine, and S. Goldstein, *Bohmian mechanics and quantum theory: an appraisal*, vol. 184. Springer Science & Business Media, 2013.

[39] E. Joos, H. D. Zeh, C. Kiefer, D. J. Giulini, J. Kupsch, and I.-O. Stamatescu, *Decoherence and the appearance of a classical world in quantum theory*. Springer Science & Business Media, 2013.

[40] N. Gisin, "Stochastic quantum dynamics and relativity," *Helv. Phys. Acta*, vol. 62, no. 4, pp. 363–371, 1989.

[41] A. Bassi, D. Dürr, and G. Hinrichs, "Uniqueness of the equation for quantum state vector collapse," *Physical review letters*, vol. 111, no. 21, p. 210401, 2013.

[42] G. C. Ghirardi, A. Rimini, and T. Weber, "Unified dynamics for microscopic and macroscopic systems," *Physical Review D*, vol. 34, no. 2, p. 470, 1986.

[43] G. C. Ghirardi, P. Pearle, and A. Rimini, "Markov processes in hilbert space and continuous spontaneous localization of systems of identical particles," *Physical Review A*, vol. 42, no. 1, p. 78, 1990.

[44] S. L. Adler, "Lower and upper bounds on csl parameters from latent image formation and igm heating," *Journal of Physics A: Mathematical and Theoretical*, vol. 40, no. 12, p. 2935, 2007.

[45] L. Arnold, *Stochastic differential equations: Theory and applications*. Wiley-Interscience, New York, 1974.

[46] L. Ballentine, "Failure of some theories of state reduction," *Physical Review A*, vol. 43, no. 1, p. 9, 1991.

[47] M. R. Gallis and G. N. Fleming, "Comparison of quantum open-system models with localization," *Physical Review A*, vol. 43, no. 11, p. 5778, 1991.

[48] P. Pearle and E. Squires, "Gravity, energy conservation, and parameter values in collapse models," *Foundations of Physics*, vol. 26, no. 3, pp. 291–305, 1996.

[49] A. Bassi, E. Ippoliti, and B. Vacchini, "On the energy increase in space-collapse models," *Journal of Physics A: Mathematical and General*, vol. 38, no. 37, p. 8017, 2005.

[50] B. Vacchini, "On the precise connection between the grw master equation and master equations for the description of decoherence," *Journal of Physics A: Mathematical and Theoretical*, vol. 40, no. 10, p. 2463, 2007.

[51] G. Lindblad, "On the generators of quantum dynamical semigroups," *Communications in Mathematical Physics*, vol. 48, no. 2, pp. 119–130, 1976.

[52] V. Gorini, A. Kossakowski, and E. C. G. Sudarshan, "Completely positive dynamical semigroups of n-level systems," *Journal of Mathematical Physics*, vol. 17, no. 5, pp. 821–825, 1976.

[53] F. Dalfovo, S. Giorgini, L. P. Pitaevskii, and S. Stringari, "Theory of bose-einstein condensation in trapped gases," *Reviews of Modern Physics*, vol. 71, no. 3, p. 463, 1999.

[54] A. J. Leggett, "Bose-einstein condensation in the alkali gases: Some fundamental concepts," *Reviews of Modern Physics*, vol. 73, no. 2, p. 307, 2001.

[55] I. Bloch, J. Dalibard, and W. Zwerger, "Many-body physics with ultracold gases," *Reviews of Modern Physics*, vol. 80, no. 3, p. 885, 2008.

[56] S. N. Bose, "Plancks gesetz und lichtquantenhypothese," *Z. phys*, vol. 26, no. 3, p. 178, 1924.

[57] S. Salinas, *Introduction to statistical physics*. Springer Science & Business Media, 2013.

[58] A. F. Verbeure, *Many-body Boson systems*. Springer, 2011.

[59] K. Huang, *Statistical mechanics*. Wiley, 1987.

[60] E. P. Gross, "Structure of a quantized vortex in boson systems," *Il Nuovo Cimento (1955-1965)*, vol. 20, no. 3, pp. 454–477, 1961.

[61] L. P. Pitaevskii, "Vortex linex in an imperfect bose gas," *Sov. Phys. JETP*, vol. 13, p. 451, 1961.

[62] K. Huang and C. N. Yang, "Quantum-mechanical many-body problem with hard-sphere interaction," *Physical review*, vol. 105, no. 3, p. 767, 1957.

[63] T. D. Lee, K. Huang, and C. N. Yang, "Eigenvalues and eigenfunctions of a bose system of hard spheres and its low-temperature properties," *Physical Review*, vol. 106, no. 6, p. 1135, 1957.

[64] E. H. Lieb, R. Seiringer, and J. Yngvason, "Bosons in a trap: A rigorous derivation of the gross-pitaevskii energy functional," in *The Stability of Matter: From Atoms to Stars*, pp. 685–697, Springer, 2001.

[65] E. H. Lieb and R. Seiringer, "Proof of bose-einstein condensation for dilute trapped gases," *Physical review letters*, vol. 88, no. 17, p. 170409, 2002.

[66] A. Elgart, L. Erdős, B. Schlein, and H.-T. Yau, "Gross-pitaevskii equation as the mean field limit of weakly coupled bosons," *Archive for rational mechanics and analysis*, vol. 179, no. 2, pp. 265–283, 2006.

[67] N. P. Proukakis and B. Jackson, "Finite-temperature models of bose einstein condensation," *Journal of Physics B: Atomic, Molecular and Optical Physics*, vol. 41, no. 20, p. 203002, 2008.

[68] J. Fortágh and C. Zimmermann, "Magnetic microtraps for ultracold atoms," *Rev. Mod. Phys.*, vol. 79, pp. 235–289, Feb 2007.

[69] M. Albiez, R. Gati, J. Fölling, S. Hunsmann, M. Cristiani, and M. K. Oberthaler, "Direct observation of tunneling and nonlinear self-trapping in a single bosonic josephson junction," *Physical review letters*, vol. 95, no. 1, p. 010402, 2005.

[70] O. Morsch and M. Oberthaler, "Dynamics of bose-einstein condensates in optical lattices," *Reviews of modern physics*, vol. 78, no. 1, p. 179, 2006.

[71] G. Valtolina, A. Burchianti, A. Amico, E. Neri, K. Xhani, J. A. Seman, A. Trombettoni, A. Smerzi, M. Zaccanti, M. Inguscio, *et al.*, "Josephson effect in fermionic superfluids across the bec-bcs crossover," *Science*, vol. 350, no. 6267, pp. 1505–1508, 2015.

[72] F. Buccheri and A. Trombettoni, "Relative phase and josephson dynamics between weakly coupled richardson models," *Physical Review B*, vol. 87, no. 17, p. 174506, 2013.

[73] Y. Shin, M. Saba, T. Pasquini, W. Ketterle, D. Pritchard, and A. Leanhardt, "Atom interferometry with bose-einstein condensates in a double-well potential," *Physical review letters*, vol. 92, no. 5, p. 050405, 2004.

[74] T. Schumm, S. Hofferberth, L. M. Andersson, S. Wildermuth, S. Groth, I. Bar-Joseph, J. Schmiedmayer, and P. Krüger, "Matter-wave interferometry in a double well on an atom chip," *Nature Physics*, vol. 1, no. 1, pp. 57–62, 2005.

[75] A. D. Cronin, J. Schmiedmayer, and D. E. Pritchard, "Optics and interferometry with atoms and molecules," *Reviews of Modern Physics*, vol. 81, no. 3, p. 1051, 2009.

[76] D. Gordon and C. Savage, "Creating macroscopic quantum superpositions with bose-einstein condensates," *Physical Review A*, vol. 59, no. 6, p. 4623, 1999.

[77] Y. Huang and M. Moore, "Creation, detection, and decoherence of macroscopic quantum superposition states in double-well bose-einstein condensates," *Physical Review A*, vol. 73, no. 2, p. 023606, 2006.

[78] C. Gross, T. Zibold, E. Nicklas, J. Esteve, and M. K. Oberthaler, "Nonlinear atom interferometer surpasses classical precision limit," *Nature*, vol. 464, no. 7292, pp. 1165–1169, 2010.

[79] M. F. Riedel, P. Böhi, Y. Li, T. W. Hänsch, A. Sinatra, and P. Treutlein, "Atom-chip-based generation of entanglement for quantum metrology," *Nature*, vol. 464, no. 7292, pp. 1170–1173, 2010.

[80] B. Lücke, M. Scherer, J. Kruse, L. Pezzé, F. Deuretzbacher, P. Hyllus, J. Peise, W. Ertmer, J. Arlt, L. Santos, *et al.*, "Twin matter waves for interferometry beyond the classical limit," *Science*, vol. 334, no. 6057, pp. 773–776, 2011.

[81] I. Kruse, K. Lange, J. Peise, B. Lücke, L. Pezzè, J. Arlt, W. Ertmer, C. Lisdat, L. Santos, A. Smerzi, *et al.*, "Improvement of an atomic clock using squeezed vacuum," *Physical Review Letters*, vol. 117, no. 14, p. 143004, 2016.

[82] R. Schmied, J.-D. Bancal, B. Allard, M. Fadel, V. Scarani, P. Treutlein, and N. Sangouard, "Bell correlations in a bose-einstein condensate," *Science*, vol. 352, no. 6284, pp. 441–444, 2016.

[83] J. I. Cirac, M. Lewenstein, K. Mølmer, and P. Zoller, "Quantum superposition states of bose-einstein condensates," *Physical Review A*, vol. 57, no. 2, p. 1208, 1998.

[84] D. A. R. Dalvit, J. Dziarmaga, and W. H. Zurek, "Decoherence in bose-einstein condensates: Towards bigger and better schrödinger cats," *Physical Review A*, vol. 62, no. 1, p. 013607, 2000.

[85] J. A. Dunningham and K. Burnett, "Proposals for creating schrödinger cat states in bose-einstein condensates," *Journal of Modern Optics*, vol. 48, no. 12, pp. 1837–1853, 2001.

[86] P. Louis, P. Brydon, and C. Savage, "Macroscopic quantum superposition states in bose-einstein condensates: Decoherence and many modes," *Physical Review A*, vol. 64, no. 5, p. 053613, 2001.

[87] I. Mazets, G. Kurizki, M. Oberthaler, and J. Schmiedmayer, "Creation of macroscopic quantum superposition states by a measurement," *EPL (Europhysics Letters)*, vol. 83, no. 6, p. 60004, 2008.

[88] G. FERRINI, *Macroscopic quantum coherent phenomena in Bose Josephson junctions*. PhD thesis, Citeseer, 2012.

[89] A. Smerzi, S. Fantoni, S. Giovanazzi, and S. R. Shenoy, "Quantum coherent atomic tunneling between two trapped bose-einstein condensates," *Physical Review Letters*, vol. 79, no. 25, p. 4950, 1997.

[90] G. Milburn, J. Corney, E. Wright, and D. Walls, "Quantum dynamics of an atomic bose-einstein condensate in a double-well potential," *Physical Review A*, vol. 55, no. 6, p. 4318, 1997.

[91] E. Merzbacher, *Quantum Mechanics*. Wiley, 1998.

[92] M. Egorov, B. Opanchuk, P. Drummond, B. Hall, P. Hannaford, and A. Sidorov, "Measurement of s-wave scattering lengths in a two-component bose-einstein condensate," *Physical Review A*, vol. 87, no. 5, p. 053614, 2013.

[93] A. Smerzi and A. Trombettoni, "Nonlinear tight-binding approximation for bose-einstein condensates in a lattice," *Physical Review A*, vol. 68, no. 2, p. 023613, 2003.

[94] D. Jezek, P. Capuzzi, and H. Cataldo, "Two-mode effective interaction in a double-well condensate," *Physical Review A*, vol. 87, no. 5, p. 053625, 2013.

[95] J. Javanainen and M. Y. Ivanov, "Splitting a trap containing a bose-einstein condensate: Atom number fluctuations," *Physical Review A*, vol. 60, no. 3, p. 2351, 1999.

[96] A. Trenkwalder, G. Spagnolli, G. Semeghini, S. Coop, M. Landini, P. Castilho, L. Pezzè, G. Modugno, M. Inguscio, A. Smerzi, *et al.*, "Quantum phase transitions with parity-symmetry breaking and hysteresis," *Nature Physics*, 2016.

[97] M. Andrews, C. Townsend, H.-J. Miesner, D. Durfee, D. Kurn, and W. Ketterle, "Observation of interference between two bose condensates," *Science*, vol. 275, no. 5300, pp. 637–641, 1997.

[98] M. Greiner, O. Mandel, T. W. Hänsch, and I. Bloch, "Collapse and revival of the matter wave field of a bose–einstein condensate," *Nature*, vol. 419, no. 6902, pp. 51–54, 2002.

[99] G.-B. Jo, Y. Shin, S. Will, T. Pasquini, M. Saba, W. Ketterle, D. Pritchard, M. Vengalattore, and M. Prentiss, "Long phase coherence time and number squeezing of two bose-einstein condensates on an atom chip," *Physical Review Letters*, vol. 98, no. 3, p. 030407, 2007.

[100] M. Lewenstein and L. You, "Quantum phase diffusion of a bose-einstein condensate," *Physical review letters*, vol. 77, no. 17, p. 3489, 1996.

[101] J. Javanainen and M. Wilkens, "Phase and phase diffusion of a split bose-einstein condensate," *Physical Review Letters*, vol. 78, no. 25, p. 4675, 1997.

[102] D. K. Faust and W. P. Reinhardt, "Analysis of a bose-einstein condensate double-well atom interferometer," *Physical review letters*, vol. 105, no. 24, p. 240404, 2010.

[103] A. Imamoglu, M. Lewenstein, and L. You, "Inhibition of coherence in trapped bose-einstein condensates," *Physical review letters*, vol. 78, no. 13, p. 2511, 1997.

[104] A. Sinatra and Y. Castin, "Phase dynamics of bose-einstein condensates: Losses versus revivals," *The European Physical Journal D-Atomic, Molecular, Optical and Plasma Physics*, vol. 4, no. 3, pp. 247–260, 1998.

[105] G. Ferrini, A. Minguzzi, and F. W. J. Hekking, "Number squeezing, quantum fluctuations, and oscillations in mesoscopic bose josephson junctions," *Physical Review A*, vol. 78, no. 2, p. 023606, 2008.

[106] R. Grimm, M. Weidemüller, and Y. B. Ovchinnikov, "Optical dipole traps for neutral atoms," *Advances in atomic, molecular, and optical physics*, vol. 42, pp. 95–170, 2000.

[107] M. Lewenstein, A. Sanpera, V. Ahufinger, B. Damski, A. Sen, and U. Sen, "Ultracold atomic gases in optical lattices: mimicking condensed matter physics and beyond," *Advances in Physics*, vol. 56, no. 2, pp. 243–379, 2007.

[108] C. Cohen-Tannoudji, "Frontiers in laser spectroscopy, proceedings of the les houches summer school of theoretical physics, les houches, 1975," 1977.

[109] C. Cohen-Tannoudji, "Atomic motion in laser light," *Fundamental systems in quantum optics*, no. 53, pp. 1–164, 1990.

[110] W. Kohn, "Analytic properties of bloch waves and wannier functions," *Physical Review*, vol. 115, no. 4, p. 809, 1959.

[111] N. Marzari, A. A. Mostofi, J. R. Yates, I. Souza, and D. Vanderbilt, "Maximally localized wannier functions: Theory and applications," *Reviews of Modern Physics*, vol. 84, no. 4, p. 1419, 2012.

[112] O. Luiten, M. Reynolds, and J. Walraven, "Kinetic theory of the evaporative cooling of a trapped gas," *Physical Review A*, vol. 53, no. 1, p. 381, 1996.

[113] E. Burt, R. Ghrist, C. Myatt, M. Holland, E. Cornell, and C. Wieman, "Coherence, correlations, and collisions: What one learns about bose-einstein condensates from their decay," *Physical Review Letters*, vol. 79, no. 3, p. 337, 1997.

[114] T. Weber, J. Herbig, M. Mark, H.-C. Nägerl, and R. Grimm, "Three-body recombination at large scattering lengths in an ultracold atomic gas," *Physical review letters*, vol. 91, no. 12, p. 123201, 2003.

[115] T. Kraemer, M. Mark, P. Waldburger, J. Danzl, C. Chin, B. Engeser, A. Lange, K. Pilch, A. Jaakkola, H.-C. Nägerl, *et al.*, "Evidence for efimov quantum states in an ultracold gas of caesium atoms," *Nature*, vol. 440, no. 7082, pp. 315–318, 2006.

[116] S. Bali, K. O' Hara, M. Gehm, S. Granade, and J. Thomas, "Quantum-diffractive background gas collisions in atom-trap heating and loss," *Physical Review A*, vol. 60, no. 1, p. R29, 1999.

[117] T. Savard, K. O' hara, and J. Thomas, "Laser-noise-induced heating in far-off resonance optical traps," *Physical Review A*, vol. 56, no. 2, p. R1095, 1997.

[118] S. L. Adler and F. M. Ramazanoğlu, "Photon-emission rate from atomic systems in the csl model," *Journal of Physics A: Mathematical and Theoretical*, vol. 40, no. 44, p. 13395, 2007.

[119] S. L. Adler and F. M. Ramazanoglu, "Photon-emission rate from atomic systems in the csl model," *Journal of Physics A: Mathematical and Theoretical*, vol. 42, no. 10, p. 109801, 2009.

[120] S. Donadi, D.-A. Deckert, and A. Bassi, "On the spontaneous emission of electromagnetic radiation in the csl model," *Annals of Physics*, vol. 340, no. 1, pp. 70–86, 2014.

[121] A. Barone and G. Paterno, *Physics and applications of the Josephson effect*. 1982.

[122] F. Cataliotti, S. Burger, C. Fort, P. Maddaloni, F. Minardi, A. Trombettoni, A. Smerzi, and M. Inguscio, "Josephson junction arrays with bose-einstein condensates," *Science*, vol. 293, no. 5531, pp. 843–846, 2001.

[123] S. Levy, E. Lahoud, I. Shomroni, and J. Steinhauer, "The ac and dc josephson effects in a bose–einstein condensate," *Nature*, vol. 449, no. 7162, pp. 579–583, 2007.

[124] L. LeBlanc, A. Bardon, J. McKeever, M. Extavour, D. Jervis, J. Thywissen, F. Piazza, and A. Smerzi, "Dynamics of a tunable superfluid junction," *Physical review letters*, vol. 106, no. 2, p. 025302, 2011.

[125] A. Smerzi, A. Trombettoni, T. Lopez-Arias, C. Fort, P. Maddaloni, F. Minardi, and M. Inguscio, "Macroscopic oscillations between two weakly coupled bose-einstein condensates," *The European Physical Journal B-Condensed Matter and Complex Systems*, vol. 31, no. 4, pp. 457–461, 2003.

[126] T. Zibold, E. Nicklas, C. Gross, and M. K. Oberthaler, "Classical bifurcation at the transition from rabi to josephson dynamics," *Physical review letters*, vol. 105, no. 20, p. 204101, 2010.

[127] M. Carlesso, A. Bassi, P. Falferi, and A. Vinante, "Experimental bounds on collapse models from gravitational wave detectors," *arXiv preprint arXiv:1606.04581*, 2016.

[128] J. Ruostekoski and D. F. Walls, "Bose-einstein condensate in a double-well potential as an open quantum system," *Physical Review A*, vol. 58, no. 1, p. R50, 1998.

[129] Y. Kagan, B. Svistunov, and G. Shlyapnikov, "Effect of bose condensation on inelastic processes in gases," *JETP Lett*, vol. 42, no. 4, 1985.

[130] P. Fedichev, M. Reynolds, and G. Shlyapnikov, "Three-body recombination of ultracold atoms to a weakly bound s level," *Physical review letters*, vol. 77, no. 14, p. 2921, 1996.

[131] M. W. Jack, "Decoherence due to three-body loss and its effect on the state of a bose-einstein condensate," *Physical review letters*, vol. 89, no. 14, p. 140402, 2002.

[132] G. Ferrini, D. Spehner, A. Minguzzi, and F. W. J. Hekking, "Effect of phase noise on quantum correlations in bose-josephson junctions," *Phys. Rev. A*, vol. 84, p. 043628, Oct 2011.

[133] H. Pichler, A. Daley, and P. Zoller, "Nonequilibrium dynamics of bosonic atoms in optical lattices: Decoherence of many-body states due to spontaneous emission," *Physical Review A*, vol. 82, no. 6, p. 063605, 2010.

[134] H.-P. Breuer and F. Petruccione, *The theory of open quantum systems*. Oxford University Press on Demand, 2002.